University of Zurich[UZH]

A New Time-Dependent Limit-Equilibrium Model to Understand Progressive Failure in Bedrock Slopes on the Grimsel Pass

GEO 511 Master's Thesis

Author
Marco Zapata Torres
16-732-182

Supervised by
Dr. Simon Allen
Leith, Kerry (kerry.leith@erdw.ethz.ch)
Aaron, Jordan (jordan.aaron@erdw.ethz.ch)

Faculty representative
Prof. Dr. Andreas Vieli

29.01.2019
Department of Geography, University of Zurich

UNIVERSITÄT ZÜRICH

MASTER THESIS

A New Time-Dependent Limit-Equilibrium Model to Understand Progressive Failure in Bedrock Slopes on the Grimsel Pass

Author:
Marco Fernando ZAPATA TORRES

Supervisor:
Dr. Leith KERRY
Dr. Jordan AARON
Dr. Simon ALLEN
Faculty Member:
Dr. Andreas VIELI

January 29, 2019

Abstract

Rockfalls can have severe consequences for the affected population and infrastructure and cause high reconstruction cost. For this reason it is important to understand rock instabilities in order to implement appropriate safety measures. Limit Equilibrium Methods (LEM) are models to asses rock instabilities which are often used due to their simplicity and reliability. Despite these advantages, LEM analyze the slope stability by assuming temporally invariant conditions (friction, cohesion, geometry, etc.). The aim of this thesis is therefore the implementation of a temporally variant condition (progressive tensile edge crack) into LEM for the planar failure in rock slopes with the objective to carry out a time-dependent analysis. A code that combines LEM with crack growth theory to evaluate the evolution of the tensile edge crack growth for single blocks was developed. The implemented code evaluates if the base provides enough stability to the block or if a progressive tensile edge crack will propagate. When a progressive tensile edge crack starts to propagate the code selects between Paris or Charles crack growth law, choosing the faster one. The code during this crack propagation records the crack opening, the length of the crack, iteration and the time until the crack reaches a critical state. In a critical state, the tensile strength between the toe of the block and the tip of the edge crack plus the resisting base forces are less than the driving forces. This will cause the block failure. To perform a back analysis of the code, which consists of plotting the field data over the code result, three different photogrammetries near Grimsel Pass (Switzerland) were made. From these photogrammetries, digital elevation models (DEM) were obtained. Then two different types of blocks with planar characteristics and a visible tensile edge crack were mapped: existing blocks (96) and failed blocks (16). Characteristics such as height, length, perimeter and slope angle were recorded. The mapped blocks were classified according to their slope angle ($< 40^\circ$,$40^\circ - 50^\circ$ and $50^\circ - 60^\circ$) and represented in different plots. Three different zones exist in each plot. In the first zone the base provides stability, in the second the tensile edge crack propagates and causes block failure and in the third the blocks topple. The results show that the existing blocks are distributed in the three areas and the failed blocks in the non-toppling area. If the blocks are located in the zone where the edge crack has propagated, this indicates that the edge crack dominated the process and that it had reached the critical length to hold the blocks in their position. For the failed blocks located in the zone where the base provides stability, the failure cause is unclear. Probably they have failed due to external events (seism, extreme rainfalls, etc.). The results of the model help to understand the evolution of the tensile edge crack propagation in planar failure rock slopes and the model can be further used to add new modules. However, the model has some limitations and the results need to be evaluated carefully.

Acknowledgements

The present master thesis would not have been possible without the guidance and help of many people. Each of them supported me in a different way and therefore I am very grateful to each of them.

A special mention goes to my supervisors Dr. Kerry Leith, Dr. Jordan Aaron and Dr. Simon Allen. Dr. Kerry Leith for supporting me with your thorough knowledge and all the interesting discussions about crack propagation and your guidance with the Matlab code which kept me constantly motivated. Dr. Jordan Aaron for sharing your knowledge about the topic, the invaluable support with the Matlab code, the formulas verification and the thesis corrections. Dr. Simon Allen for the corrections and the interesting inputs from a more geographical point of view.

To Dr. Martin Ziegler who allowed me to use his data and help me with the realization of the Photogrammetric models.

To all my friends. My profound gratitude goes in particular to Anika Bail for all the time you invested to do the final English revision. To Emanuel Bueechi for the constant English corrections. To Joan Delort for providing the transport to Grimsel Pass and your help to obtain the photos. To Andrea Graber for your immense patience and support during all this time. Finally to my family for the moral and financial support.

Contents

List of Figures

List of Tables

List of Abbreviations

CAGr	Central Aar Granite
CGrGr	Grimsel Granodiorite
DEM	Digital Elevation Model
DGPS	Differential Global Positioning Systems
EF	External Factors
FOS	Factor of Safety
FOSA	First Order Second Moment Approach
GCP	Ground Control Points
GIS	Geographical Information System
IP	Internal Parameters
ISO	Sensitive Image Sensor
J(PUJ)	Post Uplift Joints
J(UJ)	Uptlift Joints
JExf	Exfoliation Fractures
KI	Stress Intensity Factor
K$_I C$	Critical Stress Intensity Factor
LEM	Limit Equilibrium Methods
LGM	Last Glaciar Maximum
MiGr	Mittagluh Granite
MSA	Monte Carlo Simulation Approach
MSMR	Modified Slope Mass Rating
PEA	Point Estimate Approach
SMR	Slope Mass Rating
SsCAGr	Southern Stripe of the Central Aar Granite
UAV	Unmanned Aerial Vehicle

Chapter 1

Introduction

1.1 Introduction

Rock slope stability analyses are important for population and infrastructure safety (Eberhardt, 2002). Rockfalls can have different consequences for society, in the worst case it causes human fatalities. Other consequences are economic impacts, which are related to loss of utility or damage to the infrastructure. Indirect economic impacts are for example the cost of closing a road or if big areas with an economy based on the transportation network are affected (Winter et al., 2014). For example in Switzerland during the 2017 the cost of rockfalls, landslides and debris flows was about 170 Million Swiss francs (Andres and Badoux, 2018).

Slope instabilities can be classified according to if they happen in soils or rocks. In the case of rockfall, there are four primary failure modes: planar, rotational, wedge and toppling failure (Kliche, 2003). Different methods and analysis (i.e kinematic methods, probability methods, etc.) exist to assess the slope stability (Raghuvanshi, 2017). In this thesis I only focus on the planar failure mode. I analyzed this failure mode with the Limit Equilibrium Method (LEM) and to it added the theory of progressive tensile crack growth. To validate the proposed model, a back analysis with the data obtained from Grimsel Pass (Switzerland) was performed.

This thesis has the following structure. First, a literature review is provided from which the specific research gap is derived. Then, the underlying theories are discussed in more detail. In the next chapter the research goals are presented. The following chapter "Methodology and Data" reviews the formulas that were used in the Matlab code and outlines the code workflow. After that the photogrametry process is explained. The obtained results and their data interpretation are presented in the subsequent chapter. Finally the conclusions are drawn.

1.2 Literature Review

1.2.1 Rockfalls

Several authors have classified modes of failures (i.e. Hocking, 1976, Hoek and Bray, 1981 Wyllie and Mah, 2005). The detachment process is divided by Varnes (1978), into five groups: slide, flow, drift, topple and fall. Goodman and Kieffer (2000), provide a detailed description of the modes of failure of slopes (including the ones classified by Varnes (1978), and some additional ones). Each of the different detachment processes can occur in debris, rock, soil or mud. In the specific case of rockfall Selby (1982), classify it like a very small landslide which removes individual blocks or superficial rocks from a cliff face.

The process of rockfall starts with the detachment of rocks from bedrocks. Bedrock slopes are exposed to different conditions of weathering (this can include physical

and chemical weathering) (Schumm and Chorley, 1964; Day, 1997). According to Jaboyedoff and Derron (2005), there are internal parameters (IP) and external factors (EF) which provide a conceptual framework to describe the slope system. Some of the most important internal parameters are: morphology, geology, fracturing, mechanical properties of rocks and soils and hydrogeology. These internal parameters can evolve to external factors which are: gravitational effects, water circulation, weathering, erosion, seismicity, active tectonics, microclimate, nearby instabilities, human activities, etc.

Plane mode or planar failure usually is controlled by a structurally weak surface (faults, joints, bedding planes, variation in shear strength between layers) or by the contact between firm bedrock and overlying weathered rock (Kliche, 2003;Raghuvanshi, 2017). Different conditions such as that the structural discontinuity plane dips (or daylight) towards the valley at an smaller angle than the slope angle face (greater than the angle of friction of the discontinuity surface) are necessary in order that a plane failure happens (Wyllie and Mah, 2005).

The stability of the slope depends on the relationship between driving forces and resisting forces (Wyllie and Mah, 2005; Kliche, 2003; Hoek, 2007; Eberhardt, 2002). As mentioned above, IP and EF are very important for the stability analysis.

1.2.2 Stability Analysis Techniques

There exist different methods to analyze the stability of the rock slopes which can be grouped into two main approaches. On the one hand there are the conventional approaches which include kinematic methods, empirical methods, limit equilibrium methods and probability methods.On the other hand there are the numerical methods which include continuum modeling, discontinuum modeling and hybrid modeling (Raghuvanshi, 2017).

Conventional Approaches

- Kinematic methods: The kinematic methods analyze the geometric conditions that are required for the movement of the rock over the discontinuity planes. However they do not consider the forces that generate this sliding. (Goodman, 1989;Hoek and Bray, 1981). In the last few years some new classifications for the lateral boundaries have been developed (Price, 2009). One of their principal characteristics is that they are represented on an stereo-net.

- Empirical methods: The empirical methods are based on rock mass classification systems, such as the Slope Mass Rating (SMR) (Romana, 1985), the Modified Slope Mass Rating (MSMR) (An-balagan, 1992) and the rock mass classification systems for slopes (Liu and Chen, 2007). In general these methods establish a relationship between the slope inclination and dip of the discontinuity. In some cases the degree of weathering, the shear strength of the slope material and geological and environmental factors are considered.

- Limit equilibrium methods: Limit equilibrium methods evaluate the forces that are responsible for the driving and resisting forces that act on the rock mass (Hoek, 2007;Hoek and Bray, 1981; Kliche, 2003; Eberhardt, 2002). The ratio of resisting forces to driving forces defines the factor of safety (FOS). If the FOS is higher than 1 it suggests a stable slope, if it is less than 1 then the slope is in a critical state of equilibrium. The factors considered are: geometry of the slope, geometry of the block, failure plane characteristics and water

and external triggering factors (Hoek, 2007;Hoek and Bray, 1981; Kliche, 2003; Eberhardt, 2002).

- Probabilistic methods: Some of the considered parameters (friction angle, dip strike, etc.) show uncertainty whereas others such as slope height, slope inclination, etc. are fixed. With these methods it is possible to incorporate the uncertain parameters in a systematic way and define the slope stability in probabilistic terms (Chowdhury, Flentje, and Bhattacharya, 2010;Kliche, 2003). In these methods a target population is considered, as well as a random sample and a biased sample (Miller and Freund, 1985). The result of these methods are a FOS with a probability distribution over a certain range. There exist three different probabilistic methods which are the First Order Second Moment Approach (FOSA), the Point Estimate Approach (PEA) and the Monte Carlo Simulation Approach (MSA).The FOSA provides values of the FOS and their variance. With the PEA the discrete values can be estimated at the mean values of the variables and mean and standard deviation of the FOS can be calculated. In the MSA, each variable has a probability of distribution and the discrete values are randomly selected (Chowdhury, Flentje, and Bhattacharya, 2010).

Numerical Methods

Rocks slopes are not homogeneous, for example they show differences in geological formation. This cause a non linear behaviour in the potential failure plane. For this reason such complex features can not be evaluated by the conventional techniques. The numerical methods include continuum, discontinuum and hybrid methods (Stead, Eberhardt, and Coggan, 2006; Eberhardt, 2002).

- Continuum modeling: This method can be applied to slopes where characteristics do not largely vary. For example it can consider heavily disintegrated rock mass overburden another geological formation. The modeling is based on finite element, finite difference and boundary element methods. For the case of continuum modeling the inputs are: constitutive model, in situ stress, shear strength parameters, etc. (Stead, Eberhardt, and Coggan, 2006).

- Discontiuum modeling: In a situation where the rock mass has discontinuities and the failure mechanism is controlled by pre-existing discontinuities, it is recommended to use this modeling. The movement of the intact rock blocks within discontinuities can be assessed for static and dynamic conditions (Stead, Eberhardt, and Coggan, 2006).

- Hybrid modeling: This modeling combines the continuum and the discontinuum modeling. The methods mentioned above are not capable to model fracturing through intact rocks if the pre-existing structures (ie. non-continuous rock joints) inside the rock mass are at the origin of the new fracturing. To tackle this problem different approaches based on fracture mechanics have been developed. With the hybrid modeling it is possible to model the evolution of non-directional physical rupture surface, with the formation, propagation and coalescence of cracks (Alzo'ubi, 2016).

1.2.3 Effectiveness and Limitations of Stability Analysis Techniques

Each technique has advantages and disadvantages, therefore they should be used appropriately.

Kinematics analysis is often used as a preliminary analysis, as it is rather easy and time efficient to perform. Furthermore, field data for this analysis can be easily collected (Raghuvanshi, 2017). But the results of this analysis are not very exact as strength parameters (discontinuities and rock mass) and acting forces on the slope are not taken into account (Alzo'ubi, 2016). Therefore this method does not allow to analyze complex geological scenarios. (Tang, Yong, and Ez Eldin, 2017) In addition, it does not provide a quantitative result of the slope stability analysis (Raghuvanshi, 2017).

Empirical methods are also not difficult to perform and can be used in a large area, and in the case of the planar failure can be applied directly on the field, but in case of complicated parameters (different lithologies, variable slope geometry) this method can not be applied.(Alzo'ubi, 2016). On the contrary, they cannot be applied in complex geologic cases, for this reason this system should not be applied for a design purpose (Alzo'ubi, 2016).

Limit Equilibrium Methods are relatively simple methods that can be easily applied and are very common methods in the engineering field even if they involve internal deformation. (Huang, 2014;Eberhardt, 2002). Several different approaches have been developed and they provide an exact solution (Alzo'ubi, 2016) (Chowdhury, Flentje, and Bhattacharya, 2010).On the other hand they can tend to over simplify the reality.

The probabilistic methods have the advantage that they provide an assessment of the uncertain parameters with the use of different simulations like Monte Carlo (Raghuvanshi, 2017; Digvijay P. et al., 2017). They also allow to take into account many variable factors (i.e. cohesion, friction, tensile strength, etc) (Alzo'ubi, 2016) and consider events which are difficult to predict such as for example extreme rainfalls or earthquakes (Kliche, 2003). But a disadvantage is that a large amount of detailed data must be collected in order to use probabilistic methods (Raghuvanshi, 2017).

Continuous or discontinuum methods can be applied where stratified discontinuties exist and is one of the principal benefits that each of the discontinuities can be explicitly modeled (Alzo'ubi, 2016). Neverthless, the continuum techniques define the rock mass as continuum which is a simplification in some cases of the discontiuum rock mass (Hack, 1998). The discontinuum methods require a defined failure surface and the current surface is not able to grow free inside the rock mass (Alzo'ubi, 2016). For accurate modeling the discontinuity needs to be indicated at block level, which can be hard to collect (Raghuvanshi, 2017).

1.2.4 Limit Equilibrium Methods

In this thesis I use a Limit Equilibrium Method for my analysis and I will therefore provide a more detailed literature review on this method here. During the last century many researchers and engineers have been working with Limit Equilibrium Methods and a large theoretical literature has been developed. For reasons of space, I will only describe the most important features of these methods. There exists various books and articles such as Fredlund (1984), Duncan (1996), Digvijay P. et al. (2017) or Huang (2014) which can be consulted for a more in-depth literature review. Limit Equilibrium Methods have been used for almost 100 years. They are commonly

used in geotechnical engineering and in soil and rock analysis. One of the first approaches was done by Petterson in 1916, when he was working in Gothenburg. He presented the stability analysis for the Stigberg Quay (Gothenburg) discretizing a sliding mass into vertical slices. Then in 1936 Fellenius introduced the Ordinary or Swedish method of slices, where he divided the soil mass into slices and found their equilibrium equating the forces and moments to zero (Steward et al., 2011). In 1969 Bailey presented the normal method (Bailey and Christian, 1969) and the simplified Bishop method in which he defined the factor of safety as the ratio of the available shear strength of the soil to that required to maintain equilibrium (Bishop, 1954).

Static Slope Stability Analyses

This analysis is based on the static equilibrium of an unstable rock mass. An unstable rock block needs to be defined (height, lenght, slope angle) and in this block the resisting and driving forces are evaluated. Then the FOS is calculated by the ratio of resisting forces to driving forces. The simplest expression for a 2D model was presented by Hoek and Bray (1981). They included the following factors in their model: sliding forces, the weight of the rock mass block, the inclination of the slope, cohesion and angle of internal friction (or angle of shearing resistance).The last one, angle of internal friction is equivalent to the Mohr-Coulumb failure criterion. They also developed additional formulas that take into account the influence of water and a tension crack at the top of the block (always perpendicular to the slope angle). Moreover, in the third version of their book, they further expanded their model to include the influence of under-cutting the toe of a slope, reinforcement of the slope and the analysis when the failure happens in a rough plane.

Several scientists have modified or added parameters to the FS presented above. Aydan and Kawamoto (1992) proposed a LEM for flexural toppling failure. Adhikary et al. (1997) proposed a mechanism of flexural toppling as well with LEM. Mauldon, Arwood, and Pionke (1998) included statistical parameters to the planar and wedge failure. Bobet (1999) studied toppling failure based on LEM , he considered water seepage into his analysis. Kemeny (2003) included the time-dependent cohesion rock degradation using subcritical crack growth in a planar sliding example with a probabilistic model. Kim et al. (2004) studied different failure modes from a perspective of Geographical Information Systems (GIS) considering kinematics and LEM's analysis. Jimenez-Rodriguez, Sitar, and Chacón (2006) analyzed quantitatively the reliability of stability analysis. He presented two blocks resting in a inclined plane separated by a tension crack and with random water level. This list only includes works that have been done in English and not every proposal is documented here.

Pseudo-Static Slope Stability Analyses

If other external factors (i.e. earthquakes or external loads) are present in the analysis, these factors are introduced as coefficients and the new analysis is called pseudo-static analysis (Hossain, 2011). Several studies have introduced these coefficients to LEM. For example Ling and Cheng (1997) included the influence of the seismic forces in a 2-D LEM. Additionally, they also included in their model a tension crack obtaining acceleration and permanent displacement of the rock mass. Yang (2007) using kinematic theorem with limit analysis studied the seismic coefficient. Hoek (2007) presented an update of the FOS in which the seismic coefficient, water pressure distribution, tension fracture and anchors are considered. Shukla et al., 2009

analyzed the FOS with different factors (water forces, horizontal seismic forces, etc).

1.3 Research Gaps

Slope stability is a topic that has been thoroughly studied by different authors and scientists as the literature review has shown. Therefore, many different methods to assess slope stability have been developed. However, most of them analyze the slope stability from an static perspective. This means that the variables remain constant during the analysis. For the case of crack growth, one solution is to use the concept of material fatigue that has been proposed by Paris, Gomes, and Anderson (1961).The concept of material fatigue originates from fracture mechanics science and has been the object of many studies in the last century (Anderson et al., 2005). It allows to include the progressive crack growth in the analysis.

Different authors such as Kirane and Bažant (2016), Pugno et al. ("A generalized Paris' law for fatigue crack growth"), Tada, Paris, and Irwin (*The Stress Analysis of Cracks Handbook, Third Edition*), Le, Manning, and Labuz (2014), Ko and Kemeny (2011), etc have used and tested the concept of material fatigue propagation (or progressive failure) to analyze crack propagation in the recent past. However, no author in the performed literature review has used or applied the concept of material fatigue in the context of the planar failure. Sellmeier (2015) is the only author that mentions a possible value of the concept for the analysis of planar failure, but she does not perform an analysis with it.

Therefore, in general terms (see Chapter 3 for the specific research goals) the goal of this thesis is to incorporate progressive tensile crack growth formulas to the Limit Equilibrium Method and perform a back analysis with the information obtained from the field data. The objective is to evaluate the evolution of the tensile crack growth in planar failure and gain knowledge to better understand this evolution.

Chapter 2

Background

2.1 Theory

2.1.1 Slope Stability

Depending on the material in the area, which can be rock or soil, different methods and analyses can be performed to assess slope stability. Often rocks contain discontinuities and they have several parameters that influence the analysis (geometric parameters and geotechnical or geological features). For this reason it is important to take into account the different geological structures as these are associated with different types of slope failure (Wyllie and Mah, 2005). Therefore different types of analysis exist (Vallejo and Ferrer, 2012). In the case of rock slopes, they are conditioned by the fracture types and their orientation in the rock mass. The most frequent failure types are : planar failure, wedge, toppling, buckling and non planar (*see figure* 2.1). However, reality is much more complex and the diagrams (*see Fig. 2.1*) are not able to show the different geological situations which can generate in the same slope more than one specific form of failure (such as ravelling, block torsion, etc) (Goodman and Kieffer, 2000). Despite these limitations, the classification of Varnes (1978) is important as different analysis methods are used for the various failure types (Wyllie and Mah, 2005).

Planar failure is one of the less complicated failure modes and there exists a lot of literature about it. This constitute a good basis for introducing new concepts and try to test them. For this reason this thesis only focuses on planar failure.

Failure Types

Plane failure (*see Fig. 2.1 (a)*) takes place along a pre-existing surface or discontinuity, this can be a fault, bedding plane, or tectonic joint. The discontinuities must be dipping out of the slope face, and the slope angle must be less than the rock friction angle in order for sliding to occur.(*see Fig. 2.1 (a)*)

Wedge failure is presented in (*see Fig. 2.1 (b)*) This kind of failure consists of two discontinuity planes whose line of intersection dips towards the slope face. As in the plane failure the slope angle must be greater than the failure plane angle (dip of the line of the intersection of the two planes) and to the friction angle as well. Toppling failure (*see Fig. 2.1 (c)*) occurs in slopes where the strata dips steeply away from the slope. Buckling occurs when the bedding planes are parallel to the slope and the dip is greater than the friction angle. Finally the non-planar failure (*see Fig.2.1 (d)*) can occur when the rock mass is heavily jointed or broken, because of this the whole body behaves as individual sets and the rock mass behaves like a soil. (Vallejo and Ferrer, 2012).

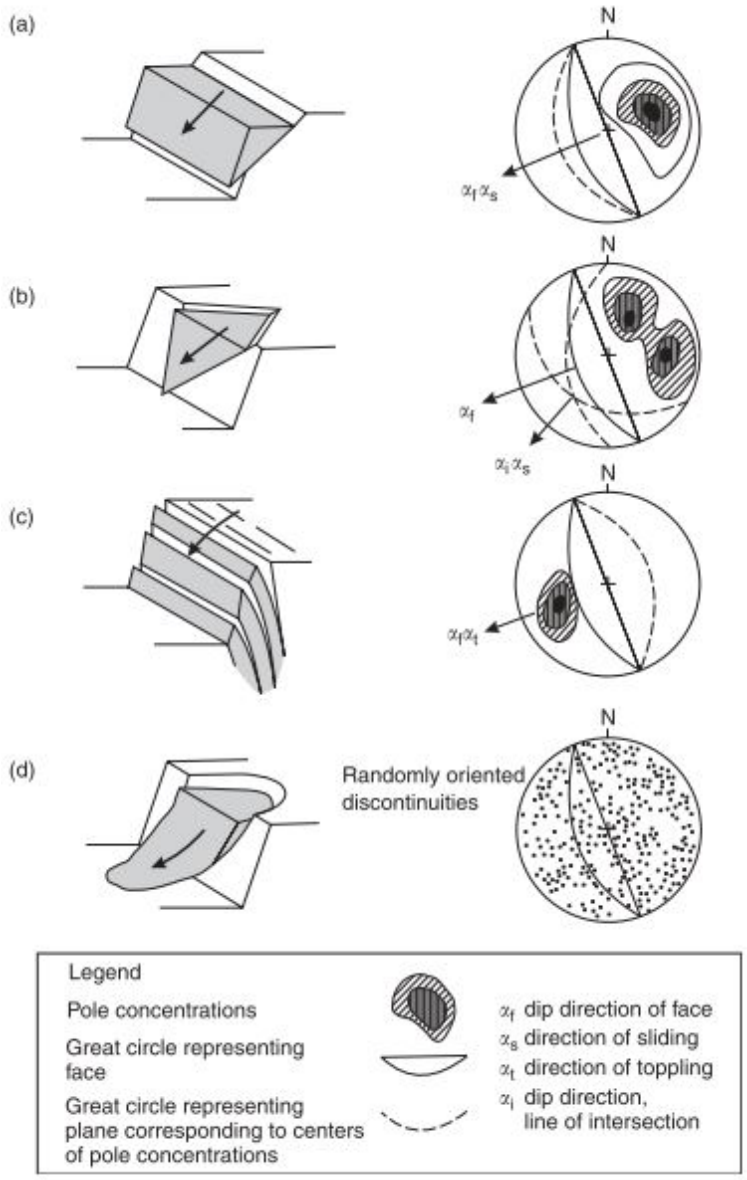

FIGURE 2.1: Types of failure in rock slopes. On the left the graphical representation, and on the right the Stereographic representation, indicating the characteristics of each of them. (Wyllie, 2014)

2.1.2 Slope Analysis

Different slope analysis's can be performed, which includes limit equilibrium (deterministic) and numerical analysis. Limit equilibrium analysis can be used to calculate the factor of safety, numerical analysis examines the stresses and strains from the slope. (Wyllie and Mah, 2005) The most common analysis is the limit equilibrium analysis to evaluate sensitivity of possible failure conditions. More advanced techniques are required for analyzing complex slope geometry, multiple or complex structural geometry, variable rock strength parameters and complex hydrological conditions (Kliche, 2003).

Limit of Equilibrium

At a determined state a block is in a limiting equilibrium condition. This moment happens just before the block falls. At this point, different forces such as driving forces (stress, moments) and resisting forces (cohesion and friction at the base) (*see Fig. 2.2*) are equal. In this moment, the ratio between driving and resisting forces is close to one. This ratio is called factor of safety (see equation 4.9) and is obtained by dividing the resisting forces against the driving forces. If the ratio is greater than one the block is stable. Otherwise it will probably fall (Kliche, 2003). According to Eberhardt (2002) this analysis method is widely used, thus numerous software's are available in the market and one can vary the used factors (cohesion, slope angle, rock type, etc.).

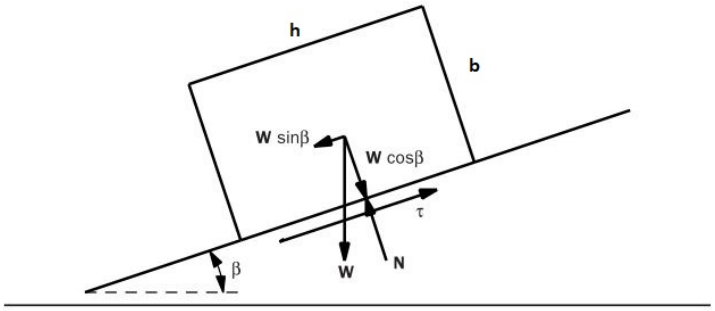

FIGURE 2.2: Mechanical approach for a limit equilibrium analysis in the case of planar failure, the corresponding equations are equation 4.2 to equation 4.8 (Kliche, 2003).

General Conditions for Plane Failure

According to Wyllie and Mah (2005) the following conditions must be satisfied: the plane on which sliding occurs must strike parallel or nearly parallel (+/- 20°) to the slope face. The sliding plane must dip less than the dip of the slope face. The dip must be greater than the angle of friction. The upper end of the block intersect the upper slope or terminates in a tension crack. And finally release surfaces provide negligible resistance to sliding, and they should be present to define the lateral boundaries.

Tension Crack-Water

Wyllie and Mah (2005), Kliche (2003) and several other authors consider the existence of a tension crack (dry or filled with water) and ground water in the analysis. However, they consider the tension crack as a static parameter, in other words no crack growth occurs.Wyllie and Mah (2005) mention that it is an indicator when a tension crack became visible that shear failure has initiated within the rock mass. He suggests that the formation of them is just the start of a complex progressive failure process of which little is known.

2.1.3 Fracture Mechanics

Failure Causes

Vallejo and Ferrer (2012) indicated that the slope stability depends on geometric conditions, such as whats required in LEM: height and slope angle, geomechanical factors such as strength, permeability, deformability and geological factors such as anisotropy or weakness area. A difference can be established between active triggering factors such as heavy rainstorms, earthquakes, application of static or dynamic loads, etc, and passive factors which includes degree of fracturing, weathering, lithology and frequency of discontinuities.

Crack Growth

Materials tend to have defects and microcracks, this generates fractures which are related to crack growth. If the crack is stable (not growing) it is denominated as stationary. If a specific critical load or deformation is reached, then crack initiation takes places and it starts to grow and is denominated as non-stationary. Very slow crack propagation under constant loading (1 mm/s or less) is called subcritical. If the crack propagates under a cyclic loading (10^{-6} mm per cycle) then it is called fatigue crack growth (Gross and Seelig, 2011). This concept was develop by P. Paris in 1961 (Paris, Gomes, and Anderson, 1961):

$$da/Dn = C(\triangle K_I)^m \tag{2.1}$$

where a = a(N) is the crack length following the N^{th} load cycle, C and m are material and climate dependent constants and $\triangle K_I$ is the amplitude of the cyclically varying mode I stress intensity factor K_I (see 2.1.3 K concept) (Eppes and Keanini, 2017).

Crack Opening Modes

From a macroscopic point of view (continuum mechanical) a crack is observed as a separation in a material which has crack surfaces. There exist three types of crack openings: Mode I, mode II and mode III (*see Fig.2.3*).
Mode I shows a symmetric crack opening with respect to x-z plane. Mode II presents displacement in the x-direction and mode III in the z-direction. These classifications can only be applied locally (near the crack tip). In continuum mechanics the extend of the influence area is important, therefore the considered process zone must be very small in comparison to the whole dimension of the body (Gross and Seelig, 2011).

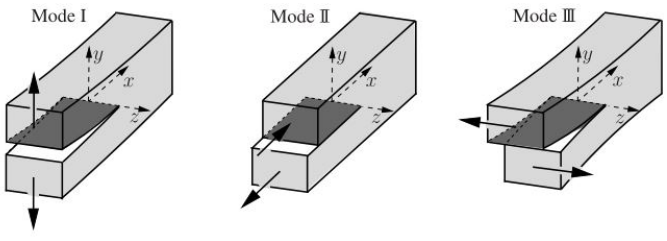

FIGURE 2.3: Classification of crack opening modes with respect of the deformation (Gross and Seelig, 2011).

K Concept

The stress intensity factor (K_I) is a linear elastic material constant, the crack-tip conditions are characterized by this constant. When the material locally fails, the constant turns into a critical stress intensity factor (K_{IC}). This critical stress intensity factor is an alternate measure of fracture toughness (Anderson et al. (2005)). In this section, I analyze case mode I crack opening, because it is directly related with the opening mode from planar failures.

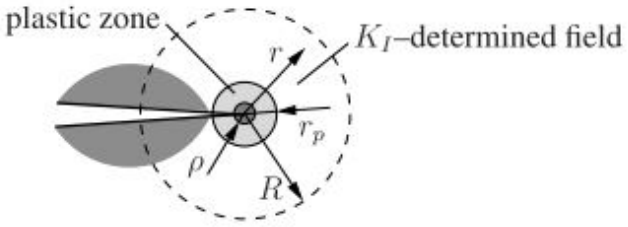

FIGURE 2.4: The figure shows the area of influence of KI. (Gross and Seelig, 2011)

The stress influence area is different for each material which is represented in the next graphic by a circle with radius R (*see Fig. 2.4*). According to Gross and Seelig (2011) the influence outside this area can not be neglected, but the largest impacted area is inner R. For the rock case, plastic or inelastic deformations appear at the crack tip (denoted by ρ). The plastic zone is r_ρ. Additionally, it is proposed that the K_I region is much larger than the areas P and r_p . These assumptions make the processes a black box, therefore it is assumed that the processes are controlled by the near K_I field. It is indicated that the stress intensity factor, and the stress are state variable or loading parameters of the area near to the crack tip. Using the stress factor, it is possible to introduce the fracture criterion. It states that the propagation of a fracture starts when the stress intensity reaches the rock critical value K_{Ic}.

K_{Ic} is a parameter which is determined by laboratory experiments (such as Brazilian test) which has the [stress][length]$^{1/2}$ units N m$^{-3/2}$ or MPa m $^{1/2}$(Gross and Seelig, 2011).

Stress Intensity Factor

Different modes of the K factors exists, it depends on the mode of loading (Mode I, Mode II or Mode III, *see Fig. 2.3*) as well depending of the test specimen configuration (Anderson et al., 2005; Gross and Seelig, 2011). In the case of planar failure (*see Fig. 2.1*) there exists a similar sample configuration that can be used. It receives the name of single edge notch test specimen (*see Fig. 2.5*) and the equations have been proposed by different authors.

Crack Opening at the Edge

Tada, Paris, and Irwin (*The Stress Analysis of Cracks Handbook, Third Edition*) have developed an equation (Equation 4.24) that based on the crack length, provides the crack opening at the edge.

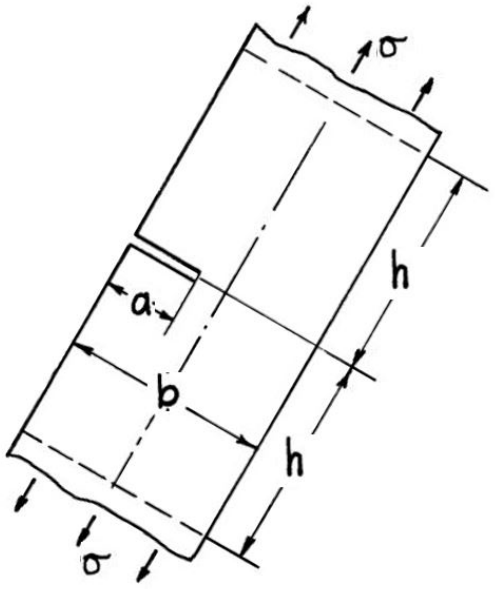

FIGURE 2.5: Stress intensity factor that can be applied to the planar fractures. (*The Stress Analysis of Cracks Handbook, Third Edition*)

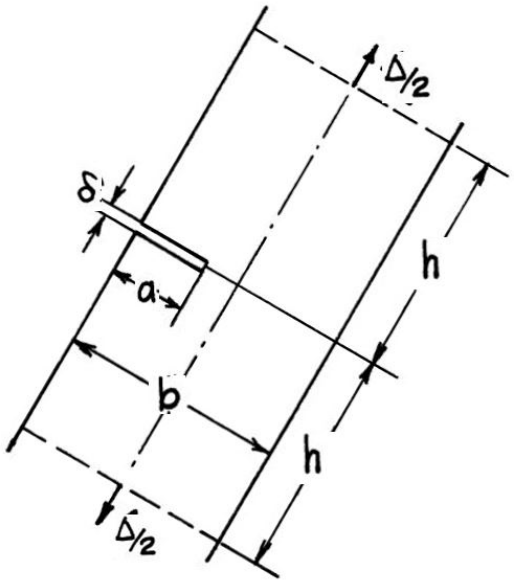

FIGURE 2.6: Longitude of the crack opening at the edge. Gross and tada have proposed equations. (*The Stress Analysis of Cracks Handbook, Third Edition*)

Crack Growth-Weathering

It has been experimentally found that the presence of water and higher temperatures are directly related to an increase in the crack rate. However liquid water is not a determining factor for subcritical cracking, while temperature is. The global annual averages range of air temperature is between 5 °C - 25 °C and at the land surface 10 °C - 20 °C (Eppes and Keanini, 2017). For this reason it is very important to have

the local temperature data.

Regarding to the lower stress intensity limit K_{th}, below which subcritical cracking does not occur exists no consensus. Using experimental data only the upper stress intensity limit K_{th} can be obtained. Therefore this parameter lacks data in a geological time context (Eppes and Keanini, 2017).

To model this climate dependency, it is first necessary to model the stress. As seen before I use Paris's Law. Then the temperature is introduced by diurnal thermal cycling. The magnitude of stress varies according to these temperatures as well from the difference in thermal expansion coefficient of the rock primary minerals and the rock's Poisson ratio (Eppes and Keanini, 2017).

Cracking Growing Dimension

The equations (eq. 4.14 and 4.15) are limited to grain scale, this means that the initial length is a_0 and is in the order of the characteristic grain size d_g. The critical crack length a_c that Eppes and Keanini (2017) use in their model is as well in the order of characteristic grain size. The stresses, in terms of intergranular stress are considered between Feldspar and Quartz. These two minerals mostly control the thermal stress and the fracture response of granite. The equation does not consider rock albedo, biologic cover, light penetration, nor fast temperature changes (Eppes and Keanini, 2017).

Accommodation of Moisture

The moisture is related to the Paris law, which includes m and C factors. m and C stands for Paris law exponent and coefficient for cyclic fatigue cracking under different environmental conditions. However there is almost no existing data for these factors for rocks (Eppes and Keanini, 2017). Data from non-cyclic subcritical cracking of rocks has been correlated using Charle's law (Charles, 1958) of subcritical crack growth (Equation 4.15).

Crack Evolution per Stress Cycle

For a single surface-initiated, representative crack that grows under cyclic heating caused by diurnal N cycles of heating.Eppes and Keanini, 2017 have developed an equation that relates the stress caused by the different minerals of the granite (4.14).

2.2 Study Site

To perform a back analysis of the proposed model of progressive tensile crack propagation, it is necessary to select a location where enough scientific information is available. Geological parameters such as rock type, tectonic settings (for example tectonic faults and joint sets), geotechnical data as well as rock parameters are needed to carry out an exhaustive back analysis. One area where these requirements are fulfilled is the Grimsel area.

During the last 12 years, in this area, several rockfalls have occurred which have been detected and analyzed (Ernst (2017). Although there are no large cities and the zone is only poorly populated, the Grimsel area has been subject to a considerable amount of research and monitoring of its geological properties. This is due to the location of important transport infrastructure, artificial dams, power lines and a geological research facility (Grimsel Rock laboratory) in the area. Furthermore, it is

also a popular destination for tourist activities. In conclusion, the Grimsel area is an important place which requires investigation and protection.

2.2.1 Geology

Grimselpass is located in the central Aar Massive (Raumer, 1993). Which consists primarily of late Variscan intrusive rocks (*see Fig. 2.8*). Large plutons are present as "Southern stripe of the central Aar Granite" (sCAGr), "Mittagfluh Granite" (MiGr) "Central Aar Granite" (CAGr) and "Grimsel Granodiorite" (GrGr). The largest plutons present in the area are the Central Aar Granite and Grimsel Granodiorite. Surrounding these plutons are older polymetamorphic gneisses and schists (Labhart, 1977; Abrecht, 1994) which name is Altkristallin (Ger.).

The Central Aar Granite is a light, coarse to middle grained granite (Sutter, 2008). Masive to foliated (foliacion direcion 157°/64° (Sutter, 2008)) or 149°/77° (Ziegler, 2013). The Mittagfluh Granite which is present in the North of the studied area is similar to the Central Aar Granite. The main difference is the amount of dark mica content, which therefore is less foliated.(Labhart, 1977). In terms of percentage it is around 35% of Quartz (For details *see Fig.2.7*).

[vol %]	Qtz	K-fsp	Plg	Bt	Wm	Chl	Epi	Author	Method
MiGr	35	35	27	3				Schaltegger	Estimated
CAGr	35	27-31	30	4-8				Schaltegger	Estimated
	32	34.1	20.9	5.5	1.6	1	2.3	Keusen	Point counted

FIGURE 2.7: Detailed composition of Mittagluh Granite and the Central Aar Granite. (Schneeberger, 2017)

Faults

Sutter (2008) classified five different tectonic fault sets in the area between Lake Gelmer and Lake Räterischboden (*see Fig. 2.9*). Set S1 are brittle discontinuities and show a mean orientation of 138°/75° (dip direction/dip angle). Near Grimsel pass, South of the study area, Set S2 is located with an orientation of 167°/73°. Throughout the area (with the exception of Southwest) he found S3 with an orientation of 190°/67° . Fault set S4 has an mean orientation of 244°/71° and only appears in the south. Set S5 shows a mean orientation 330°/74°.

Joint Sets

Sutter, 2008 has intensively studied and described the area, there he indicates the existence of six different joint sets (*see fig. 2.10*). J_1, J_2 and J_{PUJ} (post uplift joint) ('exfoliation joints')are the principals in the region while J_3, J_4 and J_{UJ} (uplift joints) are minors.

Then K_1 139°/71° is the most frequent joint in the area. In the south there is a change of direction of 15° clockwise. k_2 198°/70° is also present in the area, and similar to K_1 it shows a change of direction of 13° to the south. Regarding K_3 the main orientation is 244°/76°, this is more abundant in the south. K_4 orientation is 330°/64° however it is not abundant in the area. J_{UJ} varies in dip direction and the range of dip is between $0° - 34°$. However, they are not found in the whole studied

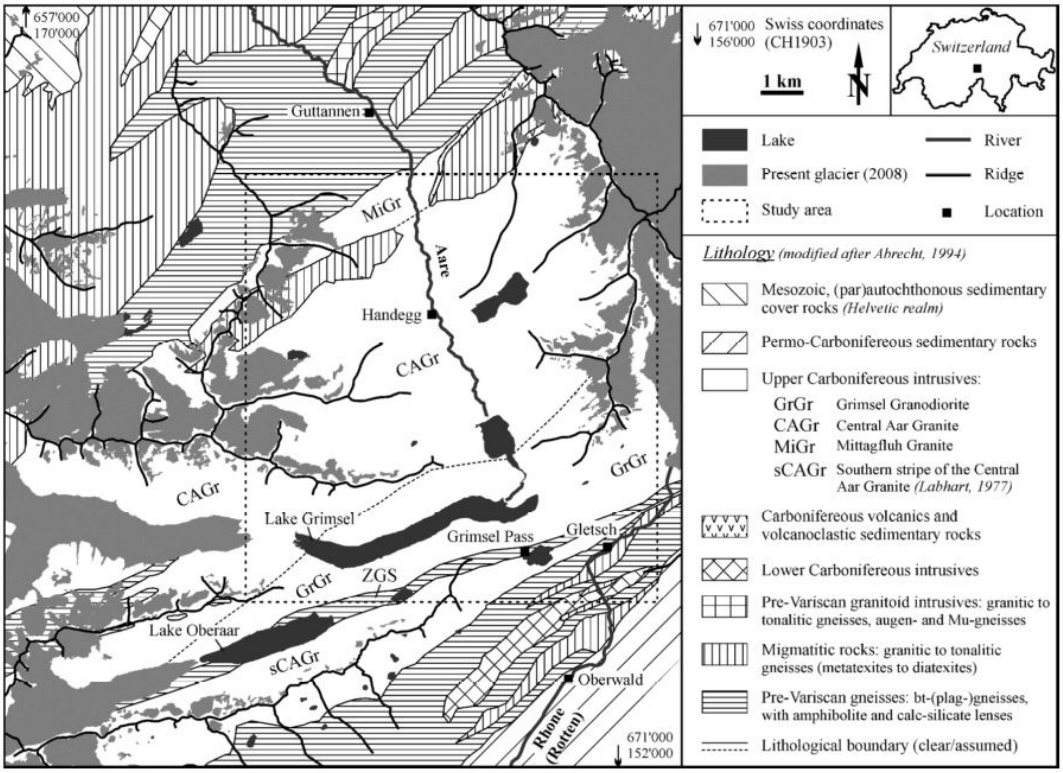

FIGURE 2.8: In the study region dominates the Grimsel Granodiorite (GrGr), in less amount is present Mittagfluh Granite, which is very similar in composition from the GrGr. (Ziegler, 2013)

area and are difficult to distinguish from the other joint sets (Ernst, 2017). In this area one can also distinguish another kind of joints. These are exfoliation joints, which are dependent on the topography. For this reason the exfoliation joints depend on their location and can be divided in four generations (Ziegler, 2013).

Slopes

Ernst (2017) has categorized the area with five different slope angles (*see Fig. 2.11*). It is represented in a map, with a color scale, between $0° - 30°$ (yellow), $30° - 40°$(light green), $40° - 50°$ (green), $50° - 60°$ (blue) and $60° - 90°$(dark blue). It is indicated that the most common slope angle in the studied area is $0° - 30°$ and the mean angle is about $33°$. Lakes are not considered in this classification and they are represented in blue.

Exfoliation

Different investigations have been performed in the area (Ernst, 2017; Ziegler, 2013; Bolay, 2013). Ziegler (2013) states that the exfoliation joints can have a topographic perturbation origin. He has demonstrated that if the near-surface in-situ stress exceeds the overburden stress then an exofliation joint develops. He performed a classification of them in the area, and divided them into four generations. Each of them have a different geologic origin time as well different directions:

- Generation 1. It originated in the Lower Pleistocene, in the main and hanging valleys and on the top of the mountains. The general fracture surface is around

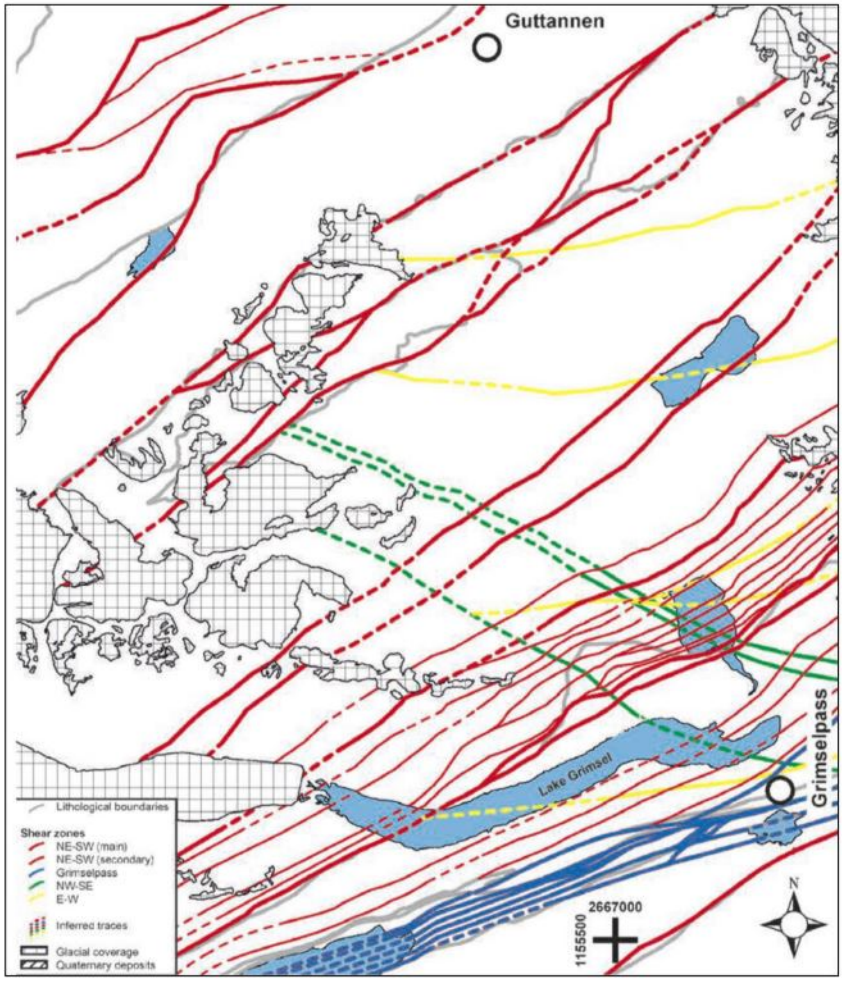

FIGURE 2.9: Map showing the four different fault zones. (Ernst, 2017)

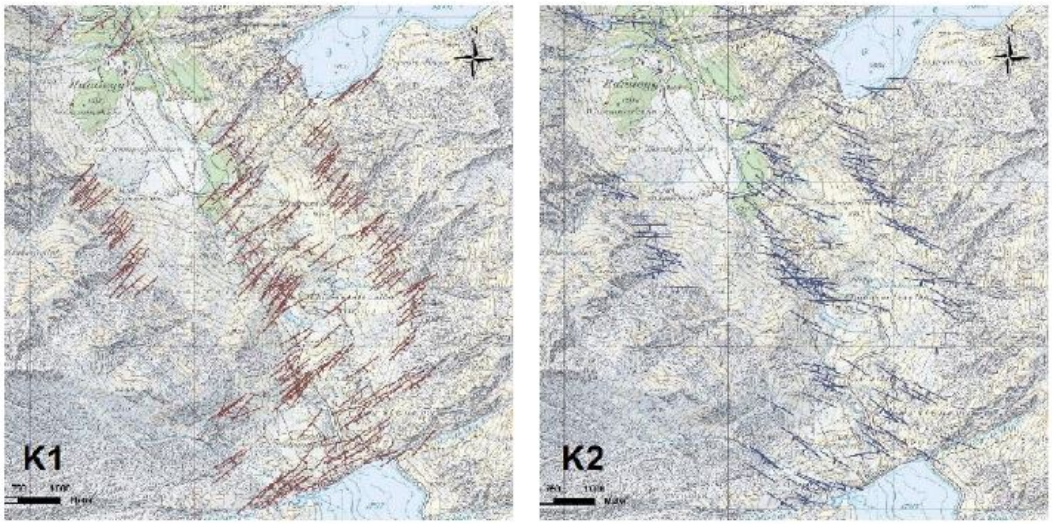

FIGURE 2.10: Most important joint sets K_1 (in red) and K_2 (blue). WIth directions: 139° /71° and 198° /70° respectively (Bolay, 2013)

30° or more. However this generation is not completely well defined due to accessibility reasons.

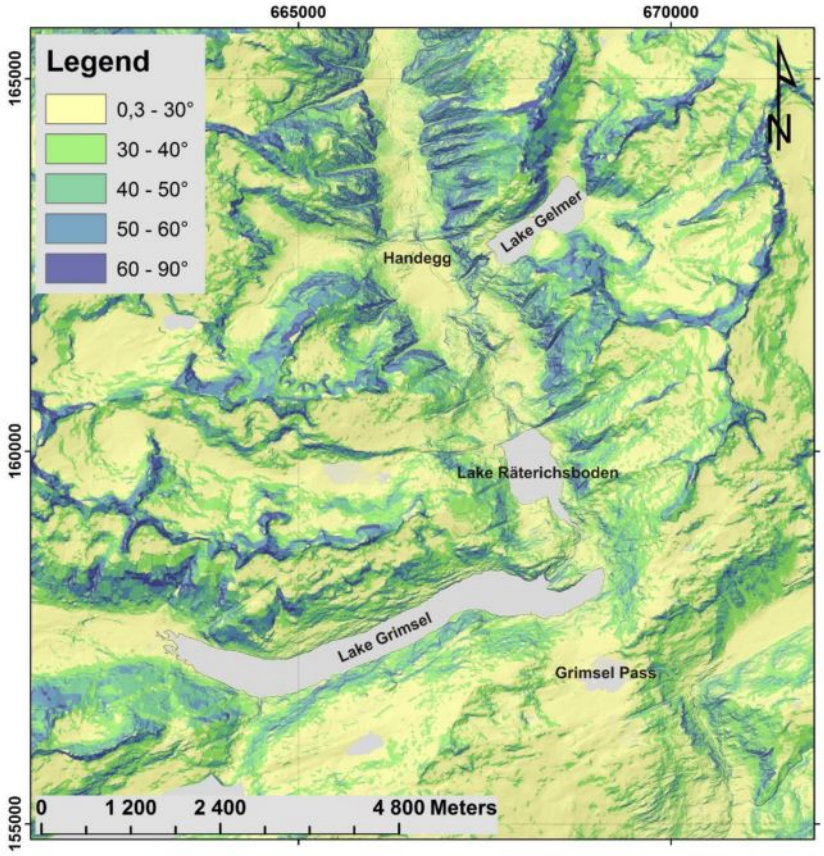

FIGURE 2.11: Map from the study area with the slopes angles. The colors indicate the different angles. Lakes are not included in the classification. (Ernst, 2017)

- Generation 2. It originated in the Middle Pleistocene. They are present in the principal valley and they curve from one valley side to the other. The spacing of this second generation is about 10 m and they reach a maximum depth of 260 m. The angle between the valley wall and the joint surface is 20°.
- Generation 3. It probably originated in the Upper Pleistocene. They were formed either during or before the Last Glaciar Maxium (LGM) because they have an direction to the bed-rock surfaces. In some cases they present a similar orientation as generation 2.
- Generation 4. It most likely originated in the Late Glacial or Holocene. They are closely spaced and are quite similar to today's topography. Another indicator that these generation is new is the existence of fresh surfaces.

The following map (*see Fig.2.12*) shows the location of the different exfoliation generations.

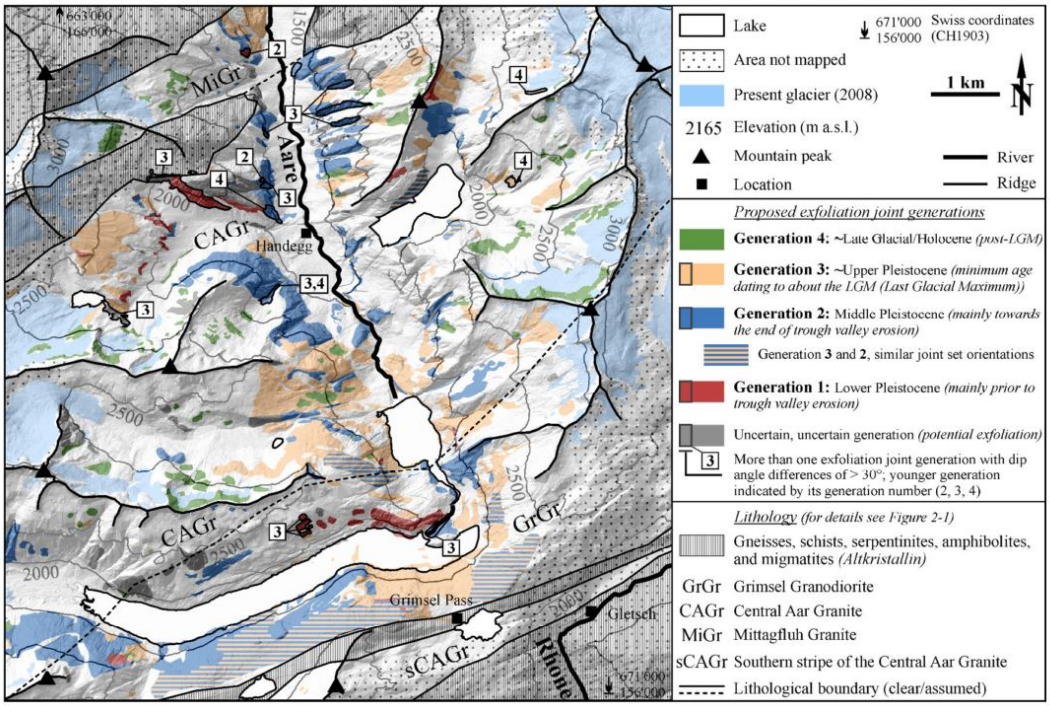

FIGURE 2.12: Proposed exfoliation generations by Ziegler in which they are differentiated by joint distributions, types and characteristics. (Ziegler, 2013)

2.2.2 Kinematic Analyses

Rock Falling Types

Ernst (2017) analyzed the joint characteristics in the area. For this analysis she has used orthophotos and different stability programs such as DIPS 7. This analysis was performed in 7 different areas near Grimsel pass (*see Fig. 2.13*).

In the performed classification by Ernst (2017) she mentions planar sliding as well wedge failure. Since the current Master topic is in planar sliding I have only focused on this. In the next graphic (*see Fig.2.14*) I show her analysis. In two areas it shows that the planar sliding probability is higher: Aaerlen (Hasli Valley (045°/75°)) and Trieebtenseewli (western slope (327°/80°)) present a probability of failure greater than 40% (*see Fig. 2.14*).

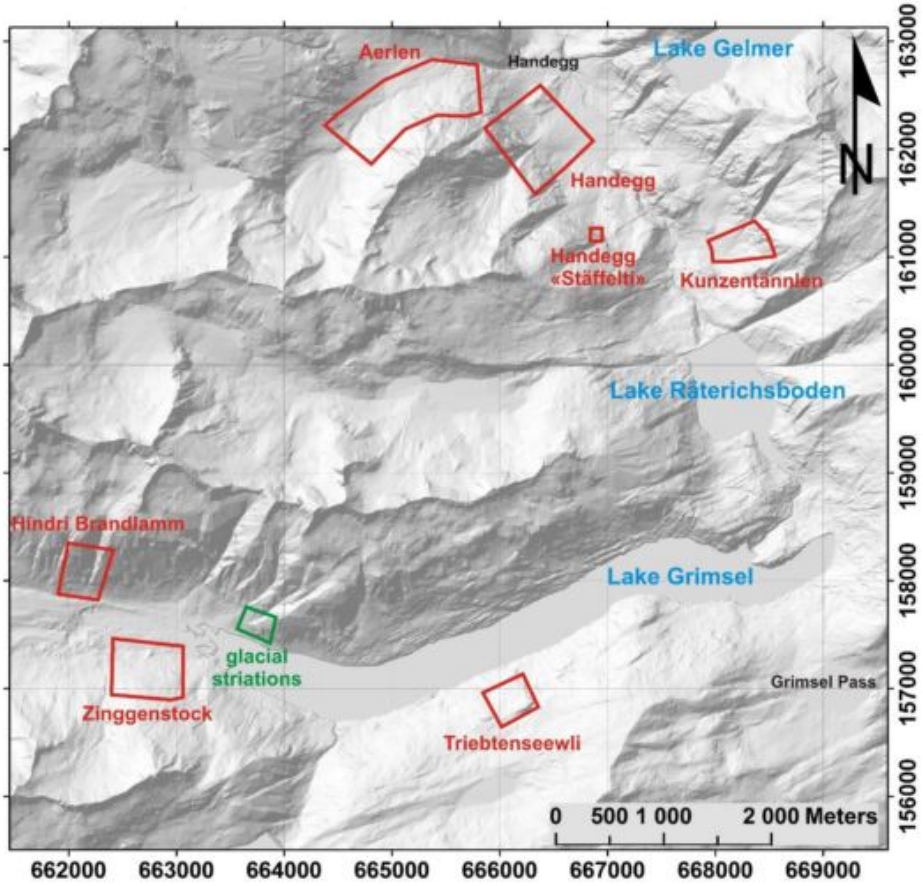

FIGURE 2.13: Ernst, 2017 Have perform an kinematic analysis from seven areas near to Grimsel Pass.

Swedge Analysis Ernst (2017) has used another program (Swedge) for the slope stability analysis. In this case different friction angles were tested 20°, 30° and 40° and four specific cases were studied dry (with-and without Exfoliation fractures (JExf), acting as basal planes) and wet (with-and without JExf) (*see figure 2.15*)

In this analysis the wet conditions have a clearly higher probability of failure, and in most of the cases it is as well higher when it is performed with JExf.

Dips Analysis

Ernst (2017) has considered for each analysis different parameters, however the Friction angle in all the sites is set to 20°. The results are expressed in terms of rock type failure probability. Ernst (2017) has analysed different types of rockfall, however I present here only where I consider that planar failure has the most importance character.

Aerlen In the case of the Aerlen site, it can be observed two slopes. For this reason, Ernst (2017) has divided it into two valleys. Aerlen (A) and Hasli (H) valley, the north-facing slope (slope A), has an 356°/62° orientation and the northeast-facing slope (slope H) has a mean orientation of 045°/75°.

These slope angles, allowed Ernst (2017) to find planar failures, because the Joint JExf A and JExf H are dipping towards the same slope direction and the angles of the joints are (in some cases) less than the slope angles. For the case of Aerlen the

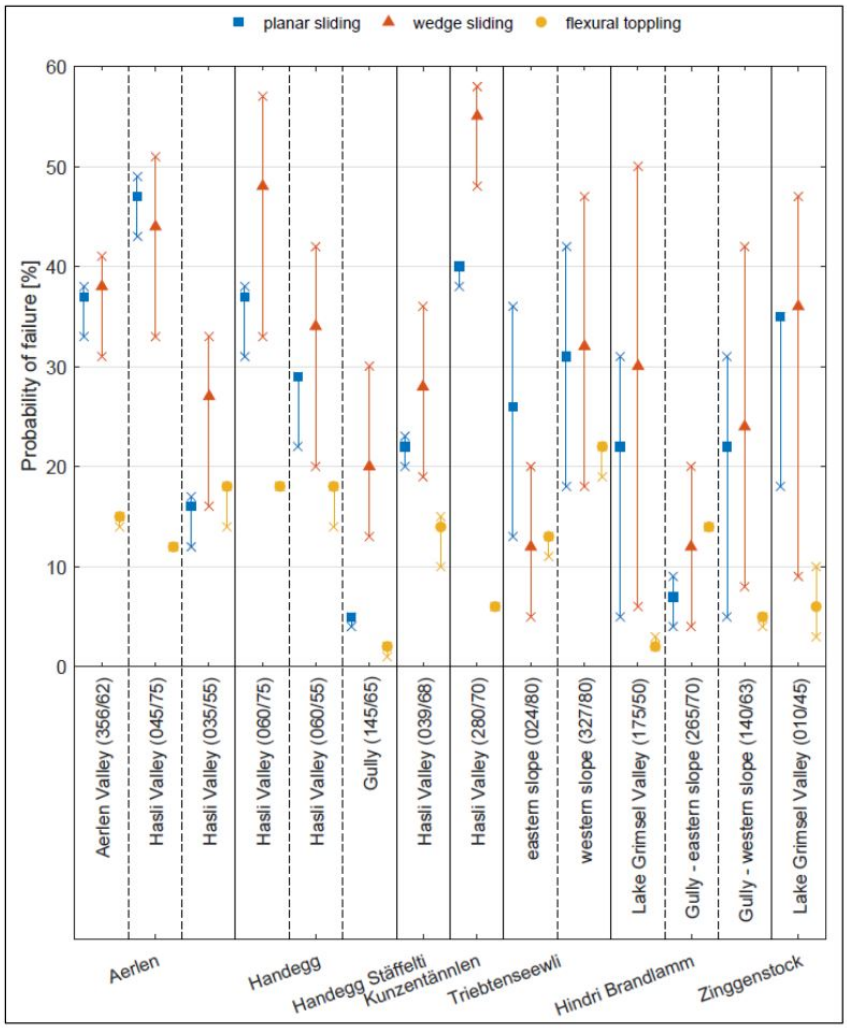

FIGURE 2.14: Planar sliding, wedge sliding and flexural toppling probability of failure analysis. Perform with Dips 7.0 From.(Ernst, 2017)

probability range is from 33% to 38%. However in the Hasli Valley it is much less probable that a planar failure happens. It just shows a 2% probability.

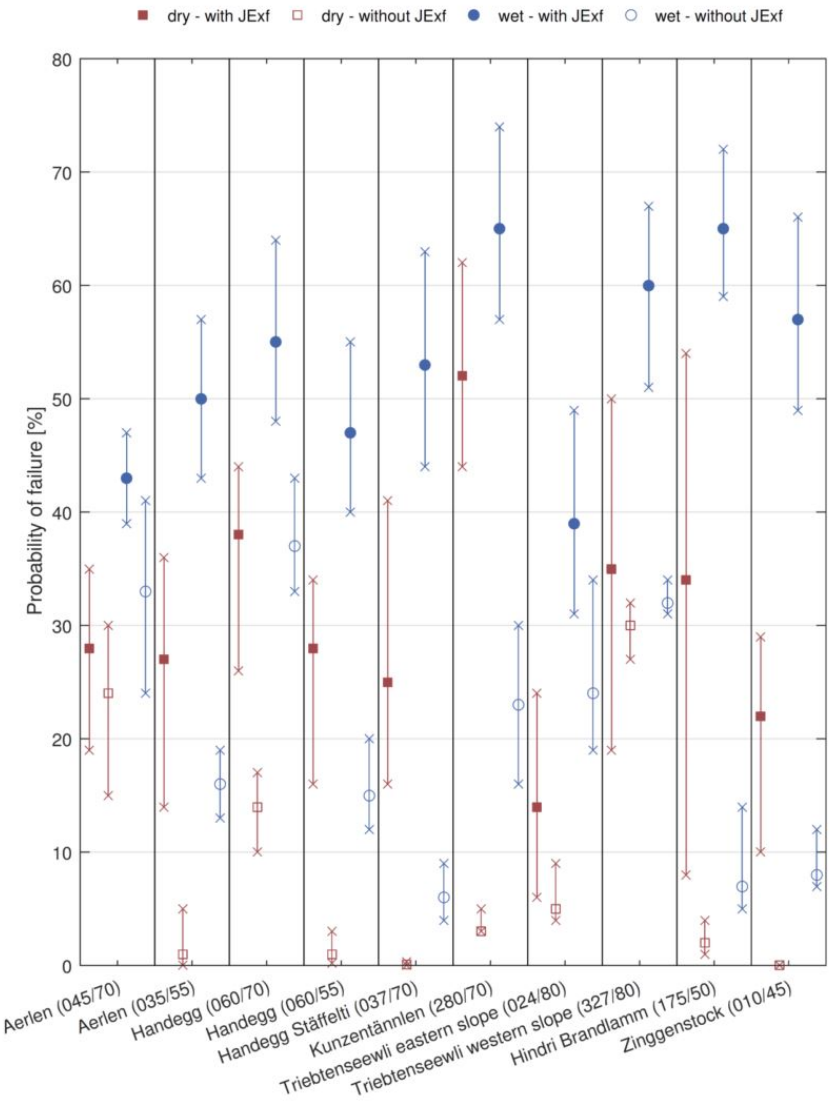

FIGURE 2.15: Four probability failure analysis cases were performed, dry and wet conditions and as well with/wihout JExf. Perform with Swedge Analysis. (Ernst, 2017)

Chapter 3

Research Goals

Limit Equilibrium Methods (LEM) provide a useful means of assessing the potential kinematic failure of rock blocks. These models assume temporally invariant conditions (cohesion, geometry, load, etc). A while a range of groundwater pressures may be investigated to assess the combination of conditions that allow failure, a time-dependant analysis (that includes the evolution of driving stress) is rarely undertaken.

The evolution of stress and strain is fundamental to the stability of blocks subjected to planar sliding. A time- dependant analysis allowed me to improve on existing probabilistic analysis by assessing the time required for sub-critical conditions (e.g tensile strength provided by shrinking rock bridges) to become critical.

For the reasons above, the primary goal of this thesis is the addition of progressive tensile crack growth to the LEM. Additionally it is necessary to perform a back analysis of the implemented numerical model and therefore it is necessary to gather real data.

In order to obtain field data, I have performed and used three Photogrammetric models (near Grimsel Pass - Switzerland). From them I have extracted the necessary block data (blocks with planar failure characteristics). Two different types of blocks were mapped: existing blocks and failed blocks. The obtained field data comprises length, height, perimeter and slope angle of the blocks. I then used this obtained field data to perform a back analysis from the implemented equations to evaluate their accuracy.

The following research questions were addressed within the scope of the thesis:

- How can the addition of progressive tensile crack growth equations to the concept of LEM (planar failure mode) classify the state (stable, growing crack, toppling) of the rock blocks?
- How can field /laboratory data be used to perform a back analysis of the equations?
- How can the obtained field data from Grimsel pass be correlated with the different outcomes from the proposed code?
- How can the model be used to understand the evolution of tensile cracks on planar rock fall in the areas around Grimsel Pass?

The outputs of this thesis will be a quantitative analysis and will provide answers to the proposed research questions. The implementation of the code will be performed in Matlab with a modular implementation. Additionally, the use of different methods, such as photogrammetric modeling and mapping with ArcGis, will be used to try reproduce the time dependency in the selected places near to Grimsel Pass.

Chapter 4

Methodology and Data

4.1 Introduction

A numerical model was developed in Matlab, which incorporates the Paris law (equation 4.14), the Charles law (equation 4.19) into the Limit Equilibrium Method for the case of the planar sliding (equation 4.10). The model also includes further equations which are presented in Chapter 4.2 (Governing Equations).

Field data was obtained in three different areas in the form of Unmanned aerial vehicle (UAV) photographs as well as manually executed terrestrial photographs near Grimsel Pass (see 4.3). Based on the data obtained three photogrammetric models were constructed. From these photogrammetric models it was possible to extract field data of blocks (length, height, perimeter and slope) with planar failure characteristics. This data was then used to perform a back analysis of the generated code (5 .3 Back Analysis).

In this chapter, the governing equations for the developed code are explained. The model implementation (including assumptions and used variables) is described. In addition, the code work-flow is analyzed. A the end, the photogrametric procedure is described. This includes the acquisition of the photos, the post-processing and the mapping of the blocks.

4.2 Model Implementation

4.2.1 Governing Equations

Detecting Toppling

Toppling failure is not covered in this thesis, however this kind of failure is very similar to planar failure. The main difference is if the ratio of the block length (h) to the height (b), is less than $\tan\beta$ (β as the dip of the failure plane) (*see Fig. 4.1*) then the block topples (Eq. 4.1)(Kliche, 2003). For this reason, I check if the block topples to exclude it from the analysis.

$$topple = \beta + \tan\left((b/2)/(h/2)\right) \tag{4.1}$$

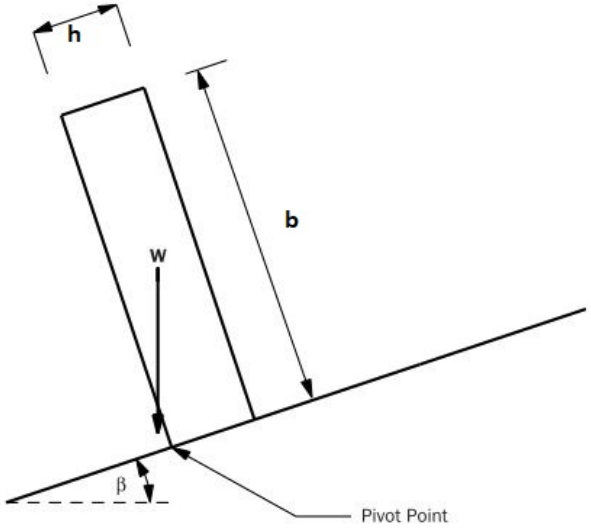

FIGURE 4.1: Toppling is governed by slenderness ratio (h/b). It controls the resultant force due to the weight of the block and with respect to the pivot point (which is located at the block base). If the pivot Point is out from the block base, then the block will topple. (Fig. adapted from Kliche, 2003)

Limit Equilibrium Method

There are several forces acting on the inclined block, (*see Fig.4.2*) along the base act: shear stress, cohesion and normal stress. To express this mathematically the following equations exist:

$$\tau = c + \sigma tan\phi \tag{4.2}$$

$$\sigma = \frac{N}{A} = \frac{W \times cos\beta}{A} \tag{4.3}$$

Replacing equation 4.3 in equation 4.2 it is obtain:

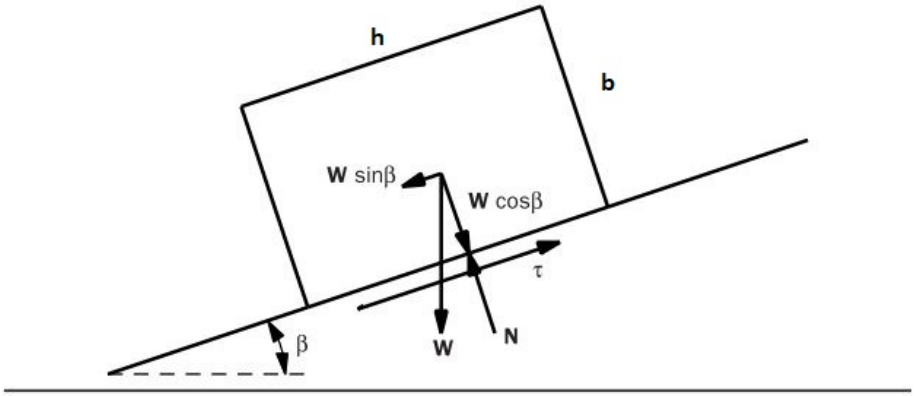

FIGURE 4.2: Mechanical approach for a limit equilibrium analysis in the case of planar failure, the corresponding equations are show from Equation 4.2 to 4.8 (Fig. adapted from Kliche, 2003).

$$\tau = c + (\frac{W \times cos\beta}{A}) \times tan\phi \tag{4.4}$$

$$W = b \times h \times \rho \times g_0 \tag{4.5}$$

$$shear force = \tau \times A \tag{4.6}$$

$$resisting force = c * A + W \cos\beta \times \tan\phi \tag{4.7}$$

$$driving force = W \sin\beta \tag{4.8}$$

Where:
τ = shear stress along the base (according to the Mohr-Coulomb failure theory)
c= cohesion along the base
σ = normal stress along the base
ϕ = angle of internal friction along the base
N = magnitude of the normal force on the base
A= area of the base
W= weight of the mass
b= height of the block
h= length of the block
ρ= density of the block
g_0= gravity
β = dip angle of the failure plane

$$Factor\ of\ Safety = \frac{resisting forces}{driving forces} \tag{4.9}$$

$$Factor\ of\ safety = \frac{cA + Wcos\beta \tan\phi}{W \sin\beta} \tag{4.10}$$

These equations are provided by Kliche (2003).

This last equation 4.10 is one of the principal equations of the code, as the progressive tensile crack growth is incorporated in this equation. Wijk (1978) introduced the concept of tensile strength. When an edge crack (a) is propagating (Chapter 4.2.3 Edge Crack Growth), there exists from the block base to the edge crack an area where the rock is intact. This area provides the tensile strength σ_{rt}. This tensile strength maintains the block stable (*see Fig.4.3*) until the crack reaches a determined length and the tensile strength is not strong enough to maintain the block stable.

To this basic analysis the progressive tensile edge crack and the resisting force from the top block is added (area under the tensile edge crack). The following equations (equation 4.11 and equation 4.12) introduce the concept:

$$tens_{height} = b - a \tag{4.11}$$

Where b is the height of the block and a is the length of the crack.

$$\sigma_{rt} = tens_{height} * \sigma_T \tag{4.12}$$

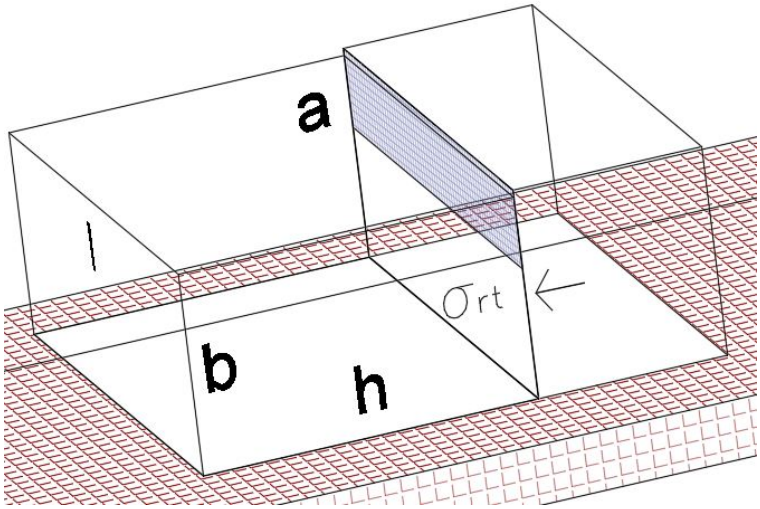

FIGURE 4.3: Block in a limit of equilibrium. The letters represent different properties of the block, l states for wide, h length and b for height of the block. In blue is represented the progressive crack growing, with a length of a and is represented as well the stress on the tension crack with σ_{rt}.

For this equation σ_T represents tensile strength which is a value obtained in laboratory experiments. σ_{rt} is a resisting force, therefore the equation 4.12 is added to equation 4.10 which results in the next equation:

$$Factor\ of\ safety = \frac{(cA + Wcos\beta \tan\phi) + (\sigma_{rt})}{W \sin\beta} \tag{4.13}$$

Edge Crack Growth

In order to find the crack growth, different authors have proposed different approaches (ie. Paris Law or Charles Law):

Paris Law For a single surface-initiated, representative crack that grows under cyclic heating caused by diurnal N cycles of heating. Eppes and Keanini, 2017 has the following equation:

$$a(N) = [a_0^{\beta} + \beta C_1 N]^{1/\beta} \tag{4.14}$$

Where a(N) is the crack length in function of the number of cycles, a_0 states for the initial crack length. $\beta = 1 - m/2$, and m has been demonstrated that has the same value of n (Equation 4.15). $C_1 = C\Delta\sigma_{max}^m \pi^{m/2}$ and C states for the Paris law coefficient (which is similar to $d_g K_c^{-m}$). N is the number of cycles and finally $\Delta\sigma_{max}$ (See 4.17) is explained in the next paragraph.

Accommodation of Moisture

$$da/Dn = C_c(K_I)^n \tag{4.15}$$

The left-hand side of the equation stands for crack growth rate,C_c stands for rock and environment constant, K_I stands for stress- and crack geometry dependent

stress intensity, and n for "subcritical crack growth index". Crack growth is dependent on chemical reactions, therefore n highly depends on the amount of moisture. Moreover Eppes and Keanini (2017) have demonstrated that m=n.

Stress Accommodation Eppes and Keanini (2017) reference the equation of Anderson et al. (2005) in which he correlates:

$$\Delta KI(z,t) = \Delta\sigma_{max} \tag{4.16}$$

Where $KI(z,t)$ is dependent, the temperature (t) and depth (z). Eppes and Keanini (2017) define the effective stress amplitude ($\Delta\sigma_{max}$) as the intergranular thermal stress caused by diurnal temperature cycle and the two primary mineral constituents. This generates:

$$\Delta\sigma_{max} = \Delta\alpha E\Delta T_0/(1-v) \tag{4.17}$$

$$\Delta T_0 = T_{(surface.max)} - T_{(infinitus)} \tag{4.18}$$

Where:
Δ T_0 $= T_{(surface.max)} - T_{(infinitus)}$, this expresses the maximum surface temperature variations produced by diurnal temperature cycling. $\Delta\alpha$ $=$ is the difference in coefficients of thermal expansion of the mineral constituents. E stands for Young's modulus and v for Poisson's ratio. Eppes and Keanini (2017) neglects the depthwise decay in the near surface temperature field because Eppes and Keanini (2017) work is on the order of characteristic grain size.

Charles Law The second crack growth approach is given by Ko and Kemeny (2011). In which Ko and Kemeny (2011) the crack growth is based on Charles (1958) the following equation:

$$\frac{\delta a}{\delta t} = A[\frac{K_I}{K_{IC}}]^n \tag{4.19}$$

where a is crack length, dt is per cycle (time) and A and n are material parameters. K_I is the Stress intensity factor (equation 4.20) and K_{IC} is the critical Stress intensity factor.

K_I Stress Intensity Factor

The stress intensity factor K_I, used in (equation 4.19) depends on the stress, the crack length as well numerical values for a relation between crack length and block height:

$$K_I = \sigma\sqrt{\pi a}F(a/b) \tag{4.20}$$

Where σ is obtained in (Eq.4.12) and stand for σ_{rt}. a represents the length of the crack, b the height of the block and h the length of the block. F(a/b) is a relation that can be obtained with different methods (Equation 4.21, 4.21 and 4.21):

- Gross, Srawley, and Jr (1964) and Brown and Srawley (1966) propose a least squares fitting based on laboratory experiments, which is 0.5% accurate for a/b =< 0.6%:

$$F = (\frac{a}{b}) = 1.122 - 0.231(\frac{a}{b}) + 10.550(\frac{a}{b})^2 - 21.710(\frac{a}{b})^3 + 30.382(\frac{a}{b})^4 \tag{4.21}$$

- The second was proposed by Tada in 1973 and is better than 1% for a/b < 0.2 and 0.5% for a/b > 0.2 :

$$F = (\frac{a}{b}) = 0.265(1 - \frac{a}{b})^4 + (0.857 + 0.265\frac{a}{b})/(1 - \frac{a}{b})^{\frac{3}{2}} \tag{4.22}$$

- The last equation is as well from Tada (1975) and is better than 0.5% for any a/b:

$$F = (\frac{a}{b}) = \sqrt{\frac{2b}{\pi a} tan \frac{\pi a}{2b}} * 0.752 + 2.02(\frac{a}{b}) + 0.37 * (1 - sin\frac{\pi a}{2b})^3 / cos\frac{\pi a}{2b} \tag{4.23}$$

The above equations can be found in (*The Stress Analysis of Cracks Handbook, Third Edition*). The variables are introduced in Figure 2.5.

Crack Opening at the Edge

The following equation (Equation 4.24) measures the crack opening (*see Fig. 2.6*) at the edge δ (*The Stress Analysis of Cracks Handbook, Third Edition*):

$$\delta = \frac{4\sigma a}{E'} V_1(\frac{a}{b}) \tag{4.24}$$

Where σ is σ_{rt} (Eq.4.12) ,a is edge crack length ,E' is the elastic constant for the plane strain E'=$E/(1 - v^2)$, in which E states for Young modulus and v for Rock Poisson ratio. b is the block height and V_1 is a relation, which can be found in the equation 4.25. The equation proposed by Tada, Paris, and Irwin (*The Stress Analysis of Cracks Handbook, Third Edition*), is expected to have an accuracy for any a/b of 1%:

$$V_1(\frac{a}{b}) = \frac{1.46 + 3.42(1 - cos(\pi a/2b))}{(cos \pi a/2b)^2} \tag{4.25}$$

4.2.2 Model Implementation

In the following subsections the code implementation for single block analysis is described (Chapter 4.2.1 Preventing toppling to 4.2.7 Progressive Crack Growth). In the next section, the variable values used in the code are presented (Chapter 4.3 Variable values) and at the end the code workflow diagram is presented (Chapter 4.4. Code Workflow).

Model Assumptions and Considerations

It is important to note that in this proposed model Eppes and Keanini, 2017 indicate some model limitations. This limitations were taken in consideration as well at the moment of applying their equations:

- The equation (equation 4.14) can only be applied to grain scale (Eppes and Keanini, 2017). For this reason the developed model is restricted to a maximal crack growth per stress cycle to grain size. However the cumulative crack growth goes from grain size to meters.
- Eppes and Keanini (2017) assume the crack model is not growing along rock imperfections such as joints or foliations because this causes a reduction in K. Therefore, in the model the cracks are supposed to grow in a intact rock.

- Eppes and Keanini (2017) model considers a intergranular thermal stress, generated from quartz and feldspar. The selected locations near Grimsel pass have rocks which main components are quartz and feldspar (Granite).
- Eppes and Keanini (2017) assume the cracks grow perpendicular to the rock surface. This is also occurring in our model due to K_I crack opening mode.
- The model from Eppes and Keanini (2017) just considers the daily thermal cycle variation, it does not consider changes in temperature (due to other cycles or abrupt temperature changes) or albedo, biologic cover or light penetration.
- The model from Eppes and Keanini (2017) neglects thermal expansion anisotropy along mineral axes.
- The crack growth always has a perpendicular direction from the block surface (or slope surface).

Variable Values Used in the Model

For the model implementation different fomulas were used, such as Charles law (see equation 4.19), Paris law (see equation 4.14) and all the equations mentioned in the (4.2 Model Implementation). They are indicated in 4.3 Matlab Workflow. These formulas use different variables. For this reason the following table (see Table 4.1) presents the following information: name of parameter, symbol, matlab used symbols, reference magnitude, calculation units and the reference from were the values were took.

Parameter	Matlab symbol	Reference magnitude	Units	Reference
Angle of internal friction	B.phi	30	degrees	Schneeberger 2017
Angle of failure plane	B.d	30-70	degrees	Ernst 2017
Cohesion	B.C	20*10^6	N/m^2	
Density	B.density	2670	kg/m^3	Schneeberger 2017
Gravity	B.gravity	9.81	m/s^2	
Tensile strenght	B.tens_strength	10*10^6	Pa	Ziegler 2012
Critical stress intensity	B.k1_critical	1.5*10^6	MN/m^1.5	Eppes 2017
Material propierties	C.A	1*10^-3	m/s	Ko and Kemney 2011
Stress corrosion index	C.n	48		Backstrom et all 2008
Initial crack length	P.a0	4.1*10^-4	m	Eppes 2017
Paris law exponent	P.m	0.6		Eppes 2017
Characteristic thermal expansion difference	P.delAlpha	3*10^-5	C^-1	Eppes 2017
Young modulus	P.E	50.6*(10^6)	Pa	Eppes 2017
Poisson's ratio	P.v	0.33		Schneeberger 2017
Fracture toughness	P.Kc	2.16*10^6	MN/m^1.5	Eppes 2017
Grain diameter	P.dg	0.7*10^-3	m	Eppes 2017

TABLE 4.1: Rock parameters used in all the calculations

4.2.3 Code Workflow

The implemented Matlab code follows a logical procedure. The entire code can be found in (Appendix C). The figure 4.4 is the summary of the whole procedure.

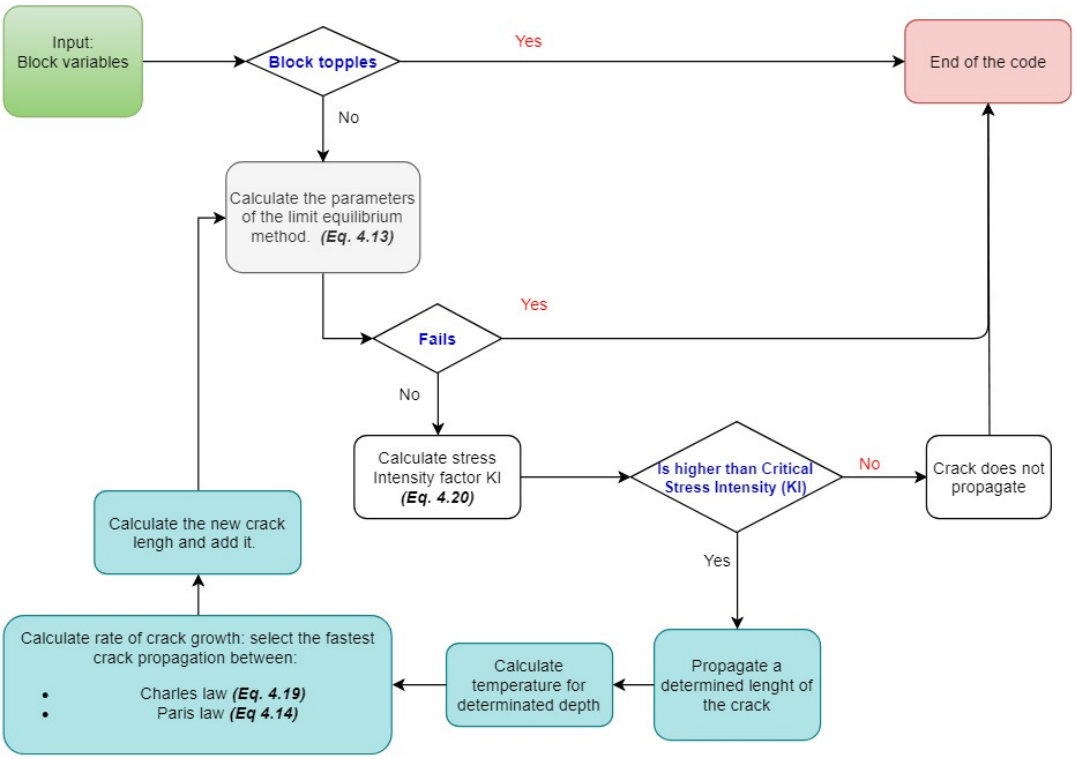

FIGURE 4.4: Matlab resume workfow for the code. The reference for the used equations are indicated in parenthesis.

There are different forms used in the code. The diamonds represent where the result must be evaluated and depending on the outcome follows different paths. Inside the rectangular blocks procedures or outcomes are indicated.

The code starts with the input of a block range of different values, block height and length (range from 0.25 to 12 m). For the slope angle the range goes from 40 to 60 in intervals of 10 degrees (these values can be be modified, as well as the intervals). The rock constant values can be modified as well (ie. cohesion, density, etc). The first step is the block topples evaluation (see 4.2.1 Preventing Toppling). If the center of mass is projected outside of block base, then the block topples and it is the end of the code (a message will indicate that the block topples), if the block does not topple, the code continues and calculates the parameters with the modified Limit Equilibrium Method (equation 4.11).

In this step, the driving forces and the resisting forces are evaluated. If the resisting forces are smaller than the driving, then the block falls and the code ends. In the opposite case, when the resisting forces are bigger than the driving, it will be calculated if the base of the block provides stability to the block. If the base provides stability then the crack will not propagate and the code will end with the result that the base provides stability. If it is higher then the propagation of the crack starts. The next step is to calculate the temperature for the particular depth of the crack and then evaluate between Charles law (equation 4.19) or Paris law (equation 4.14) to see which is faster. The one that is faster will dominate the crack length growth. With this new crack length the modified Limit Equilibrium Method (equation 4.13)

is once more calculated until the crack is large enough to make the whole block fall. In the following sections the process is explained in much more detail.

Detecting Toppling

The first procedure performed is to detect toppling (Equation 4.1). If the angle of the failure plane plus the angle between the base and the center of gravity is less than 90° then the block does not topple (*see Fig. 4.1*)(Goodman and Bray, 1976). If the block topples, the process is interrupted, a message "the block topple" appears and it is the end of the code. If the block does not topple, then it calculates the Limit Equilibrium Method.

Limit Equilibrium Method

The analysis of the single blocks was performed with the Limit Equilibrium Method. The equation 4.10, where the factor of safety is obtained is taken as base.

Block Stability

There exists three possible outcomes from this analysis, that the base provides stability (progressive tensile edge crack is not propagating), unstable edge crack (the crack will propagates, or growing crack) or the block topples. The following terminology is used (*see Fig. 4.3*)):

- σ_{rb}= resisting stress (provided by the base of the block)
- σ_d = driving stress (driving force)
- σ_{rt} = stress on the tension crack (remain surface between the base of the block and the tip of the edge crack).

This generates the next equation:

$$\sigma_{rt} = \sigma_d - \sigma_{rb} \tag{4.26}$$

Equation 4.26 states that, if the resisting stress (σ_{rb}) plus the stress on the tension crack (σ_{rt}) is greater than driving stress (σ_d) then the block is stable. Then the crack will not grow and a message will appear: the base provides stability. Otherwise if the driving stress (σ_d) minus the resisting stress (σ_{rb}) is greater than 0, then the edge crack will start a sustained crack growth. The crack will start growing until the edge crack stress (σ_{rt}) plus resisting stress (σ_{rb}) are lower than the driving stress (σ_d). During the crack growth the code records the time, number of iterations, and length of the crack.

Stress Intensity of the Tension Crack Tip

It is assumed that if the Critical Stress Intensity factor (K_{IC}) of the granite is 1 500 000 M N $m^{-1/2}$ (Eppes and Keanini, 2017) then the crack will generate stress until it reaches the (K_{IC}), where it then fails.

Eppes and Keanini (2017) indicate the existence of the Threshold Stress Intensity Factor (K_{th}) (the minimum stress that is required for cracks to start a sustained subcritical crack growth) for the edge crack. It is assumed that the Threshold Stress Intensity Factor (K_{th}) is around 20% of Critical Stress Intensity factor (K_I) (Eppes and Keanini, 2017). However discrepancies exist about the exact value of the threshold.

Segall (1984) indicates that it is 10%, while others like Le, Manning, and Labuz (2014) indicate that exists a range (however it does not indicate what the range is). Pugno et al. ("A generalized Paris' law for fatigue crack growth") show 5% for a 1045 steel sample. For this reason I do not consider any threshold and the progressive edge crack starts growing at the time the base can not hold the driving stress, however the iteration time will be high.

$$stable\ edge\ crack = K_I\ edge < K_I\ critical \tag{4.27}$$

The crack stress will propate until it reaches the critical stress intensity. This K_I is calculated with the equation 4.20, and different numerical values for F(a/b), in which a stands for crack length and b for block height. This relation can be obtained from the equations (equation 4.21, equation 4.22 and equation 4.23). They correspond to the following methods whit different percentage accuracy:

- Gross (1964) and Brow (1966)
- Tada (1975)
- Tada (1975)

Edge Crack Opening

As it can be complicated to measure the crack depth in the field, Tada, Paris, and Irwin (*The Stress Analysis of Cracks Handbook, Third Edition*) have developed an equation that relates the length to the crack opening (see equation 4.24 and equation 4.25).

Temperature Cycle

As indicated in Chapter 1.1.4 Fracture Mechanics- Crack Growth- weathering, one of the factors that generates stress in the rock is the change of temperature. To reproduce this change of temperature an annual temperature variation was implemented in the code. The model was provided by Kerry Leith and it reproduces the temperature during one year (2016) from Finland (South of Långören), where they installed a monitoring system which included a weather station that records temperature to a depth of 1m depth (Leith et al., 2017). This can be correlated with the existing temperature measurements in the area around Grimsel Pass. The depth of the propagating crack growing is correlated with the temperature decay in the rock. This is correlated to Paris law (equation 4.14) with the equation (equation 4.18) in which the maximum temperature variations produced by diurnal temperature cycling are introduced.

Progressive Crack Growth

Wtih consideration of the above points, the code starts the analysis with a combination of different block sizes as well as the defined Variables (See 4.3 Variable Values). It then goes through the diurnal temperature variation cycle with the corresponding iterations for the edge crack growth. Once the edge crack has reach a determined length, it causes the block to fall.

4.2.4 Equations Verification

In this section, I conduct a verification of the different equations implemented in the code. The authors often present a graph where they use their respective formula. I try to reproduce the same results that they show in their papers or research.

Stress Intensity of the Tension Crack Tip

Numerical values for the stress intensity factor used in (equation 4.20). In the Fig. 4.5 the three methods are compared:

- Gross (1964) and Brow (1966) (equation 4.21).
- Tada (1975) (equation 4.22).
- Tada (1975) (equation 4.23).

Based on the relationship between crack length (a) and height of the block (b), the best fitting of the different methods is used. From the plot, I can affirm that the stress intensity factor was correctly implemented.

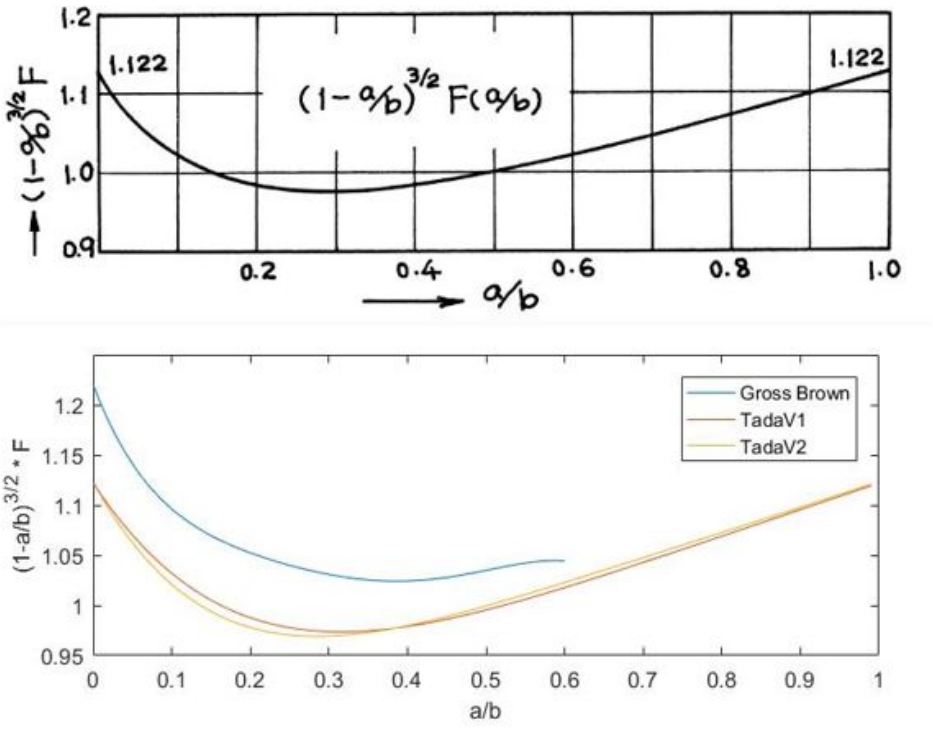

FIGURE 4.5: On the top, Proposed numerical values of F (a/b). At the top, graphic from Tada, Paris, and Irwin (*The Stress Analysis of Cracks Handbook, Third Edition*). On the bottom, corroboration of the values.

Edge Crack Opening

This equation is implemented (*see Fig.4.6*) in the code to record the edge crack opening (equation 4.24 and 4.25). From the plot I confirm that the Edge crack opening implementation was correct.

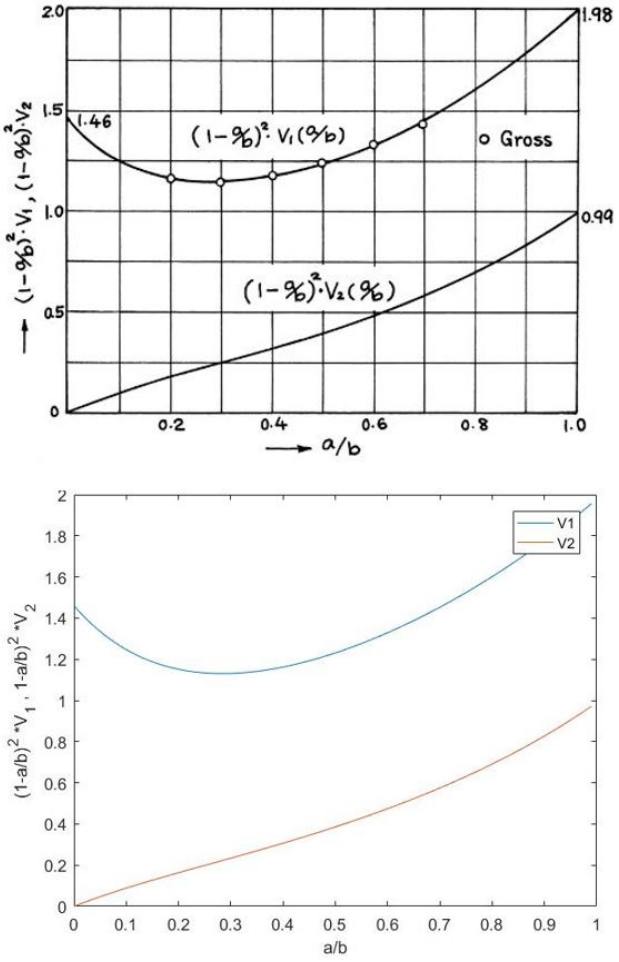

FIGURE 4.6: To corroborate if the edge crack opening code was implemented correctly a corroboration was performed.(*The Stress Analysis of Cracks Handbook, Third Edition*)

Progressive Crack Growth

For the progressive crack growth, two possibilities exist: (equation 4.19) which expresses the possible crack length per cycle from Ko and Kemeny (2011) and (equation 4.14) from Eppes and Keanini (2017). To test if the code was correctly implemented, a comparison with the published reports was made.

Charles Law For the case of the formula proposed by Ko and Kemeny (2011) I was able to reproduce the same results. (*see Fig. 4.7*)

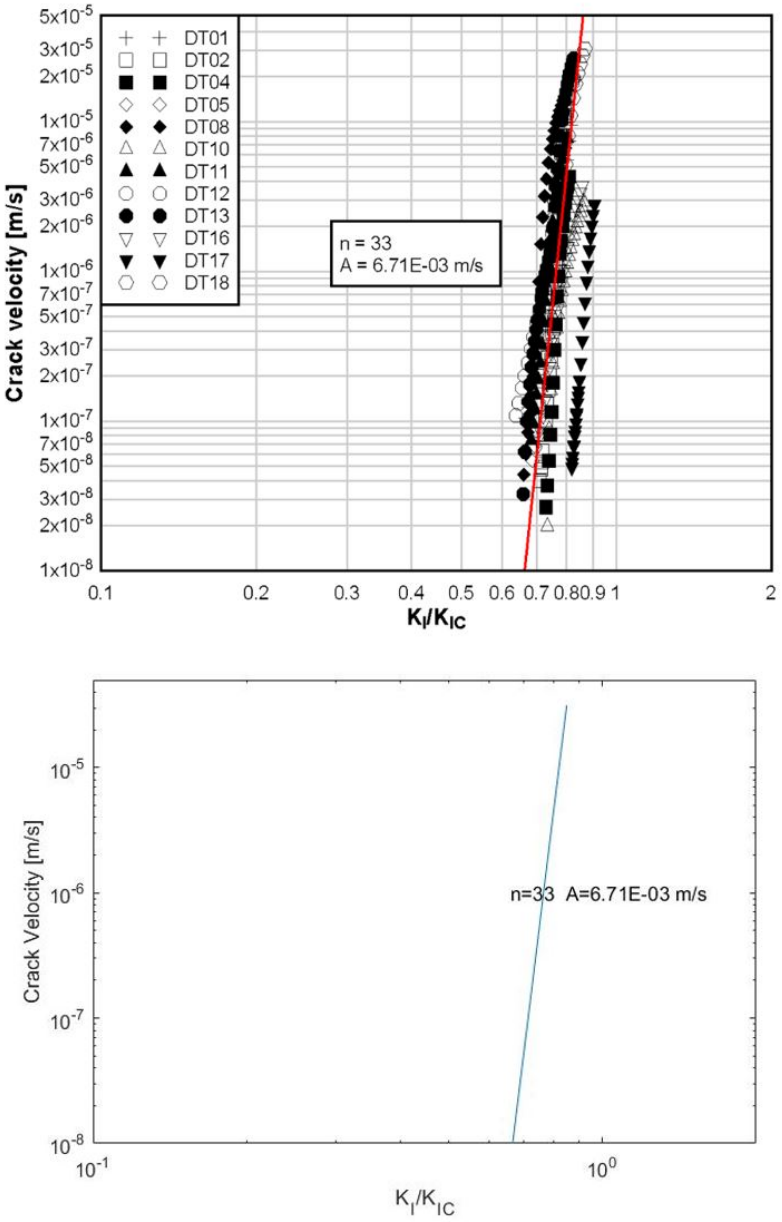

FIGURE 4.7: On the top, Charles law with experimental data from Ko and Kemeny (2011) at the bottom, results of the implemented code.

Paris Law In the case of the equation used in Eppes and Keanini (2017), (see equation 4.14 and description), a crack evolution per stress cycle is proposed. The equation can be applied for a single surface initiated crack under cyclic heating (which can be applied to Grimsel slopes). They have tested their equations with respect to a model from Delbo et al. (2014). Delbo et al. (2014) has tested a crack growth model in the laboratory for two different meteoritic rocks. In the experiment they were tested in the climatic chamber for 76 and 331 temperature cycles which sum a total of 407 cycles. The model goes up to 10^7 and 10^8(respectively) cycles where they stopped it as the crack length reached the rock diameter (5mm approximately in both cases). For the first sample, Sahara, the initial crack size is 0.41 mm and for Murchison 0.76 mm. After 400 cycles they present a crack growth length of 0.13 mm and 0.03 mm respectively (*see Fig. 4.8*).

At the moment of verifying the equation 4.14 , m is the Paris law exponent which is used in $\beta = 1 - m/2$, then β is used as exponent : $1/\beta$. I found that by using the given values the corroboration was not possible. If m is larger than 2 when β is used as root (with a negative base), then an imaginary result is generated.By dividing the value m by 100 and dividing the final crack length by 10^6 I was able to obtain almost the same results (*see Fig. 4.8*).
The exact number of thermal cycles used by Eppes and Keanini (2017) is not available, for this reason I used approximated values. It is visible in the graph of Eppes and Keanini (2017) that in the case of the Sahara sample a notable crack growth starts at 10^6 thermal cycles. In my results this crack growth starts at 10^5 thermal cycles. In the case of the Murchison sample the results of Eppes show that the crack growth starts at 10^8 thermal cycles. However, in my results it starts at 10^5 thermal cycles.

For this reason, the m value in the implemented code, was 0.6 (see table 4.1) and then the crack length results divided by 10^6. Eppes and Keanini (2017) (equation 4.14) use the parameter m (Paris law exponent) and assign a value (varying with humidity content) of m = 77.6 for 10% humidity and of m = 58 for 80% humidity.

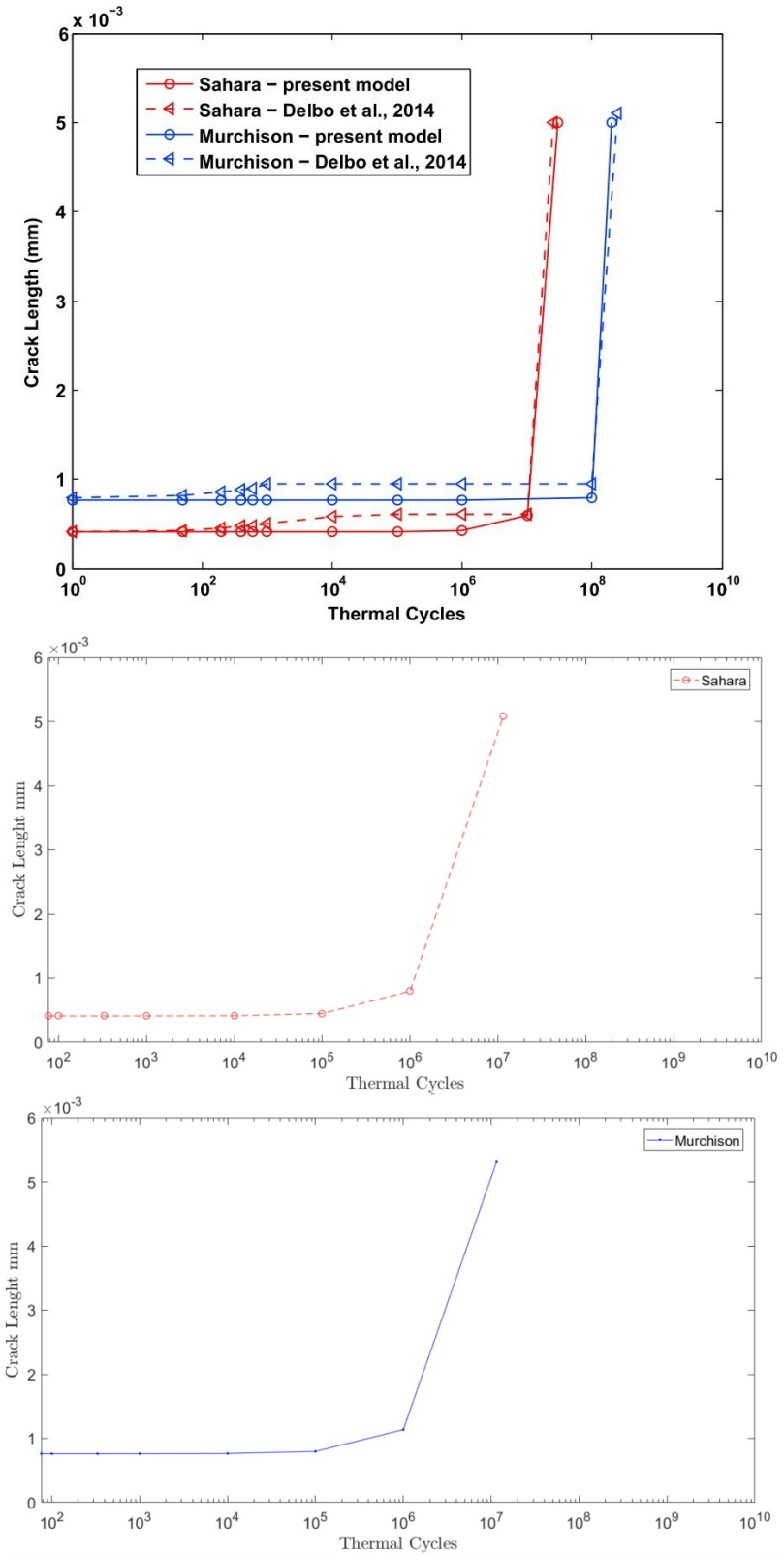

FIGURE 4.8: Thermal cycles to propagate a crack. At the top are the results of Eppes (Eppes and Keanini, 2017) equation for crack growth used to reproduce the laboratory test and model from Delbo et al., 2014. At the bottom are my results.

4.3 Photogrammetric Slope Model

In the present thesis, metric 3D images obtained from three areas near Grimsel pass (*See Fig. 4.9*) were used to map blocks that fulfill the characteristics of planar failure mode (Chapter 2 .1.1 Slope stability). The measured block properties were height, length, perimeter and slope angle.

The photogrammetric principle works similarly to visual perception. Two images of the same object with slightly different objective positions are obtained. They are then used to construct a 3D model. Subsequently, it is necessary to georeference the images to gain a real dimension of the model which allows the measure of the above mentioned block properties.

For two areas (East from Grimsel lake and near Handegg), an Unmanned Aerial vehicle (UAV) was used and for the area Tschingelmad a base photogrammetry was performed (*see Fig. 4.9*). In the case of UAV images, they were obtained by Ziegler Martin (2018) and referenced with ground control points (GCP) using Differential Global Positioning Systems (DGPS) measurements or GPS base station for inaccessible rock slopes. In the case of base photogrammetry, the photos were taken in September 2018 and the control points were provided by Ziegler Martin as well. In the case of the UAV the camera used was a Sony ILCE-6000, and the pictures were 6000 x 4000 pixel with 350 dots per inch (dpi) and a focal length of 19 mm. Throughout this procedure the ISO (sensitive image sensor) was 100. For the base photos, the camera used was Nikon D5300, the pictures were 6000 x 4000 pixel with 400 dpi and the focal length was 52 mm. The ISO was set to 200.

4.3.1 Images Requirement

The images always require the same distance from the objective (parallel) and angle to the slope. RAW pictures are recommended, then they can be converted to TIFF. The parameters ISO and the focal depth must be low and high (respectively) enough to capture all the desired objectives (for further information see Agisoft, 2018).

4.3.2 Software Processing

The program Agisoft PhotoScan 1.4, searches for the common points on the loaded photographs, matches them, locates the position of the camera and refines the calibration parameters. After this step, a sparse point cloud is obtained. Then, it is necessary to generate a dense point cloud. The third phase is to generate a surface. Different surface possibilities are available such as Mesh and/or DEM 3D. Lastly, the generated surface can be textured (Agisoft, 2018) (*see Fig. 4.10*).

From the obtained surface (*see Fig. 4.12*) it is possible to measure the following block parameters (*see Fig. 4.13*):

- Height
- Length
- Perimeter

Once the DEM was obtained, it was exported to ArcGIS ArcMap to obtain the corresponding slopes. (*see Fig. 4.11*)

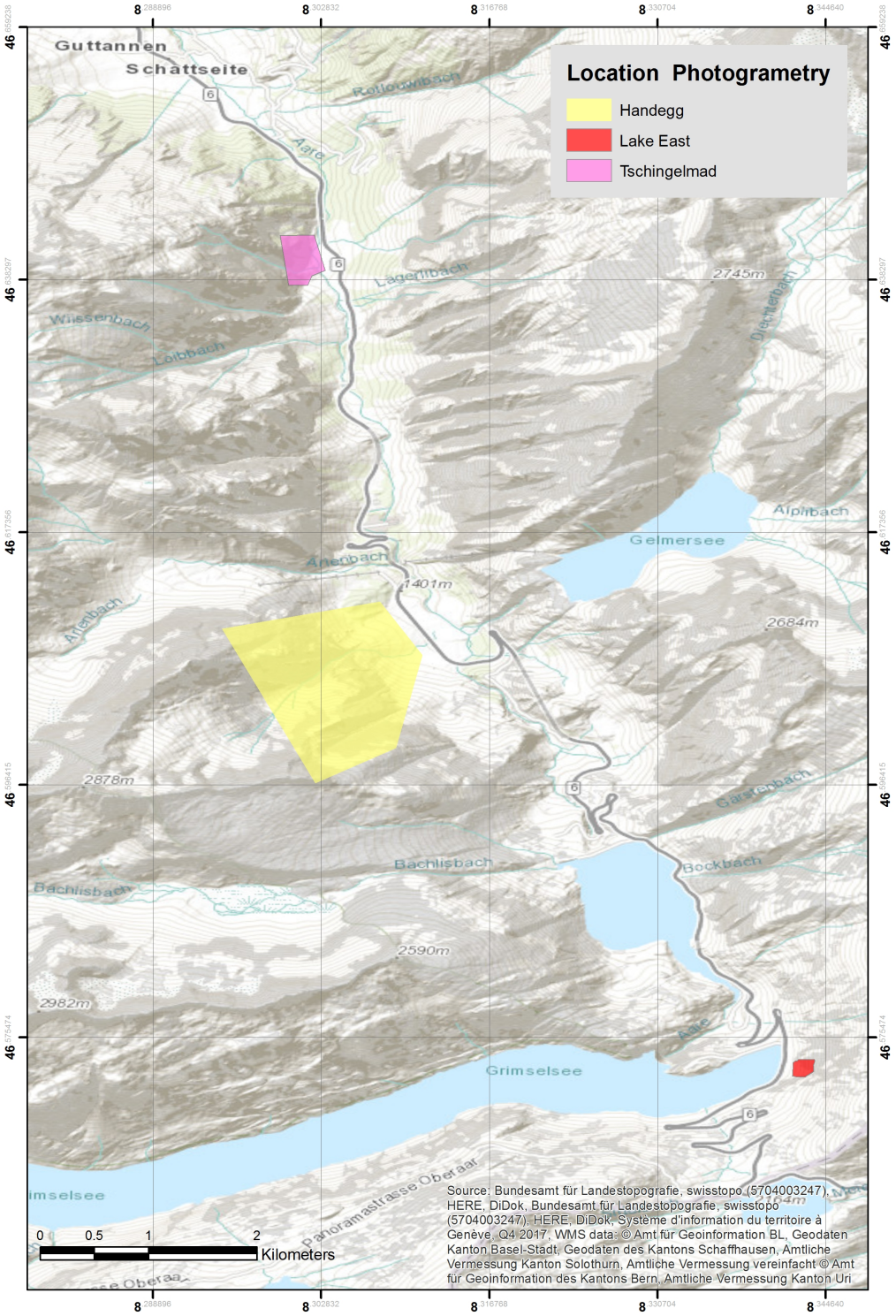

FIGURE 4.9: Location of the three different photogrammetric models. Tschingelmad (North) was captured with terrestrial photographs. Handegg (central of the map) and Lake East (South) in the map were taken with an UAV.

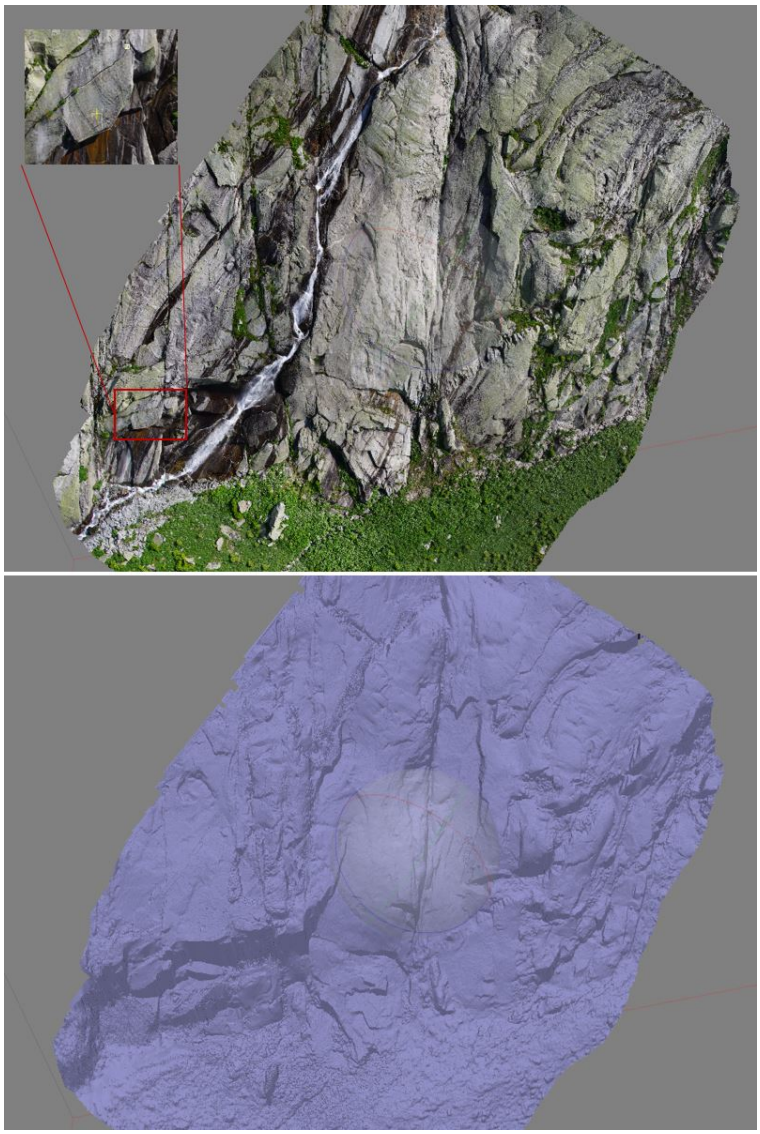

FIGURE 4.10: 3D model from the East of Grimsel lake. In both cases the product is obtained using Agisoft Photoscan. Above is the textured mode, and in zoom one single block as example. At the bottom is the generated DEM

4.3.3 Existing and Failed Blocks Mapping

The principal task was to measure in situ blocks. In the selected in situ blocks had either a visible top cracks or were limited with another superior block (*see Fig. 4.13*). When mapping failed blocks, it can be complicated to precisely define if the failed block had broken off in one single piece, in multiple pieces or if there had ever been a block or not. However, in some cases the difference of color of the fresh surfaces (*see Fig. 4.14*) helps to identify the boundaries, because fresh surfaces are brighter than older ones. Another characteristic of fresh surfaces is the lower amount of lichen. For both cases (existing blocks and failed blocks), measuring the height is complicated, After mapping all of the blocks, the data was exported to Matlab to verify the proposed model.

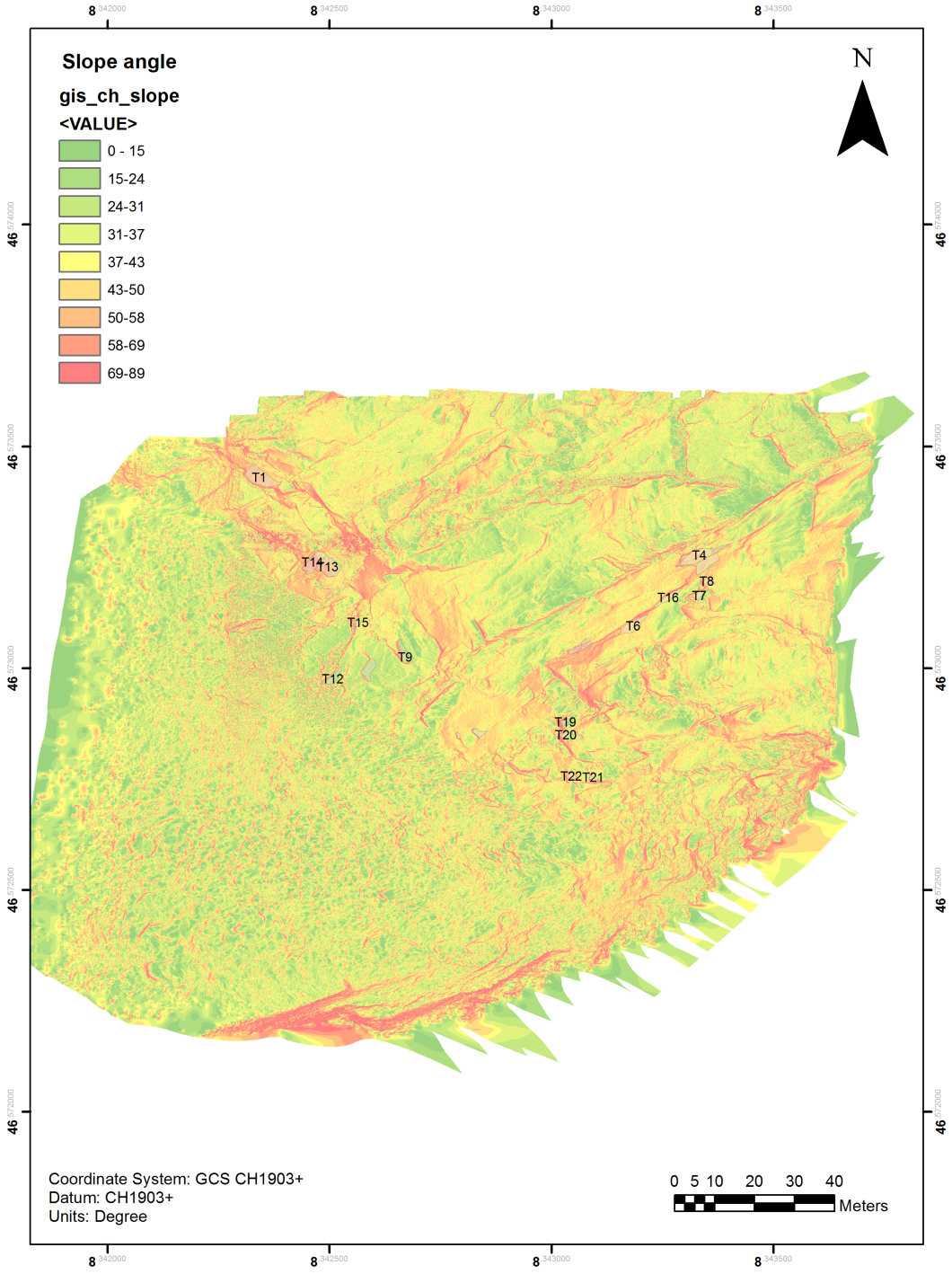

FIGURE 4.11: Slope angles generated in ArcMap for the Rock slope located East from Grimsel Lake. With the DEM obtained from the Agisoft Photoscan. The numbers represent the number of the block

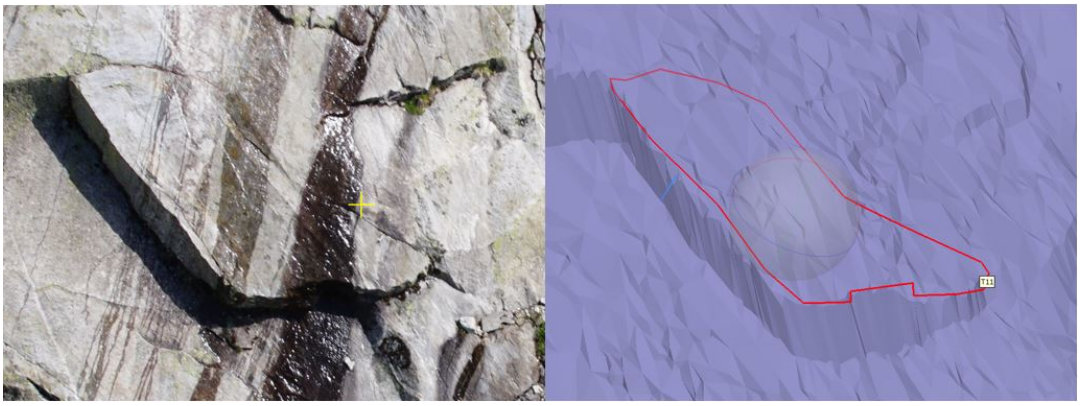

FIGURE 4.12: On the left, you can observe the single block with the presence of a fracture at the top. On the right side the DEM of the proposed block in red.

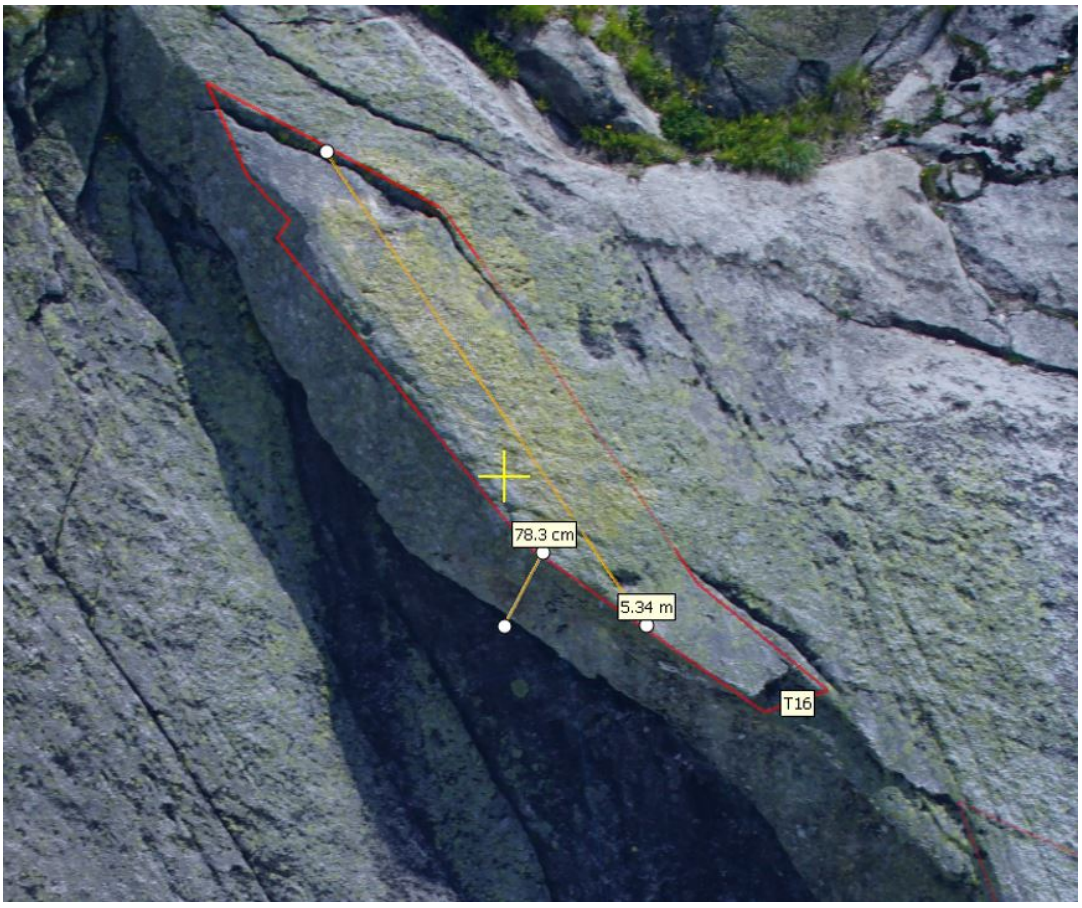

FIGURE 4.13: Block from the area denominated Lake East, Block T16, the mean height and length are measured in the corresponding planes.

FIGURE 4.14: Failed block (B3) from Lake East. It is possible to identify the area were the block was due to a brighter coloration of the Granite.

Chapter 5

Results

5.1 Code Results

5.1.1 Range of Block Parameters

Once the code was implemented in Matlab (*see Fig.4.4* or for the complete code see Appendix C), three simulations using the the corresponding parameters (*see Fig.4.1*) were performed.

The main difference between the three simulations is the slope angle. The first one is for 40° degrees, the second one is 50° degrees and the third one for 60° degrees (*see Fig 5.1*). For the three performed simulations, different block height and length ranges were simulated. The range goes from 0.25 m to 12 m with an interval of 0.25 m for each calculation in each respective case.

The output of the simulation is a plot (*see Fig.5.1*) for each of the different slope angles. In the horizontal axis different lengths are plotted and in the vertical axis different heights. Four different areas are shown:

- A zone in sky blue which indicates that the base provides stability, which means that the crack will not grow.
- The blue zone indicates that the crack grows and eventually the block will fail.
- The yellow zone indicates that the block will topple.
- The orange zone indicates that the crack grows but only Paris law will influence the growth until it falls.

The first analysis of 40° degrees (*see Fig.5.1*) shows an estimated slope of 50° degrees. This slope divides the blocks that topple (yellow zone) from the ones which the base provides stability (sky blue zone) and the ones in which the crack propagates (blue zone). The division between the blocks where the base provides stability is at 4 meters.
This would mean that a block of 4 m length, 1 m height and at 40° degrees, will be in the zone where the base provides stability and no crack will propagate.
For the case of a block with 4 m of length (same block length as the previous example), but 4,5 m of height at 40° degrees it be located in the zone where a crack will start to propagate until the block fails. For the last case of 40 degrees, 4 m of length and 6 m of height, the block will topple.
A similar analysis can be performed for the case of 50° and 60° degrees. Every time the slope angle increases, the limit between blocks that topple/don't topple decreases. The same relationship can be observed between the limit for the blocks of which the base provides stability (sky blue area) /crack propagation which leads to failure (blue area). For example, in the case of 40° degrees the division between

the area where the base provide stability/crack propagation to failure is 4 m (block height). For 50° degrees is 2 m (block height). Finally for 60° degrees is 1.5 m (block height). This indicates that at steeper angles the height of the block where the base provides stability decreases.

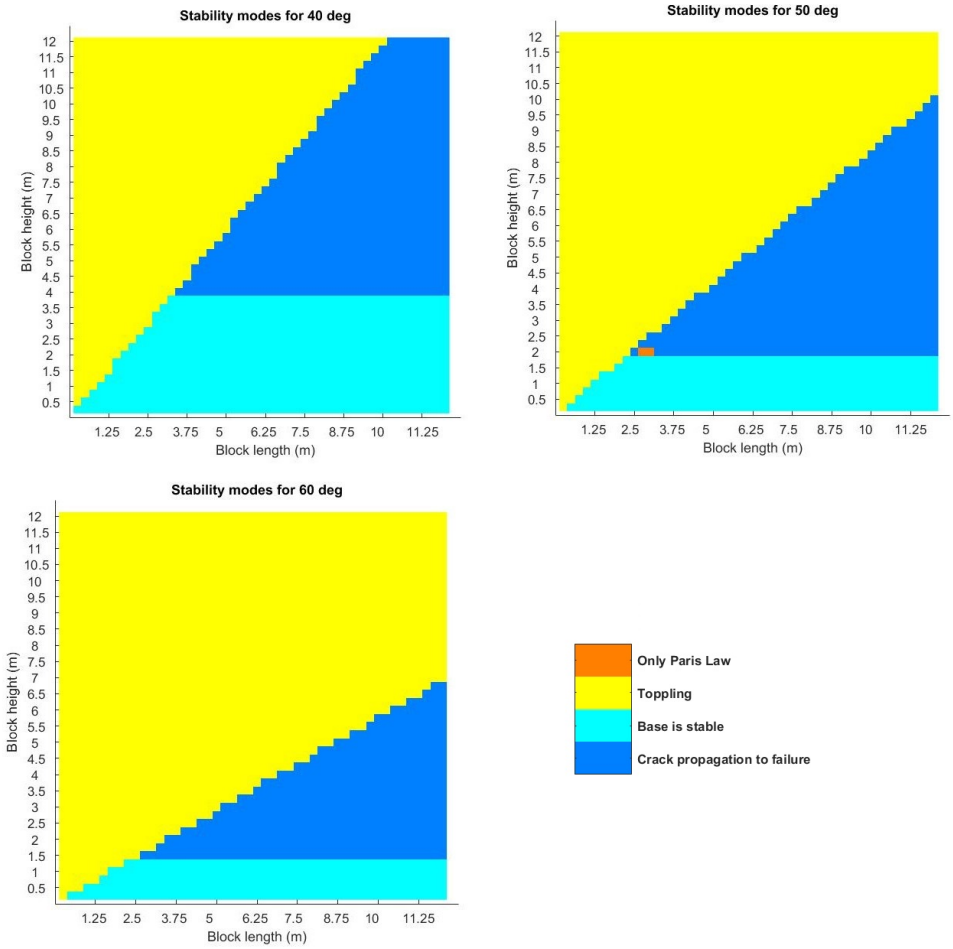

FIGURE 5.1: Results of the analysis performed. Three different angles, for 40°, 50° and 60°. Four zones are observed in the graph, depending on the blocks characteristics, it will be plotted in a specific zone. These zones include: the base provides stability, the crack is propagating to failure, the block should topple and the crack expands but only Paris law dominates the expansion.

Crack Opening Edge

Using the equation 4.24 and 4.25 it is possible to obtain the crack opening at the edge. In the *figure 5.2* is presented the crack opening at the edge one year prior to the different block falls. The various of crack opening's are in the order of 0.02 mm to 0.2 mm. The blue zone (color scale of 0) represents areas where the block topples or where the base provides stability and the edge crack does not expand.

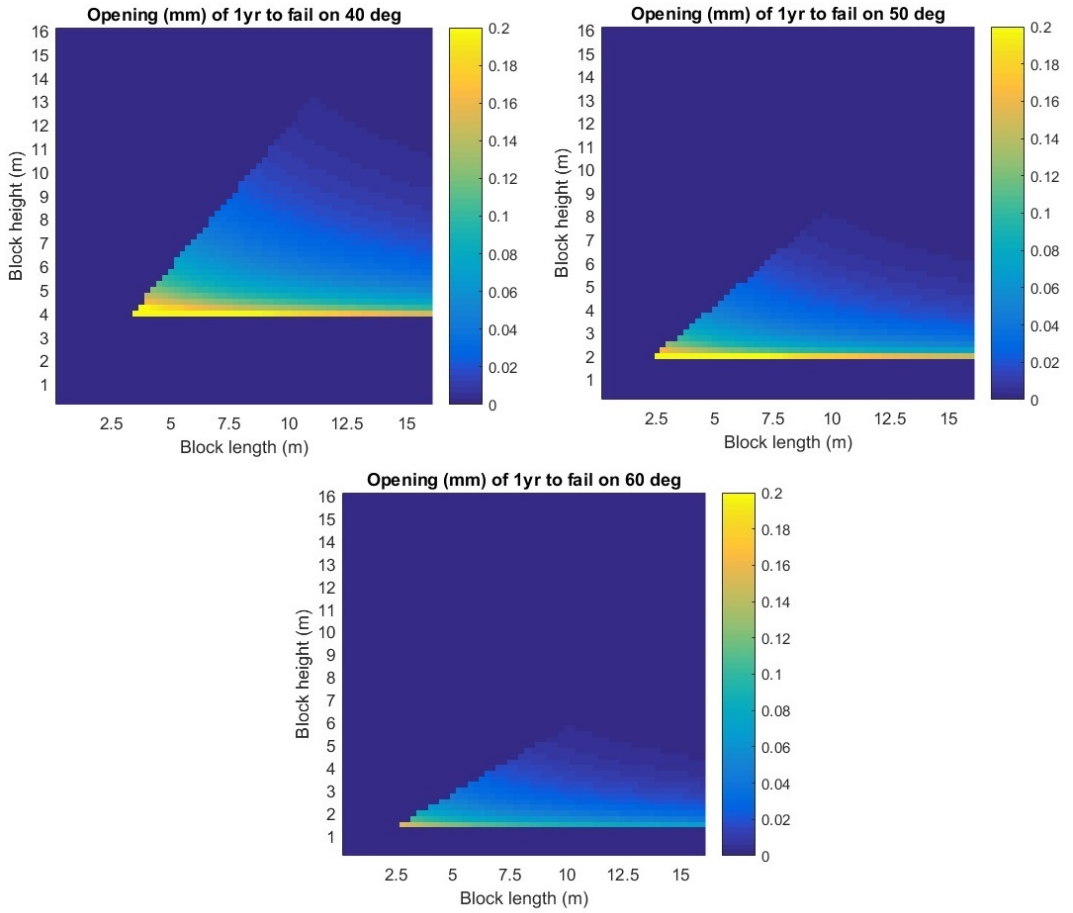

FIGURE 5.2: The code also analyses the crack edge opening (equation 4.25). Here are the results for one year before the block falls. Three different angles are plotted: 40°, 50° and 60°.

5.1.2 Defined Block Parameters

In the implemented code it is possible to perform an analysis using a range of parameters (Section 5. Range of Block Parameters) or is possible to provide a specific block height, length and slope angle. The code analyzes the single block parameters using the same work-flow (*see Fig. 4.4*). What is different is the output, the results are five different plots (*see Fig. 5.3*). In all of the cases, the horizontal axis represents the year. The black line indicates that the edge crack propagation is larger with the analysis Paris equation (equation 4.15) than the Charles equation (*see Fig. 4.18*). When Charles law is larger, then the line is coloured red.

- The first plot examines the duration of the performed iteration.

- The second plots the edge crack length (in percentage of the block height).
- The third indicates the edge crack stress intensity (in a percentage of critical stress intensity).
- The fourth indicates the crack opening in terms of meters.
- The last one presents the variation from mean crack extension

The examined block has dimensions of 6.5 m length, 5 m height, and 40° Degrees (Fig. 5.3).

- The first plot, as mentioned before indicates the iteration process. For the first 3,5 x$10^4 log_{10}$ years (x axis) the time that the iteration lasts is 10^{2}.69 when the Eppes equation dominates. As soon as the Charles law starts to dominate the process, the last of the iteration value decreases until 10^{-}7.4 year. This indicates that the iteration is much faster when the Charles law dominates the tensile edge crack growing.
- The second plot shows that during the first $14*10^4$ years Eppes equation dominates the crack growth. The edge crack growth is almost linear. As soon as the Charles equation dominates the process, the line goes almost perpendicular until reaching 74 % of the total block height when it falls.
- In the third plot, the edge crack stress intensity as a percentage of the critical stress intensity increases smoothly for the first five million years, just reaching 6.58 %. In 10 million years it reaches 18% and in the next 4 million years the percentage increases up to 57% just before Charles law starts to dominate. Then in the last 400 000 years the value escalates much faster up to 100% when the block fails.
- The next plot has a very similar plot shape due to the fact that the edge crack opening is directly related with the edge crack lenght. The values on the crack opening are in the order of 0.1 to 0.2 millimeter.
- In the last plot, the variation reaches a value of 0.01 % mean crack extension with the Eppes equation and then once the Charles equation dominates, it reaches a maximum of 0.4% per year.

The time when Paris law dominates the progressive crack growth (due to uncertainties during the Paris law validation) may be +/-10^1 factor less. This difference is shown at the moment of Paris law validation (*See section 4.4.3 Paris Law*).

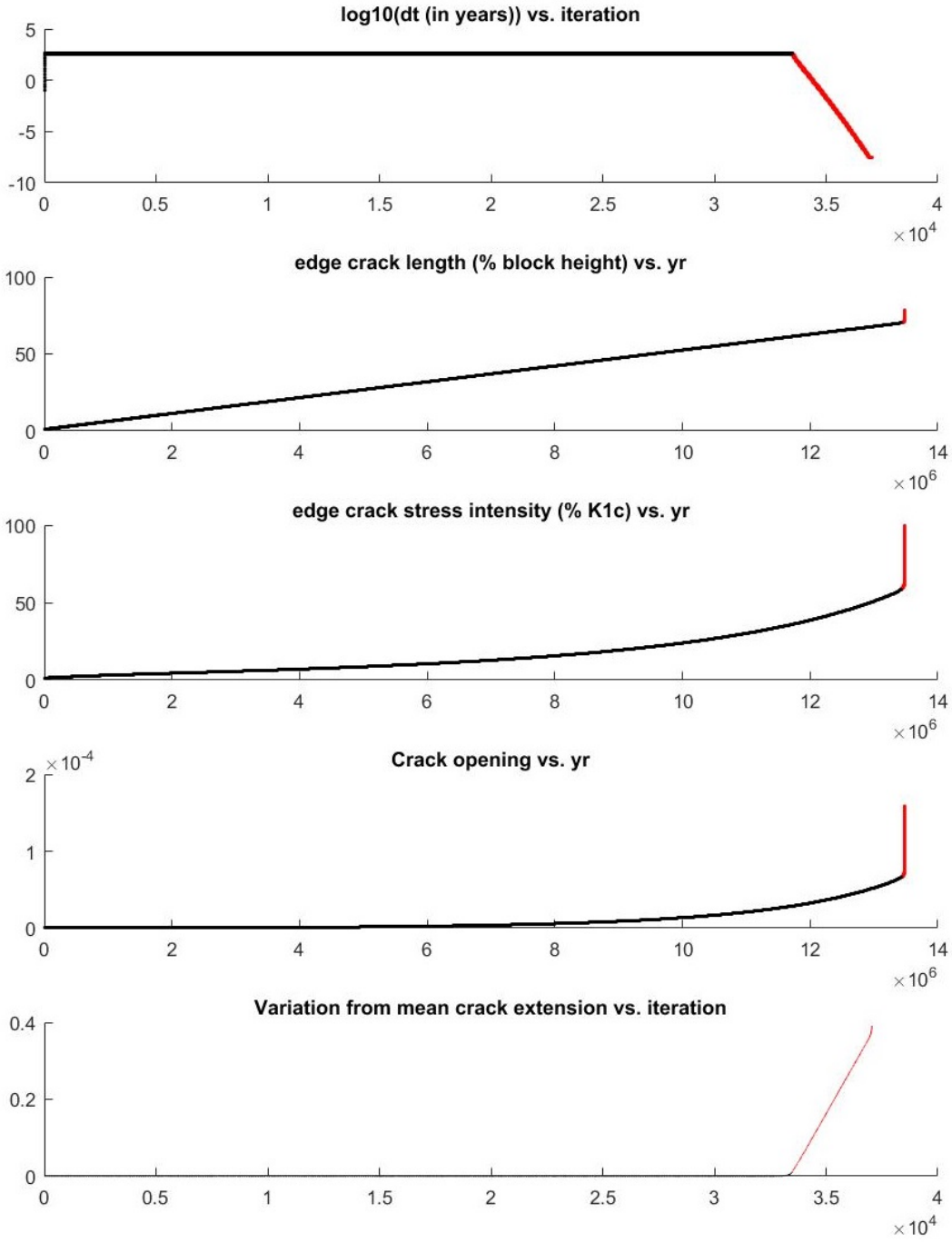

FIGURE 5.3: Matlab results for a single block of 6.5 m length, 5 m height, and at 40 Degrees. The black line represents the obtained parameters from the Eppes equation (equation 4.15), and the red line is obtained with the Charles law (equation 4.18). In the first plot, years (log10) vs iteration is plotted. The second plots crack length in terms of a percentage of the total block height. The third plot shows the Stress intensity / Critical stress intensity vs years. The fourth plot shows crack opening at surface vs years. The last one is the variation from mean crack extension vs year.

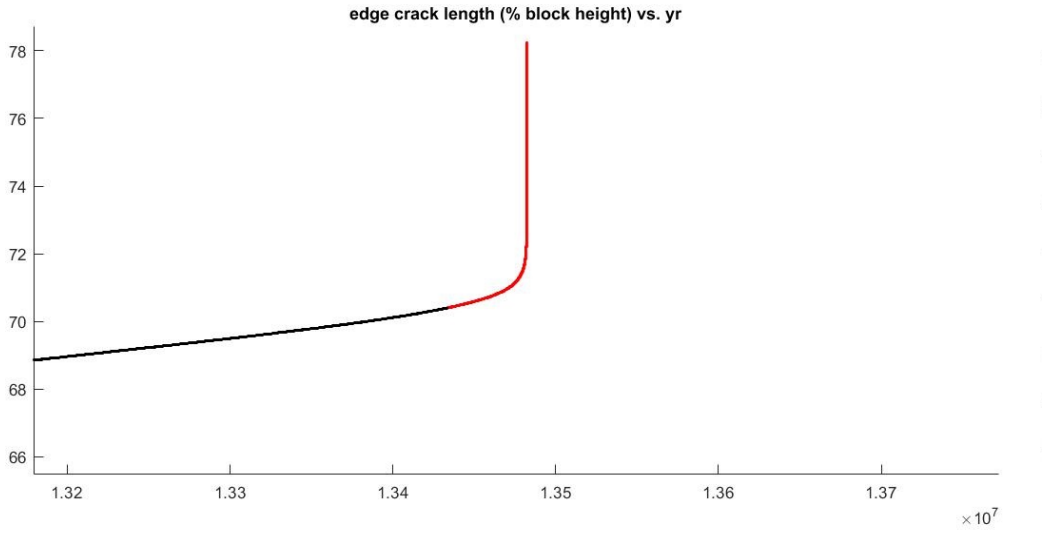

FIGURE 5.4: Zoom from the figure 5.3 for the transition Paris law - Charles law for edge crack length

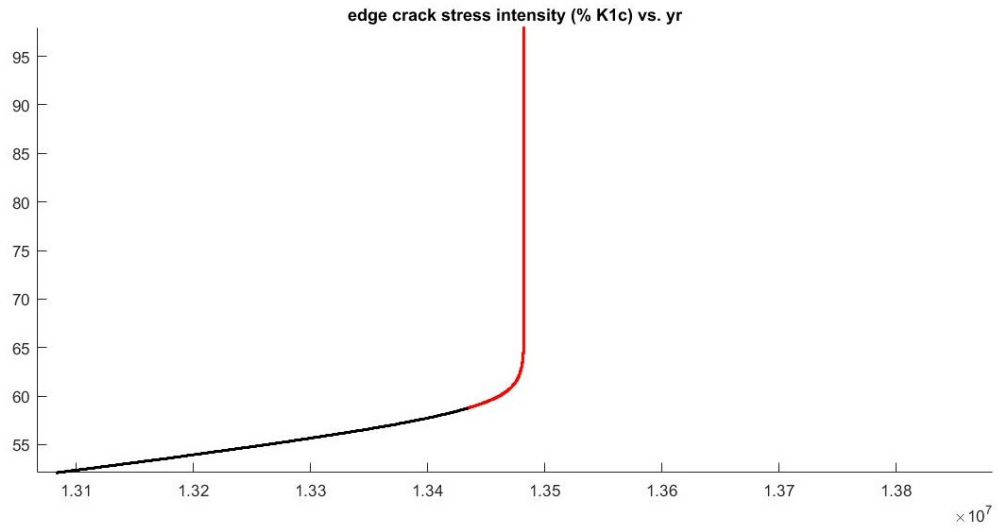

FIGURE 5.5: Zoom from the figure 5.3 for the transition Paris law - Charles law for the edge crack stress intensity

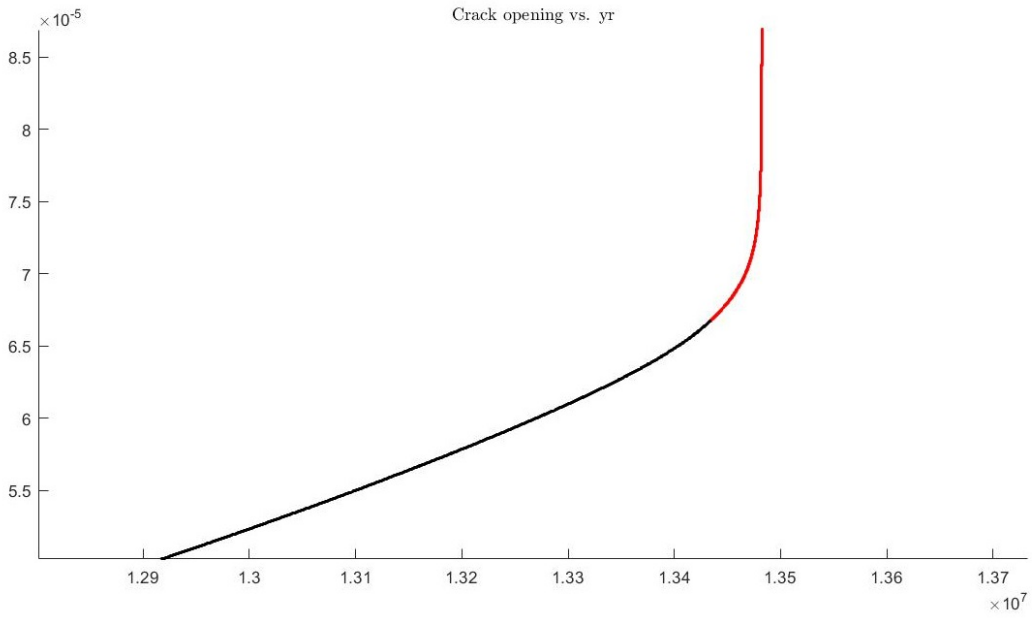

FIGURE 5.6: Zoom from the figure 5.3 for the transition Paris law - Charles law for the edge crack opening

5.2 Field Results

Three different areas have been mapped (*see Fig. 4.9*): at the north Tschingelmad (*see Fig.5.7*) , in the central part of the valley, Handegg (see Fig. 5.8) and at the south Lake East (see Fig. 5.9).

FIGURE 5.7: Area denominated Tschingelmad, photogrammetry performed with terrain photography.

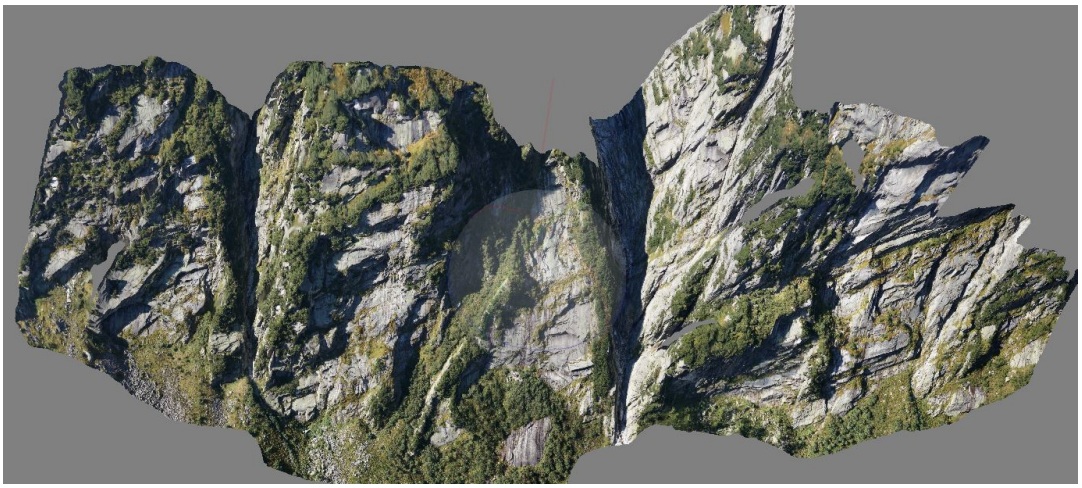

FIGURE 5.8: Photogrametry of the area denominated Handegg, was performed with a UAV.

I have developed two classifications: existing blocks (*see fig. 5.12*) and missing blocks (blocks that do not exist anymore and that I suspect have fallen) (*see Fig. 5.14*). In the following subsections the number of blocks and their length, perimeter, height and the angle is defined. In the case of height, it was difficult to measure directly because it was only possible to measure with existing surfaces and in some cases the surface was not totally perpendicular to the slope surface. In some cases trigonometry was used to calculate this angle. The missing blocks were in some cases quite difficult to interpret or to calculate the real dimension, for this reason the data must be used with caution. The blocks were classified according to their slope angle. The used range goes from 30°-40°, 40°-50°, 50°-60° and more than 60°. Depending on the existence of the mentioned angles. Unfortunately at the moment

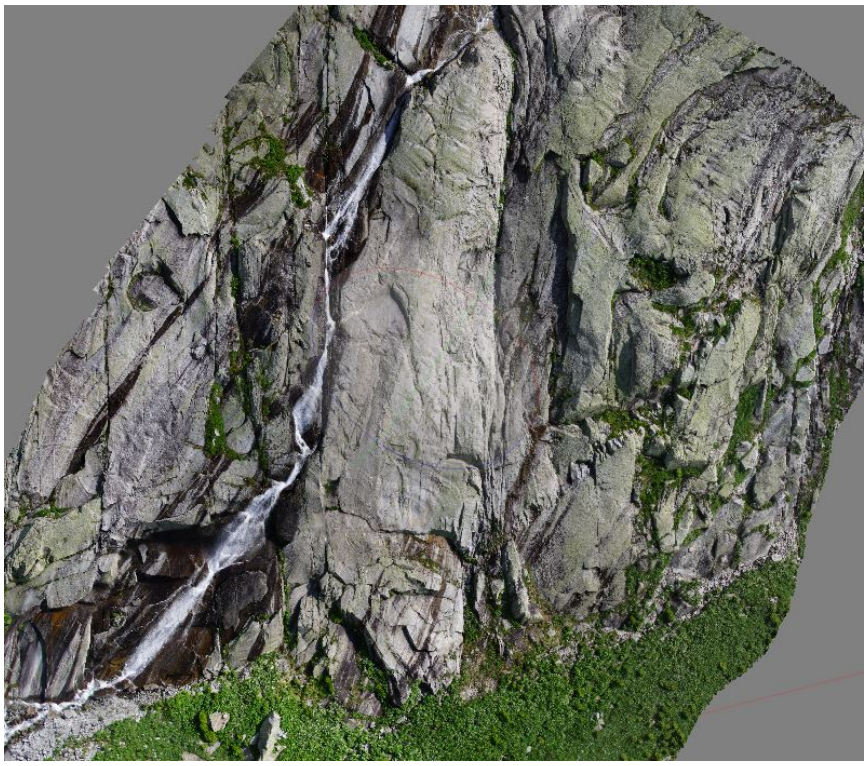

FIGURE 5.9: Area denominated Lake East, photogrametry performed with an UAV.

of performing the photogrammetry I only had control points to reference the image, but no control points to control the resolution of the images and to exactly determine what size was visible or not.

In the three areas it was possible to map 94 existing blocks and 16 failed blocks (See Appendix A)in total. The blocks details are specified in the corresponding section (Tschingelmad, Handegg and Lake East).

5.2.1 Tschingelmad

In the area, 19 existing blocks have been mapped (*See Fig. 5.10*). With a minimum of 0.79 m length, 2.53 m perimeter, 0.4 m height and 46° degrees. The maximum values are 6.43 m length, 24.3 m perimeter, 2.188 m height, and 67° degrees (See Appendix A).

In the *figure 5.11* the 19 existing blocks are plotted. In this case there is no clear correlation between the height/length and the angle of the block.

For the Case of failed blocks in Tschingeldmad, it was not possible to determine them. Therefore no results for this area is presented.

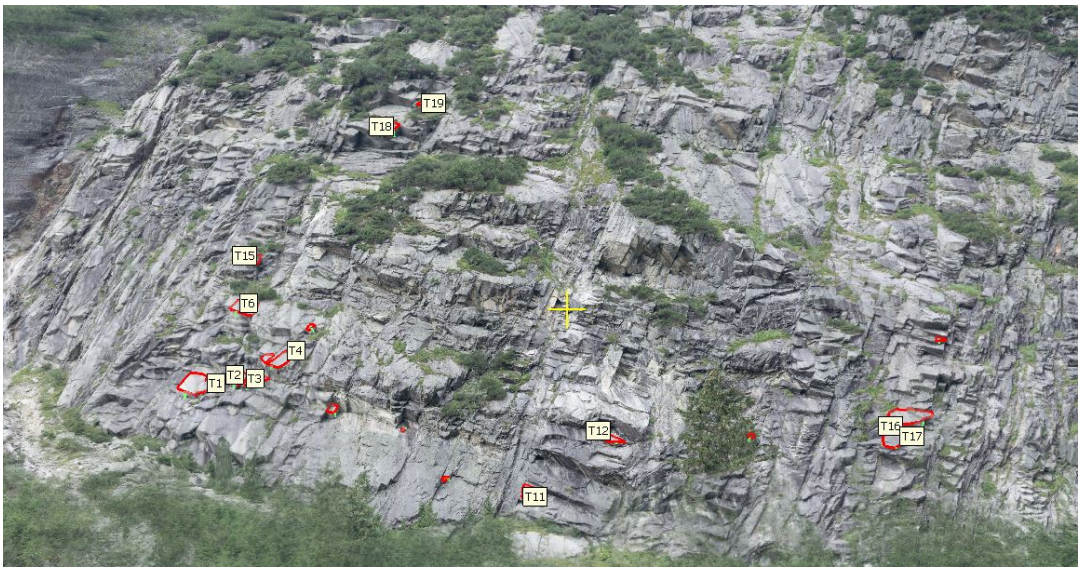

FIGURE 5.10: Tschingelmad, the red polygons are the existing blocks. In the area failed blocks were not mapped due to non-recognizable characteristics.

5.2.2 Handegg

In this area, there are 54 existing blocks (*see Fig. 5.12*) and 13 failed blocks (*see Fig. 5.14*) . With a minimum of 0.54 m length, 8.79 m perimeter, 0.48 m height, and 33° degrees. The maximum values for different blocks are 15.1 m length, 77.25 m perimeter, 12.36 m height, and 69° degrees (See Appendix A).

In the Figure 5.15 the x-axis shows the length of the block, and the y-axis the height. The different slope angles are classified with different colors. The linear correlation between slope angles less than 40° degrees, $40° - 50°$ and more than 60° has a similitude. However, the linear correlation for angles between $50° - 60°$ does not show a similar angle with the other lines.

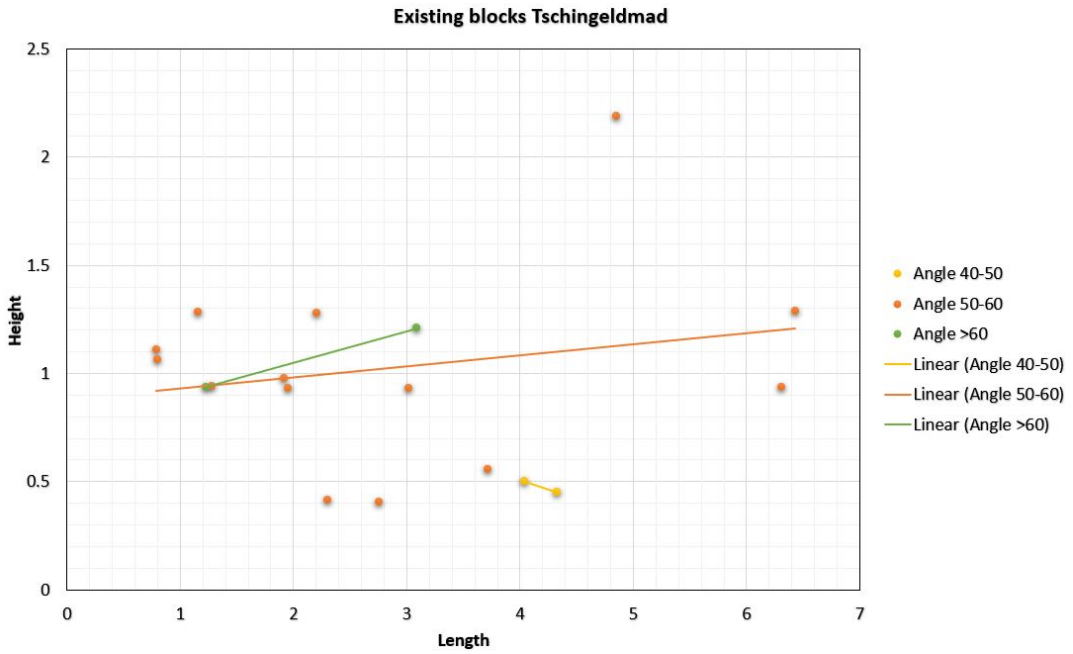

FIGURE 5.11: Tschingelmad, correlation between Height/lenght and the angle. No clear correlation is visible

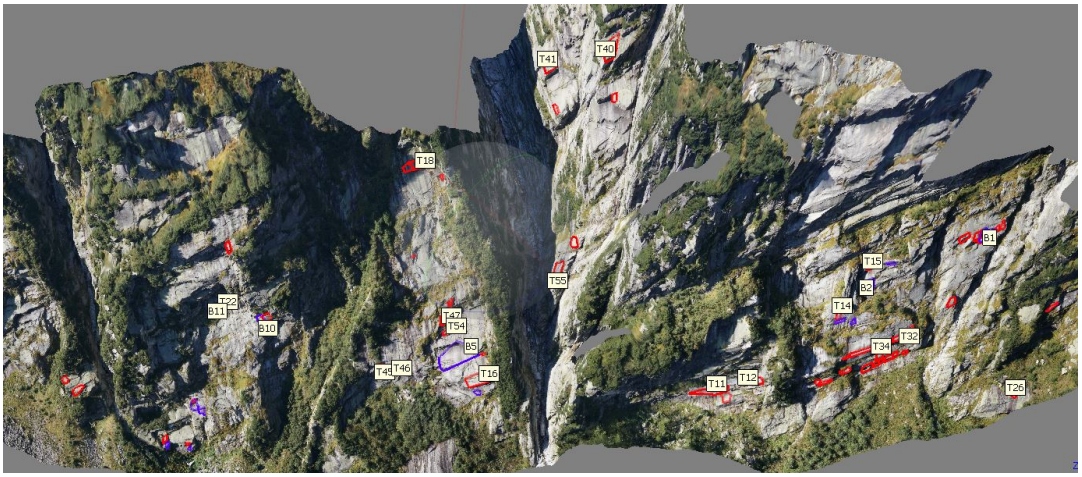

FIGURE 5.12: Handegg: Map blocks, in red the existing blocks and in violet the failed blocks

For the case of failed blocks, it was possible to map 13 blocks. One with less than 40° degrees. Therefore the linear correlation is only represented for $40° - 50°$ and $50° - 60°$ degrees (*see Fig.5.16*).

FIGURE 5.13: Handegg: Close-up to see the existing blocks.

FIGURE 5.14: Handegg: Same area shown in *Fig.5.13*. Showing two failed blocks that were identified. They are limited with a violet polygon. There is a central one and the other is in the bottom left part of the picture.

5.2.3 Lake East

In this area, there are 22 existing blocks (*see Fig. 5.17*) and 3 failed blocks. The minimum values are 0.6 m length, 5.15 m perimeter, 0.31 m height, and 28° degrees. The maximum values are 8.42 m length, 40.75 m perimeter, 3.29 m height, and 52° degrees (*See fig. 5.18*) (See Appendix A) . In the plot no correlation between the two

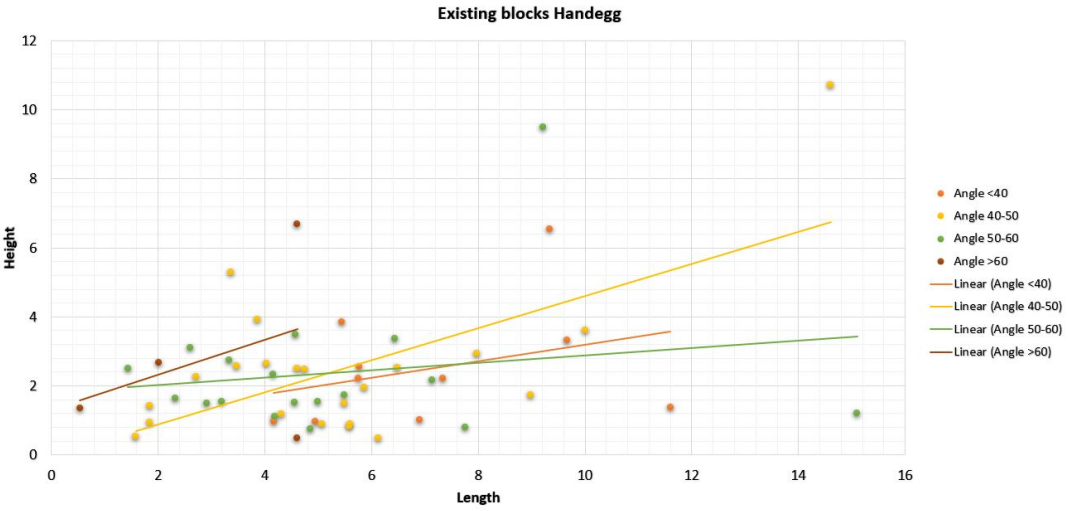

FIGURE 5.15: Handegg, existing blocks. It exists a correlation between the blocks at different angles and their correlation line , with exception from angles bigger than 60° degrees.

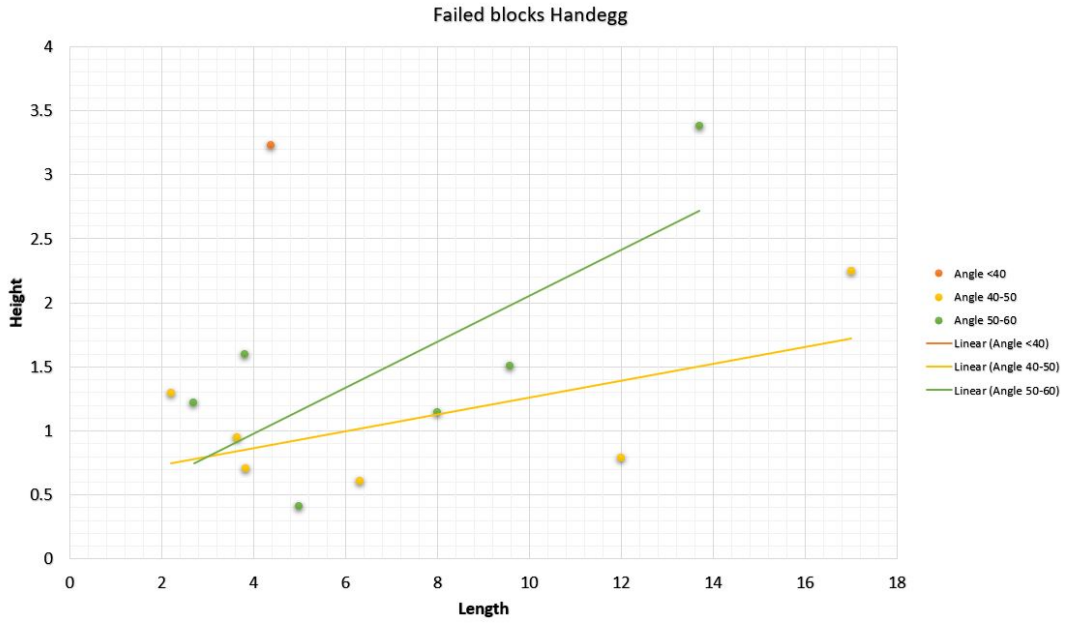

FIGURE 5.16: Handegg, failed blocks. Just two different classifications. In total 13 blocks were mapped.

slopes is visible. In the case of blocks in a slope angle of more than 50 degrees it was only possible to find one block with these characteristics. Therefore, no slope is created for this range.

In the case of failed blocks in the Lake East area, it was only possible to identify three blocks (*see Fig. 5.19*).

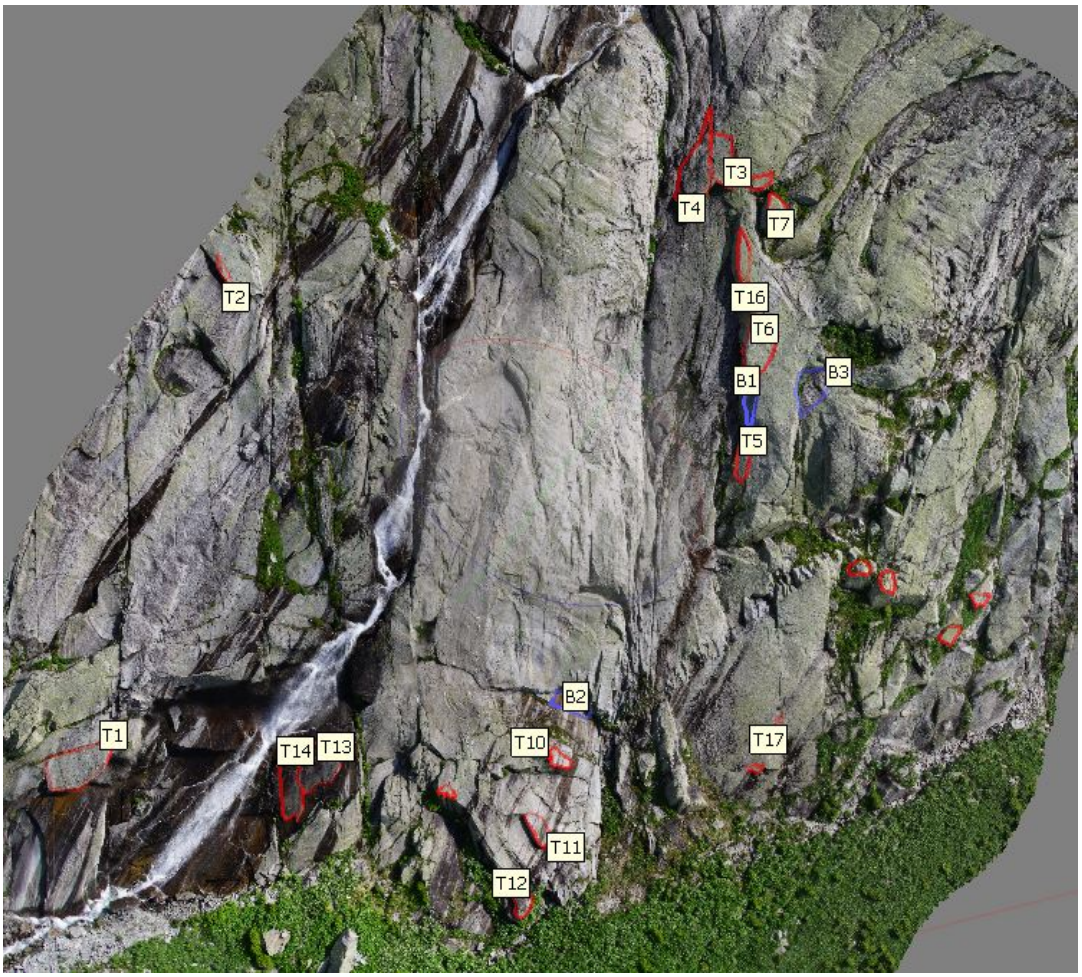

FIGURE 5.17: Existing blocks in the area Lake East. One can observe 19 map blocks in red and 3 missing in violet.

5.2.4 Block Summary

In the three areas it was possible to map 94 existing blocks and 16 failed blocks in total. The complete list is found in (Appendix A). The blocks details are specified in the corresponding section (Tschingelmad, Handegg and Lake East).

In the next plot (*see Fig. 5.20*), all the existing blocks from Handegg, Lake East and Tschingelmad are plotted. In blue are the blocks with an angle less than $40°$ degrees, in orange angles between $40° - 50°$ and in Grey angles between $50° - 60°$ degrees. There is no range greater than $60°$ due to the fact that only 2 blocks within this range exist. There is no visible correlation between the different slopes and the different angles.

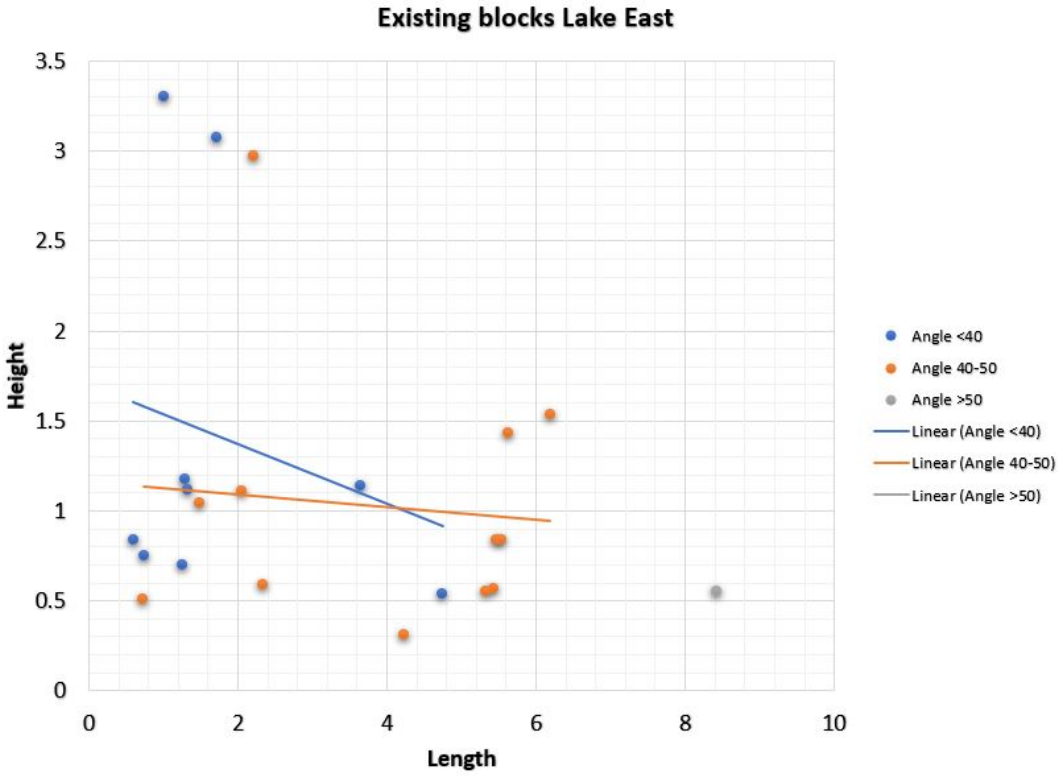

FIGURE 5.18: Correlation of the height/length- angle, it has a very low correlation. For the case of blocks with an angle > than 50° there is no correlation because just one block exist where the angle is more than 50°

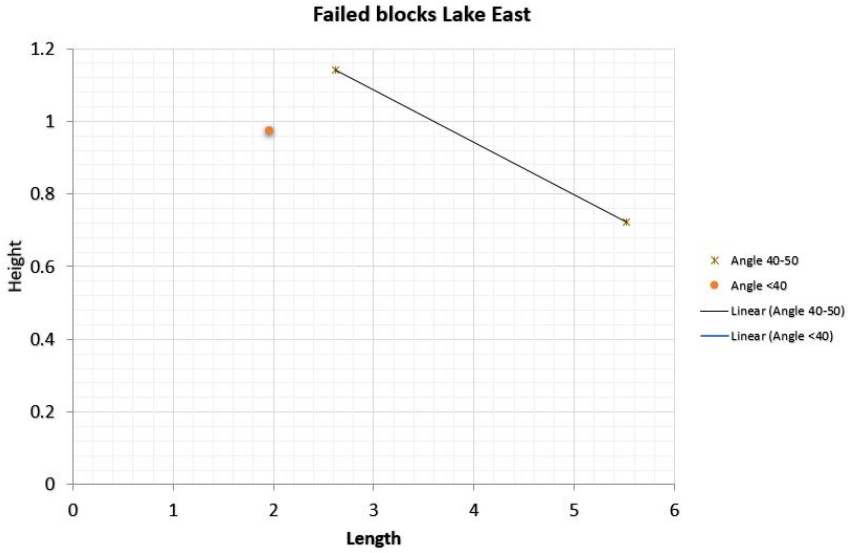

FIGURE 5.19: Lake East, failed blocks, 3 blocks were mapped for this area.

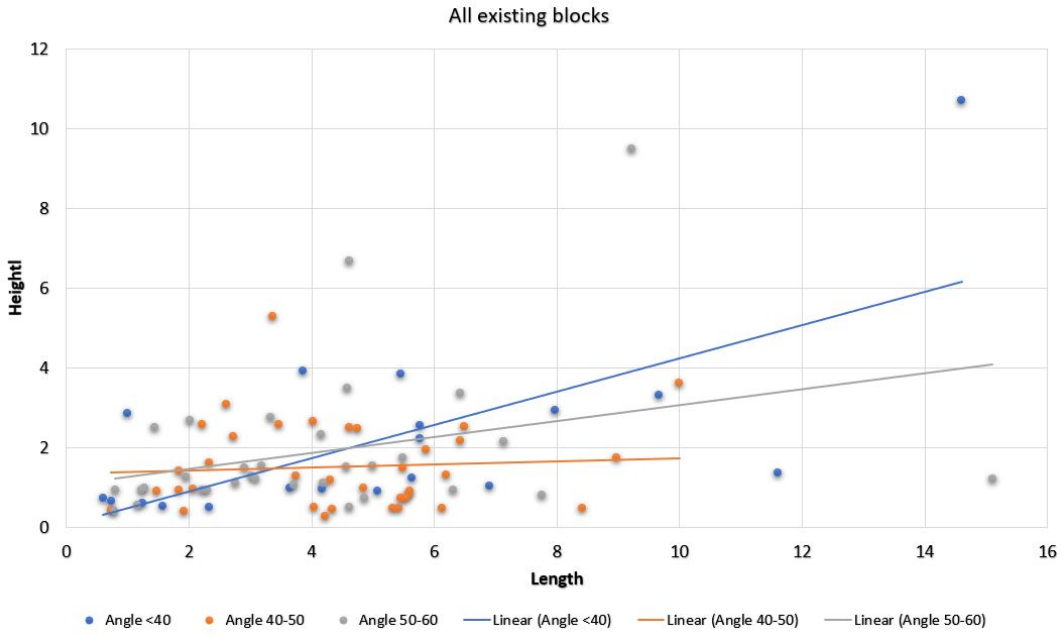

FIGURE 5.20: Plot showing all the different blocks from Handegg, Lake East and Tschingelmad, 3 angle ranges exist and they go from less than $40°, 40° - 50°$ and $50° - 60°$.

5.3 Back Analysis

The last step of the analysis is to combine the obtained field data (mapped existing and not-existing blocks from the three areas) (5.2.4 Block Summary) with the obtained model (see Fig.5.1). For this step all 94 mapped existing blocks and 16 failed blocks data were imported to the Matlab code and plotted.

In the section 5.2.4 Block Summary, it is indicated that 3 different ranges of slope angles were classified based on the field data. For this reason, in the Matlab code the same angle ranges were taken (see Fig. 5.1). In all of the cases, the regions or zones are the same as the ones presented in Chapter 5.1 Matlab Results (see Fig. 5.1). Four different zones were defined:

- The yellow zone indicates that the block topples.
- The blue zone indicates that the tension crack propagates to failure.
- The sky blue zone indicates that the base provides stability.
- The orange zone indicates that only the Paris law equation dominates the crack evolution.

The existing blocks are represented with black circles and the failed blocks are represented with red circles. In the blue zone (tension crack propagates to failure) a line is shown that divides the area in two. This line is generated from the crack opening edge results (*see Fig. 5.2*). Above this line the results of the edge crack opening are under 0.12 mm which is probably due to the resolution of the performed photogrametry not being visible (Chapter 5.1.1 Crack Opening Edge).

In the first plot (*see Fig. 5.21*) (for less than 40°), almost all of the existing blocks are plotted in the sky blue zone which indicates that the base provides stability. With the exception of two blocks that are in the toppling zone and one that is in the blue zone. In the case of the failed blocks only two blocks exist. Both are in the area that indicates that the base provides stability. One is very close to the toppling zone and another failed block is 0.70 m from the limit zone of block crack propagating zone. The line inside the blue zone, indicates that above it (according to crack opening) the edge cracks should not be visible.

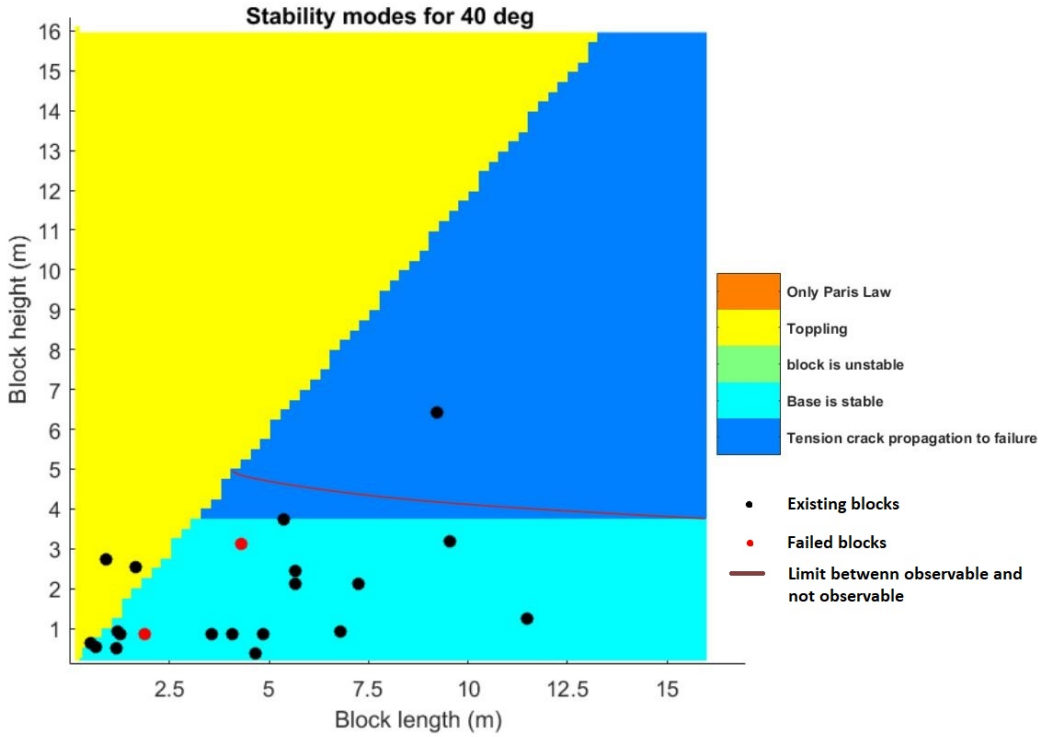

FIGURE 5.21: Results of the developed code (different areas) and the field blocks (in blue the existing and in red non-existing) for the case of 40°

In the case of the plot for $40^\circ - 50^\circ$ degrees (*see Fig. 5.22*), the existing blocks are distributed in the three zones. Three are located in the toppling zone and two very close to the propagating crack zone.The rest can be found in the propagating crack zone and where the base provides stability. From the failed blocks 7 are located in the zone where the base provides stability and only one is located in the zone where the tension crack propagates to failure.

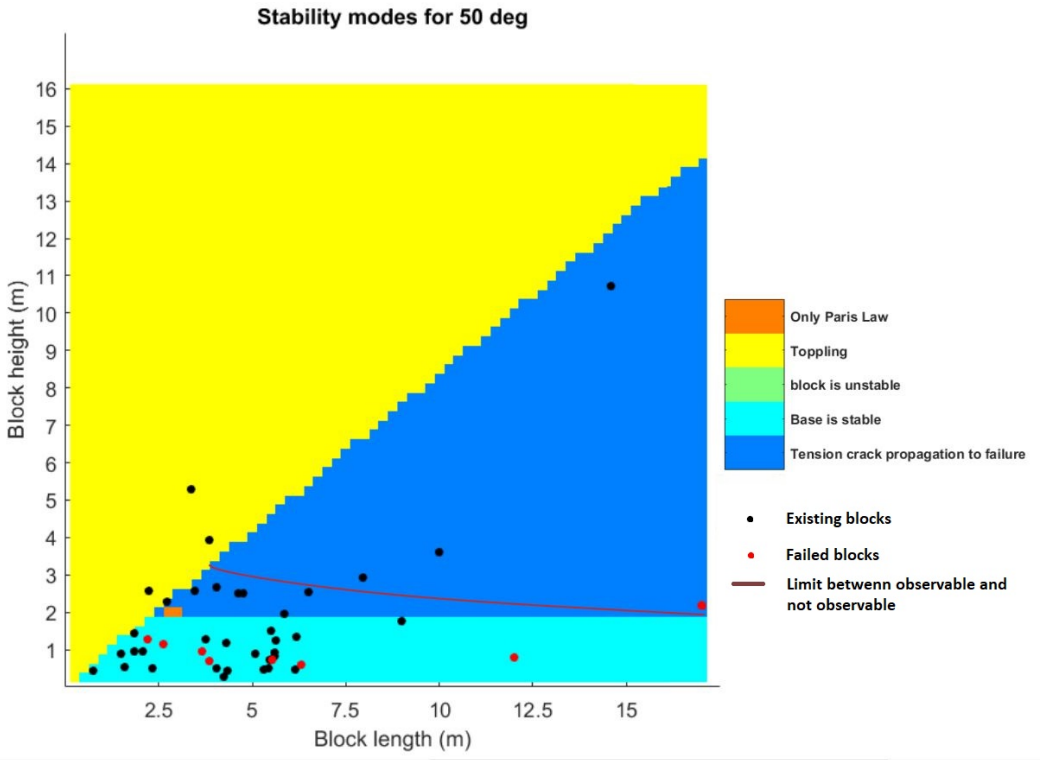

FIGURE 5.22: Result of the developed code (different areas) the field blocks (in blue the existing and in red non-existing) for the case of 50°

In the last case, when the angle is between $50^\circ - 60^\circ$ degrees (*see Fig. 5.23*), the majority of the existing blocks are plotted in the non-toppling zone. Only 9 of them are plotted in the toppling zone and in many cases they are very close to the non-toppling zone. 15 are located in the zone where the base provides stability and 8 are in the zone where the tension crack propagates to failure. For the failed blocks, all of them are plotted in the non-toppling zone. Three of them are plotted in the propagating crack zone and the other three are in the blue sky zone: the base provides stability. However two from these three, that are in the zone where the base provides stability are very close to the zone where the tension crack propagates to failure.

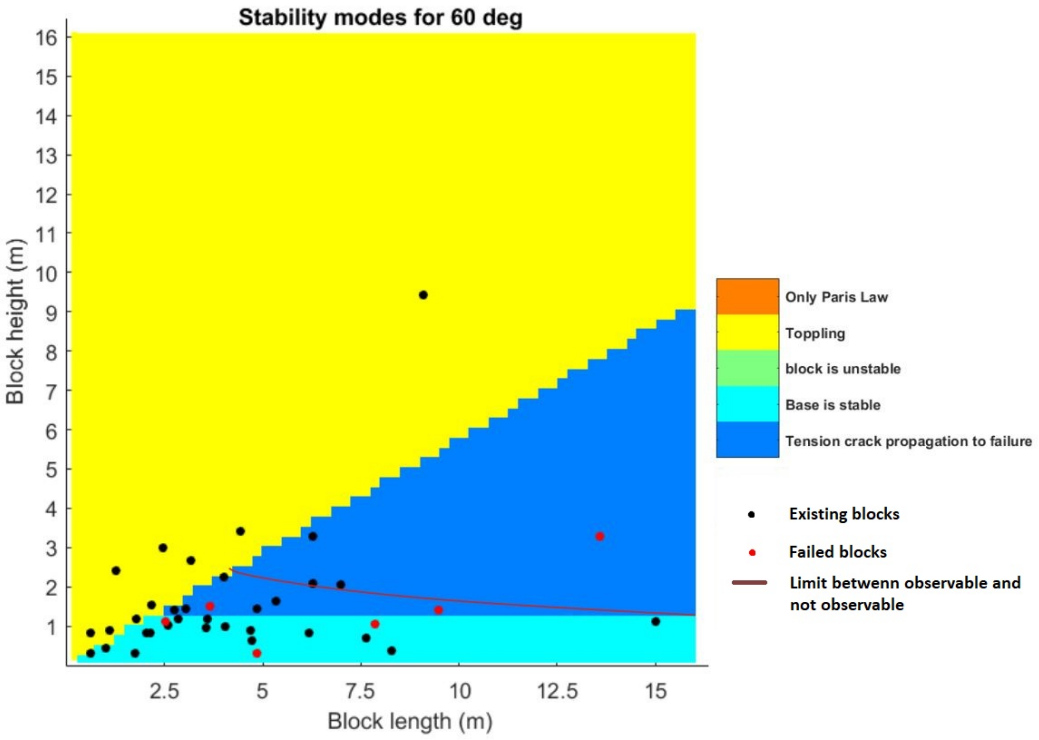

FIGURE 5.23: Results of the developed code (different areas) and the field blocks (in blue the existing and in red non-existing) for the case of 60°

Chapter 6

Data Interpretation and Discussion

6.1 Matlab Code

The implemented equations (4.2 Governing Equations) in the matlab code (see fig. 4.4) have introduced the evolution of stress and strain to the LEM by adding the assessment of the time required for a progressive tensile edge crack to reach a critical condition.

The developed code follows a logical cycle which is a simplification of reality. However, it has the following limitations:

- Regarding the forces that act on the block, the analyzed block does not take into consideration the tension that is generated on it from the lateral blocks (Kliche, 2003).
- The $K_{(I)}$ factor is for a intact rock (Eppes and Keanini, 2017), therefore the generated code can only reproduce new cracks. Rocks are often rich with pre-existing cracks (Erismann and Abele, 2001) for this reason the model only reproduces new cracks.
- During the whole analysis the base block area remains constant. This mean that the base provides the same resisting force throughout the entire analysis. However, it is possible that the entirety of remaining rock bridges on the base also degrade with time, reducing the cohesion strength per unit area.
- One single edge crack in the proposed model is developed. In reality it is possible that multiple cracks expand at the same time (Wang and Cao, 2017).
- The model does not consider earthquakes or extreme rainfall, nor the stress generated from the ice (Erismann and Abele, 2001). These events can trigger the block fall.
- Paris law (Equation 4.15) and Charles law (Equation 4.19) were used to determine the edge crack growth rate. Both formulas provided the edge crack growing length. The largest result (for each determined depth) was used.
- The model considers the cyclic variation of the temperature for one year. It does not consider extreme climate events. This change is only applied for the Paris equation because it is the only equation that includes temperature change (Equation 4.15).

Due to the mentioned factors the outcome of the model is limited. The different output zones (see fig. 5.1) that the code provides (base provides stability, the edge crack will propagate, topple, etc.) are strongly dependent on the slope angle. At bigger slopes angles, the ratio of block height to block length decreases. For the

crack opening edge values (5.2) the results are directly correlated with the edge crack length. The larger the edge crack length, the larger the edge crack opening is.

The crack opening (see fig. 5.2), contrary to what I expected, is not larger at larger block heights. The results show that for a block with the same length but different heights, the larger crack opening is larger for small heights. From these final results, which are directly correlated with the edge crack length, I can confirm that the edge crack length is also larger for blocks with small heights.

Fixed Parameters

In the case of single block evaluation (see fig. 5.3), the time evaluation depends on Paris Law (eq. 4.24) or Charles law (eq. 4.15). At the moment of Paris law implementation, I could not reproduce the exact same results proposed by Tada, Paris, and Irwin (*The Stress Analysis of Cracks Handbook, Third Edition*). My formula verification show a difference of a factor of 10^1 years less when the crack starts to propagate (See section 4.5.3 Paris Law). For this reason the displayed times do not accurately represent the reality. However, it is a good indicator to how the crack propagation would look like in comparison to the crack propagation of Charles law.

From the fixed parameters evaluation I obtain that in general Paris law dominates the tensile edge crack growing. From all the time that takes to the block to fall, Paris law dominates more than the 90% of all the time and just on the last 10% dominates Charles law.

6.2 Photogrametry

In the case of Photogrametry, the three different places: Tschingelmad, Handegg and Lake East *(see map. 4.9*) need to be georeferenced. After this georeferencing and photo alignment I have obtained for each photogrametry an alignment error.

- For Tschingelmad, the error is quite high at 3.3 m.
- The error for Handegg was 0.7 m which is acceptable.
- Finally in the Lake East photogrammetry the error is just 0.16 m.

In the case of Tschingelmad this high error is due to the large height of it. Due that this photogrametry was performed with terrestrial photographs the higher areas present a higher distortion. In the second and third cases the pictures were obtained from a drone. Therefore the error is less.

In the case of Tschingelmad, this generates a model of low quality since the mapped blocks have (in most cases) a height of less than 1 meter. Regarding the amount of map blocks, for Tschingelmad I mapped 19 existing blocks, and no failed blocks were identified. The Handegg area has the most amount of map blocks, with 54 existing blocks and 13 failed blocks. Finally in Lake East area, I mapped 22 existing blocks and 3 failed blocks. In terms of percentage of mapped blocks Tschingelmad represents 20%, Handegg is 56% and Lake East 23%. For this reason the error in respect to map blocks is acceptable. However, some uncertainties exist at the moment of mapping the blocks. Firstly, there is no methodology to mapping single blocks. In this work all the blocks were mapped without distinguishing special characteristics (i.e. no lateral blocks, just one lateral block, etc). However, some blocks have different possible configurations of surrounding blocks (one lateral block, two

lateral blocks, one lateral and a top block, etc). This could be a source of variation in the back analysis.

In the task of mapping missing blocks, it was performed only visually (it do not exist a register to compare them). However it is quite complicated to recognize the limits of the missing blocks. Moreover I don't know what triggered the fall of these blocks

6.3 Back Analysis Results

After obtaining the results from the implemented code (*see Fig. 5.1*) I plotted the results of block mapping (5.2 Field Results) over them in the three established angle range (40° , 50° and 60° grades). The results (*see fig.* 5.21, 5.22 and 5.23) show some of the blocks out of the areas where ideally plotted. A perfect (Hypothetical) result would be that the existing blocks were not plotted in the toppling zone. They could be in the other zones (crack propagation to failure zone or the base provides stability zone). The failed blocks could be in both zones. If they are in the zone where the base provides stability then they have probably failed, but not due to a tension crack propagation, rather to a base that has lost the cohesive strength per unit area. If they are in the blue zone then we can suppose that the triggering factor was the tension crack propagation to failure.

In addition the proposed model has assumptions, limitations (4.3.1 Model assumptions and considerations and 6.1 Matlab Code) and errors from the results obtained from the block mapping at the field (see 4.3 Photogrammetry). In my point of view one of the principals factors that limits this back analysis is the previous existence of joints and structural discontinuities in the area around Grimsel pass. As well as the query about if the the external trigger factors (extreme temperatures, earthquake,etc) have caused the block fall.

Despite these limitations in the implemented code (4.4) there is still room for improvement. The code has been developed in different modules and each module can be independently modified. For example, the local temperature variation and the rock parameters, such as cohesion or Young modulus can be replaced for each specific location. Moreover, it is possible to add different sections.

6.4 Recommendations

During the realization of this thesis I have thought about different approach's and procedures to assess or to implement into the chosen formulas. However, it took me a long time to locate the problem with the Paris Law formula implementation. For this reason I have not further develop the model. Despite this, I would like to mention what can still be done/included in future investigations. The code has been written in modular form, so it is possible to add more components to it. I would like to mention the relevant points for future investigation:

Central Cracks and Multiple Cracks

In this thesis the only crack that is included is edge crack. Although, in reality, it is possible that one will need to deal with multiple cracks (Gross and Seelig, 2011), central crack or base crack as the one show in Fig. 6.1.

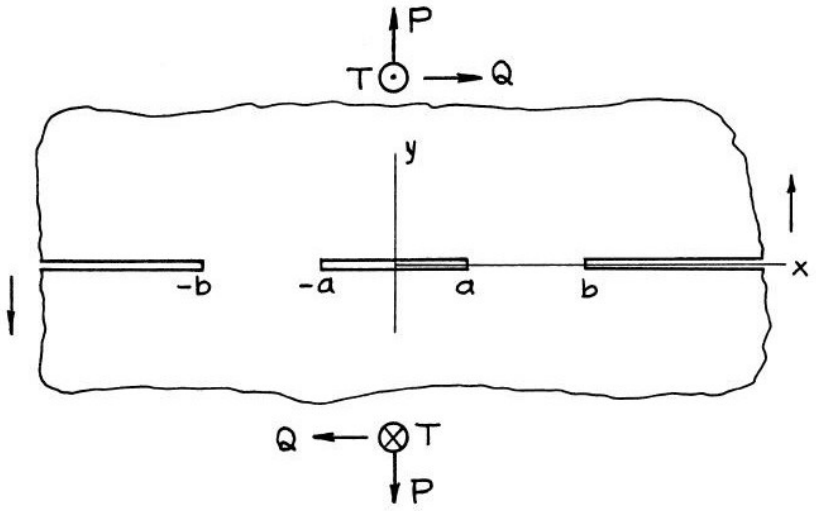

FIGURE 6.1: Tada, Paris, and Irwin (*The Stress Analysis of Cracks Handbook, Third Edition*) proposes an approach for the stress analysis of cracks at the base in the case of rock sliding

Water

Different authors include groundwater in the LEM analysis. The presence of groundwater generates forces. This can also be included into the model (Kliche, 2003).

Seismic Activity

The seismic activity can be included as vibrational forces. This is often included as a factor that reduces the normal forces (Kliche, 2003).

Block Geometry

The geometry of the proposed block was always rectangular. However in some occasions the block is truncated or have a different form. This can also be modified.

Multiple Block Analysis

In this current thesis one single block was analyzed. However the possibility exists to assess it with more blocks that interact or have an affect on the forces with the one analyzed.

Photogrammetry

The data obtained from the failed blocks was performed only visually (exist no record to compare it). I have no evidence other than some indications such as: difference of rock color or presence of lichens. I also do not know when it happened, or the trigger. For this reason this data can only be used as a reference. A solution for this problem will be to perform a photogrammetry some years after from the same area. Then compare the two different DEMs and obtain the exact dimensions of missing blocks. Finally perform a more accurate model validation with the new data. It will also be important to measure the resolution of the photogrammetry in order to obtain better quality.

Chapter 7

Conclusions

The aim of this thesis was the implementation of a variant condition (progressive tensile edge crack) into the Limit Equilibrium Method to carry out a time-dependent analysis. At first a short introduction of the different stability analysis techniques was written to provide a general context. Then a more specific review of LEM and the progressive tensile edge crack was provided. From this specific review the formulas that were used in the model implementation were obtained. Afterwards the model was implemented and a back analysis with Grimsel data was performed. The obtained results led to the following conclusions for the proposed research questions.

How can the addition of progressive tensile crack growth equations to the concept of LEM (planar failure mode) classify the state (stable, growing crack, toppling) of the rock blocks?

The process of a logical procedure to simulate progressive tensile edge crack growth and to consequently generate a planar rock falling was successfully implemented (*see Fig. 4.4*). It enabled an evaluation of different dimensions of blocks in a possible planar failure (*See Fig. 5.1*). Resulting from this evaluation were three different zones: where the block topples, where the base provides stability and where the crack is propagating until it will fail. The code is implemented to allow for the analysis of a single block with user-defined variables and goes through a series of steps (*see Fig. 4.4*). It also allows the user to evaluate the time iteration, the edge crack grow, the edge crack intensity, the crack opening and the crack length variation. However, due to the time scale I was not able to exactly reproduce the Paris equation results (see 4.5.3 Paris Law). There exists a difference of a factor of +/-10^1 years. Therefore, the time results can be used as a reference, however they still need to be adjusted.

How can field /laboratory data be used to perform a back analysis of the equations?

So far in the performed literature review (see Chapter 2) there is no directly correlatable data that can be used to assess the progressive edge crack growth for LEM. Large amounts of data from compressing the sample (Brazilian test) exist. However, these do not represent the constant load from a block in the case of planar failure (in the test the load increases). Nonetheless, data does exist from fracture growth from fracture mechanics. In the last few years investigators have tried to correlate climate factors that cause crack growth as Eppes and Keanini (2017), that uses the tension generated between the mineral components under diurnal temperature variation. He does not provide data that can be used to perform a LEM black analysis. However, he provides a correct way in which to approach the progressive tensile edge

crack growth. Due to this lack of data I decided to perform a Photogrammetric analysis of different rock areas (Chapter 4.3), in which existing and failed blocks were mapped. Then the obtained field data was used to perform a back analysis of the implemented equations.

How can the obtained field data from Grimsel pass be correlated with the different outcomes from the proposed code?

The required geometry block variable inputs in the implemented code are height, length and slope angle. It is possible to obtain this data from photogrammetries. From the three performed photogrammetries (see 4.3 Photogrammetry) two were quite successful in terms of accuracy. Tschingelmad had a considerable location error of 3.3 m, Handeg and Lake East have an error of 0.7 m and 0.16 m respectively which is acceptable. However, in terms of number of plot blocks, the amount of mapped blocks in Tschingelmad only represents 20% of the total blocks. Therefore, I still consider the use of the data helpful. Mapping the blocks is time consuming, as there is no automation to search the blocks under planar failure and record them. Neither is there an established classification. A total of 95 blocks were mapped. However, there is uncertainty as to whether they are dominated by the existing joints. Failed blocks were also mapped, but only 16 were possible to record. The task was complicated due to a lack of two information sources: it was performed visually and there is no previous or current photogrammetry from the area to compare them. For this reason, this data is used as an indicator. Once all the respective data was gathered, I was able to obtain the code plot results (*see Fig. 5.1*). Over it I plotted the field data results (94 existing blocks and 16 failed blocks. *See Fig. 5.20*). In the case of existing blocks, the vast majority (87%) is located in the zone where the base provides stability or where the edge crack is propagating. In the case of failed blocks, theoretically all of them should be located in the edge crack propagation zone. However, only four of them are located in this zone, which means that only 40% of the blocks have fallen due to the edge crack propagation. The cause of the other 60% is unclear (external factors or toppling). However, these results are not precise due to the block analysis simplifications and the errors in the field data (obtaining and post processing).

How can the model be used to understand the evolution of tensile cracks on planar rock fall in the areas around Grimsel Pass?

The implemented model has some limitations and constraints with the accuracy. One of the biggest limitations in the used formulas in regards to code implementation (Chapter 6) is that the K_I (Stress intensity factor) is used for an intact rock, while in reality the rocks in Grimsel Pass have several joints. It is very probable that the cracks tend to grow in the discontinuities rather than in other planes. Neither account for external factors such as earthquakes or heavy rainstorms.Additionally, when performing the back analysis, the obtained field data only shows an accuracy of 40%. For all the above mentioned reasons, the model can not be used to accurately predict the time it takes for a block to fail.

Although I did not get the optimum results with the field correlation, there is still room for improvement. Adding more modules to the code or modifying approaches could lead to more accurate real-life outcomes.

Appendix A

Mapped Blocks

A.1 Existing Blocks

A.1.1 Tschingelmad

Tschingelmad					
Name	Lenght	Perimeter	Height (m)	Calculated height	Angle
T17	4.3	21.2	0.4	0.4	46.9
T19	4.0	19.0	0.5	0.5	48.4
T16	3.7	22.9	1.3	1.3	50.7
T18	6.4	20.2	2.2	2.2	52.1
T1	4.9	24.3	1.1	1.0	52.2
T12	1.9	20.1	0.4	0.4	52.5
T15	2.8	15.3	1.1	1.1	52.8
T9	0.8	2.5	0.4	0.4	53.1
T5	2.3	8.3	1.1	0.9	54.6
T2	3.0	14.0	1.5	1.3	54.8
T14	1.2	6.3	0.6	0.6	55.2
T6	3.7	18.1	1.2	1.1	55.4
T10	0.8	3.6	0.9	0.9	56.8
T4	6.3	17.3	1.1	0.9	57.1
T8	2.0	7.4	1.3	1.3	57.4
T3	2.2	14.0	1.1	0.9	59.4
T7	1.3	5.8	1.1	1.0	59.6
T13	1.2	4.6	0.8	0.9	61.4
T11	3.1	10.8	1.2	1.2	67.2

TABLE A.1: Principal characteristics of the mapped blocks

A.1.2 Handegg

Handegg					
Name	Lenght	Perimeter	Height (m)	Calculated height	Angle
H20	4.9	16.4	1.1	1.0	33.5
H18	7.3	39.7	2.6	2.2	33.7
H10	9.3	32.0	7.5	6.5	35.0
H16	9.7	64.7	3.8	3.3	35.9
H26	11.6	34.5	1.6	1.4	36.2
H21	4.2	13.4	1.1	1.0	36.2
H43	5.8	27.1	2.5	2.5	37.2
H55	6.9	42.7	1.0	1.0	37.5
H17	5.8	29.4	2.6	2.2	38.9
H12	5.5	37.2	4.5	3.9	39.6
H47	8.0	43.0	3.4	2.9	40.0
H54	5.1	34.5	1.0	0.9	40.1
H48	1.6	8.8	0.6	0.5	41.2
H39	3.9	19.9	4.5	3.9	41.6
H40	14.6	53.7	12.4	10.7	42.1
H49	5.6	31.1	1.0	0.8	42.7
H24	5.6	20.8	1.1	0.9	42.8
H15	5.9	33.2	2.0	2.0	43.6
H41	10.0	42.0	4.2	3.6	44.6
H19	4.3	12.8	1.4	1.2	44.7
H5	2.7	16.7	2.6	2.3	45.9
H38	4.6	24.0	2.9	2.5	46.4
H23	1.8	11.8	1.6	1.4	46.7
H44	1.8	10.3	0.9	0.9	47.0
H7	3.5	16.5	3.0	2.6	47.2
H8	4.7	28.7	2.9	2.5	47.2
H46	3.4	52.6	6.1	5.3	47.5
H50	6.1	23.4	0.6	0.5	48.4
H22	6.5	42.7	2.9	2.5	48.8
H11	9.0	77.3	2.0	1.7	49.3
H13	5.5	22.3	1.7	1.5	49.3
H3	4.0	22.8	3.1	2.7	49.9
H1	2.6	13.9	3.6	3.1	51.1
H25	2.3	25.0	1.9	1.6	51.5
H14	15.1	36.0	1.4	1.2	52.8
H6	5.0	23.3	1.8	1.6	53.3
H9	3.2	24.5	1.8	1.5	53.7
H30	4.9	19.8	0.9	0.7	54.2
H51	2.9	12.9	1.7	1.5	54.7
H45	7.1	44.9	2.5	2.2	54.7
H53	6.4	27.3	3.9	3.4	55.9
H34	3.3	62.1	3.2	2.7	56.3
H37	4.2	15.1	2.7	2.3	56.4
H52	9.2	26.6	11.0	9.5	56.5

TABLE A.2: Principal characteristics of the mapped blocks

H23	1.8	11.8	1.6	1.4	46.7
H44	1.8	10.3	0.9	0.9	47.0
H7	3.5	16.5	3.0	2.6	47.2
H8	4.7	28.7	2.9	2.5	47.2
H46	3.4	52.6	6.1	5.3	47.5
H50	6.1	23.4	0.6	0.5	48.4
H22	6.5	42.7	2.9	2.5	48.8
H11	9.0	77.3	2.0	1.7	49.3
H13	5.5	22.3	1.7	1.5	49.3
H3	4.0	22.8	3.1	2.7	49.9
H1	2.6	13.9	3.6	3.1	51.1
H25	2.3	25.0	1.9	1.6	51.5
H14	15.1	36.0	1.4	1.2	52.8
H6	5.0	23.3	1.8	1.6	53.3
H9	3.2	24.5	1.8	1.5	53.7
H30	4.9	19.8	0.9	0.7	54.2
H51	2.9	12.9	1.7	1.5	54.7
H45	7.1	44.9	2.5	2.2	54.7
H53	6.4	27.3	3.9	3.4	55.9
H34	3.3	62.1	3.2	2.7	56.3
H37	4.2	15.1	2.7	2.3	56.4
H52	9.2	26.6	11.0	9.5	56.5
H28	4.2	24.4	1.3	1.1	57.2
H2	4.6	20.3	4.0	3.5	57.6
H27	7.8	24.8	0.9	0.8	58.0
H32	5.5	46.8	2.0	1.7	58.3
H35	1.4	17.2	2.9	2.5	58.6
H33	4.6	22.1	1.7	1.5	60.4
H29	4.6	15.5	0.6	0.5	60.5
H31	4.6	25.0	7.7	6.7	60.7
H36	2.0	27.2	3.1	2.7	66.0
H4	0.5	10.4	1.6	1.4	69.9

TABLE A.3: Continuation of table A.2. Principal characteristics of the mapped blocks

A.1.3 Lake East

Lake East					
Name	**Lenght**	**Perimeter**	**Height (m)**	**Calculated height**	**Angle**
L8	1.29	8.261	1.175	1.01757985	28.62
L9	1.33	8.429	1.119	0.96908243	28.62
L12	4.75	13.08	0.53989	0.46755846	29.48
L19	1.72	7.994	3.073	2.66129607	32.75
L7	3.65	10.358	1.137	0.98467088	35.85
L15	1	6.835	3.298	2.85615178	35.91
L2	0.6	10.845	0.839888	0.72736434	37.75
L21	1.25	6.602	0.700704	0.60682746	38.86
L10	0.74	9.028	0.749193	0.64882017	39.88
L11	2.33	13.782	0.589724	0.51071597	40.67
L16	5.63	17.007	1.429	1.2375503	41.65
L18	0.73	5.15	0.507659	0.43964559	42.39
L17	1.48	9.325	1.045	0.90499655	42.78
L5	5.43	13.466	0.565484	0.48972351	42.9
L6	5.46	19.614	0.83585	0.72386733	44.54
L20	2.22	7.473	2.974	2.57555955	45.12
L22	2.06	7.42	1.113	0.96388627	45.27
L3	5.53	16.771	0.836848	0.72473163	45.57
L4	6.19	28.367	1.533	1.32761694	46.04
L13	5.32	40.752	0.549599	0.4759667	49.11
L1	4.23	24.305	0.311437	0.26971235	49.84
L14	8.42	23.347	0.549599	0.4759667	52.76

TABLE A.4: Principal characteristics of the mapped blocks.

A.2 Failed Blocks

A.2.1 Handegg

Handegg					
Name	**Lenght**	**Perimeter**	**Height (m)**	**Calculated height**	**Angle**
T4	4.4	18.1	3.2	3.2	35.0
T5	17.0	93.8	2.2	2.2	40.0
T7	3.7	19.1	1.1	0.9	42.0
T2	12.0	33.4	0.9	0.8	43.0
T3	2.2	16.1	1.3	1.3	43.0
T8	3.8	13.9	0.8	0.7	46.0
T11	6.3	30.7	0.7	0.6	48.0
T12	2.7	22.1	1.4	1.2	52.0
T13	5.0	17.4	0.5	0.4	52.0
T6	9.6	32.8	1.7	1.5	54.0
T9	3.8	32.7	1.8	1.6	54.0
T10	13.7	49.2	3.9	3.4	55.0
T1	8.0	40.6	1.3	1.1	57.0

TABLE A.5: Principal characteristics of the mapped failed blocks

A.2.2 Lake East

Lake East					
Name	**Lenght**	**Perimeter**	**Height (m)**	**Calculated height**	**Angle**
L2	2.0	13.3	1.1	1.0	35.0
L3	2.6	20.9	1.3	1.1	43.0
L1	5.5	13.5	0.8	0.7	43.0

TABLE A.6: Principal characteristics of the mapped failed blocks

Appendix B

Code Results

B.1 Crack Length

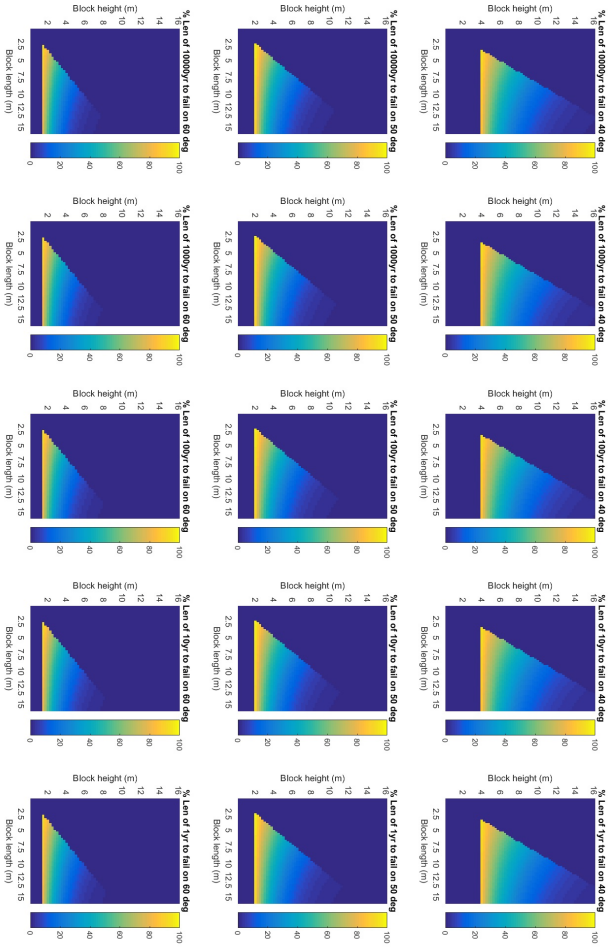

FIGURE B.1: Full range of results for crack length, the plots show the crack opening for different years and angles

B.2 Crack Opening

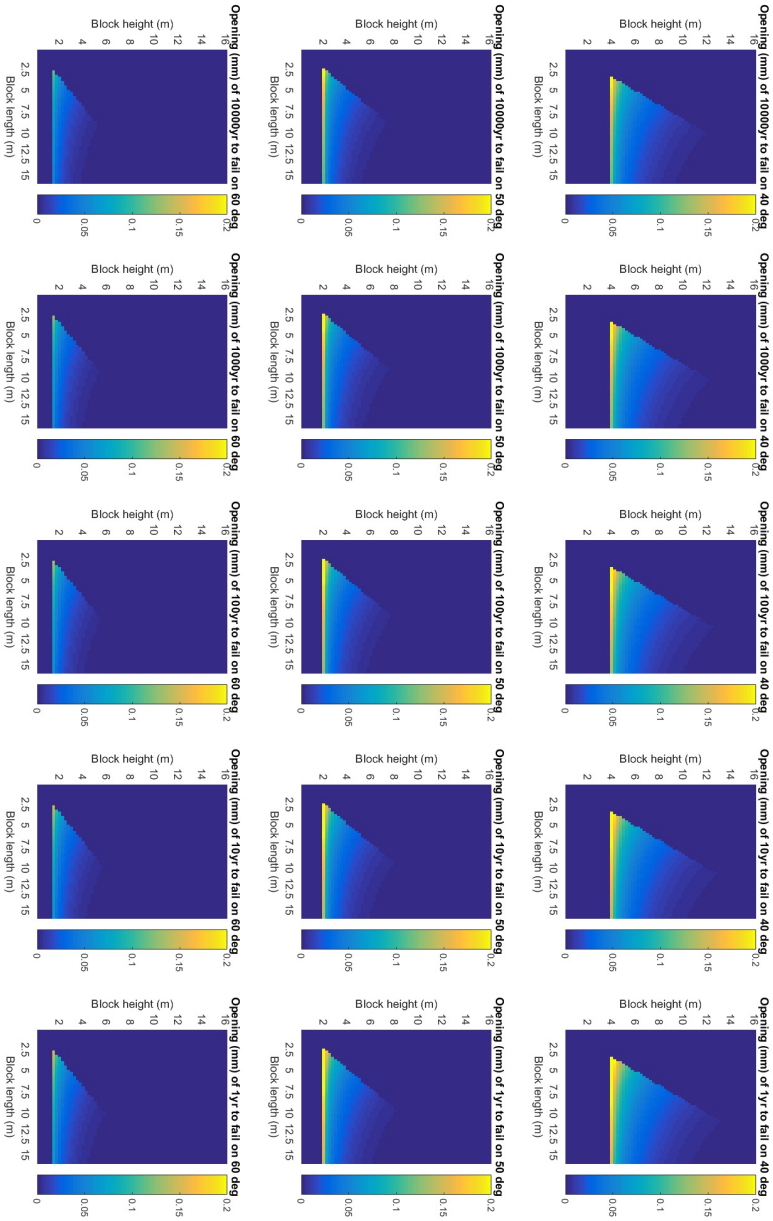

FIGURE B.2: Full range of results for crack opening, the plots show the crack opening for different years and angles

Appendix C

Matlab Code

```
close all
clear variables
clc

set(0,'defaulttextinterpreter','Latex');
%% 1 Inputs
%
```

```
%% Block variables
B.l= 5;                 % (meter) lenght of the base.
B.h=5;                    % (meter) height of the B.
B.d= 40;                  % (degrees) diF angle of failure plane

B.phi=30; %49             % (degrees) typical value for angle of internal friction *
    phi
B.C= 20*10^3;             % (Pa= N/m^2 = kg/m*s^2 = J/m^3) cohesion
B.density = 2670;         % (kg/m^3) density of granite %Schneeberger 2017 Table 2.6
B.gravity = 9.81;         % (m/s^2)
B.tens_strength=10*10^6;  % (Pa) Tensile strength of Granite
B.k1_critical = 1.5*10^6; % (MN/m^1.5) Critical stress factor of the granite. If
    this value is overcome then the crack develops
B.cl_e_prop = 0.01;       % edge crack length as proportion of block height.
B.cl_e = B.h*B.cl_e_prop;
B.cl_c=0;                 % center crack


%%% Field data
%
%  %Import the Existing blocks
%         % Import the data
%         [~, ~, raw] = xlsread('E:\Documents\UZ\Courses\Master Arbeit\Compile
    blocks.xlsx','Tabelle2','A5:E99');
%
%         %Kerry file
%         %[~, ~, raw] = xlsread('D:\03 MSc\2018\Zapatorres\Compile blocks.xlsx','
    Tabelle2','A5:E99');
%         raw(cellfun(@(x) ~isempty(x) && isnumeric(x) && isnan(x),raw)) = {''};
%         cellVectors = raw(:,1);
%         raw = raw(:,[2,3,4,5]);
%
%         % Create output variable
%         data = reshape([raw{:}],size(raw));
%
%         % Create table
%         Compileblocks = table;
%
%         % Allocate imported array to column variable names
%         Compileblocks.Name = cellVectors(:,1);
%         Compileblocks.Dipangle = data(:,1);
%         Compileblocks.Length = data(:,2);
%         Compileblocks.Height = data(:,3);
%         Compileblocks.PerimeHerbasearea = data(:,4);
%
%         % Clear temporary variables
%         clearvars data raw cellVectors;
%
```

```
% %Import the non existing blocks
%          % Import the data
%         [~, ~, raw] = xlsread('E:\Documents\UZ\Courses\Master Arbeit\Compile
    Non_e_blocks.xlsx','Tabelle2','A5:E20');
%          %Kerry file
%         %[~, ~, raw] = xlsread('D:\03 MSc\2018\Zapatorres\Compile Non_e_blocks.
    xlsx','Tabelle2','A5:E20');
%         raw(cellfun(@(x) ~isempty(x) && isnumeric(x) && isnan(x),raw)) = {''};
%         cellVectors = raw(:,1);
%         raw = raw(:,[2,3,4,5]);
%
%         % Create output variable
%         data = reshape([raw{:}],size(raw));
%
%         % Create table
%         CompileNoneblocks1 = table;
%
%         % Allocate imported array to column variable names
%         CompileNoneblocks1.Name = cellVectors(:,1);
%         CompileNoneblocks1.Dipangle = data(:,1);
%         CompileNoneblocks1.Length = data(:,2);
%         CompileNoneblocks1.Height = data(:,3);
%         CompileNoneblocks1.PerimeHerbasearea = data(:,4);
%
%         % Clear temporary variables
%         clearvars data raw cellVectors;
%
%% Thermal model variables
%if we need it, calculate the thermal model, otherwise load the data files
T.Thermal_dz = 0.025; %vertical resolution of thermal model - in meters
%[T, Tvar] = Thermal_model(T.Thermal_dz)

%load('D:\03 MSc\2018\Zapatorres\Tvar.mat');                                    %
    Kerry computer file
load('E:\Documents\UZ\Courses\Master Arbeit\Matlab\Simple block\Tvar.mat');     %
    Marco computer File
T.Tvar = Tvar; clear Tvar


%% Charles Law variables
C.A=1*10^-3;   %m/s Avro granite . B?ckstr?m et all 2008... referenced from Ko and
    Kemney(2011) p17
C.n= 48 ;      %Stress corrosion index. B?ckstr?m et all 2008 Table 2

%% Solver variables
S.yr = 365*24*60*60;        % Year in seconds
S.kyr = 1000*S.yr;          % K years
S.maxIter = 100000;         % Number max of iterations
S.minDT = 1;
S.maxDT = 10^9*S.yr;
S.initialDT = 0.1*S.yr;
S.time = 0;
S.mm = 0.001;
S.propEst = 1*S.mm;     %this is the distance we'd like our crack to propagate (m)

%Switch the solvers
%S.plotInt = 400;        %Defined block parameters in B.h and B.l
S.plotInt = nan;         %interval for plotting results (in iterations)

%% Paris Law variables

P.a0= 0.41*(10^-3);%4.1*10-7; %2.3*10^-3              %mm Initial crack lenght,
    related to grain diameter
P.m=0.6; %60 From table 1 EPPES          %Subcritical crack growth index = Paris law
    exponent
P.delAlpha=3*10^-5;%From table 1 EPPES  %C^-1  Characteristic thermal expansion
    difference
P.E= 50.6*(10^9);  %From table 1 EPPES  %Pa Young modulus Granite
if exist('Tvar', 'var')
    T.Tvar = T.Tvar;
else
    T.Tvar= 29;                         %Celcius T surf max - T infinitus
```

```
end

P.v=     0.33;                          %Rock Poisson's ratio   %Schneeberger 2017
    Table 2.6
P.dg = 0.7*10^-3; %7*10^-3;             % diameter of the grain  %From table 1 EPPES
P.Kc = (2.16 *10^6);                    %Granite fracture toughness

P.B=1-P.m/2;                            %Eppes text for Eq. 5 m = subcritical growth
    index
P.c= P.dg*P.Kc^-P.m;                    %Eppes table 1. Paris law coefficient
P.G = P.E/(1-P.v^2);                    %bulk modulus


%% ------------------------------------------------------------------------

%%Calculations
%
    %-------------------------------------------------------------------------

%if we don't want to plot the evolution of a single crack, then run a
%parametric search
if isnan(S.plotInt)
    %Load a list of parameters
    d_Var = 40:10:60;
    l_Var = 0.25:0.25:12;   %[0.2 0.4 0.6 0.8 1];%1:32;  %1:10;
    h_Var = 0.25:0.25:12;   %[0.2 0.4 0.6 0.8 1]; %[0.01 1 2 3 4 5 6 7 8 9 10];
        %1:10;
else
    d_Var = B.d;
    l_Var = B.l;
    h_Var = B.h;
end

steps = length(d_Var)*length(l_Var)*length(h_Var);

f = waitbar(0,'1','Name','Calculating cracks...',...
    'CreateCancelBtn','setappdata(gcbf,''canceling'',1)');

setappdata(f,'canceling',0);
cnt = 0;
critRec = [];
for i = 1:length(d_Var)
    for j = 1:length(l_Var)
        for k = 1:length(h_Var)
            % Check for clicked Cancel button
            if getappdata(f,'canceling')
                break
            end
            cnt = cnt+1;
            % Update waitbar and message
            waitbar(cnt/steps,f,sprintf('%s%2.1f%s%2.1f%s%2.1f','Phi = ', d_Var(i),
                'deg Len = ', l_Var(j), 'm Height = ', h_Var(k)))
            B.d = d_Var(i);
            B.l =   l_Var(j);
            B.h =   h_Var(k);
            [crackSummary(i,j,k).dt, crackSummary(i,j,k).k1_e, crackSummary(i,j,k).
                delCrack, crackSummary(i,j,k).charlesProp, crackSummary(i,j,k).cl_e,
                 crackSummary(i,j,k).time, crackSummary(i,j,k).exitCode] = crackIt(B
                , T, C, P, S);
            %record if the crack successfully propagated
            if crackSummary(i,j,k).exitCode == 0
                %this has the indices of phi, length, height
                critRec = [critRec; i j k];
            end
        end
    end
end
%delete the waitbar
delete(f)

%if we don't want to plot the evolution of a single crack, then
```

```
%plot a summary of results
if isnan(S.plotInt)
    %plot all the info for the single block failure times
    singleBlockPlots(S, critRec, crackSummary, d_Var, l_Var, h_Var)
end


%%
    ------------------------------------------------------------------------------------------

%%Functions
%
    %-------------------------------------------------------------------------------------------


% Propagate a crack
function [dt, k1_e, delCrack, charlesProp, cl_e, time, exitCode] = crackIt(B, T, C,
    P, S)
    exitCode = 100;
    isTopple = checkTopple(B.d,B.h,B.l);
    %if the block isn't toppling
    if isTopple == 0
        %get the initial driving and resisting forces
        [sigma_d, sigma_rb, sigma_rt] = blockStability (B.phi, B.l, B.d, B.C, B.h, B
            .density, B.gravity, B.tens_strength, B.k1_critical, B.cl_e, B.cl_c);
        %get the actual tensile stress in the intact rock below the tension crack
        sigma_t = sigma_d-sigma_rb;
        %if the block is stable
        if (sigma_rb + sigma_rt) > sigma_d
            %if the stability depends on the tension crack
            if (sigma_d - sigma_rb) > 0
                %calculate crack propagation with time
                i = 1;
                dt = S.initialDT;
                %record the starting day of the year
                DoY = 1;
                %get the initial crack length
                cl_e(i) = B.cl_e;
                %get the initial crack opening
                delCrack(i) = getCrackOpening(B.h,cl_e(i),sigma_t,P.G);

                %get the initial time
                time(i) = S.time;
                %while the crack length is less than the block height and the max
                %iterations haven't been reached
                while cl_e(i) < B.h && i <= S.maxIter
                    %re-calculate the driving and resisting forces with the new
                        crack geometry
                    [sigma_d, sigma_rb, sigma_rt] = blockStability (B.phi, B.l, B.d,
                        B.C, B.h, B.density, B.gravity, B.tens_strength, B.
                        k1_critical, cl_e(i), B.cl_c);
                    %get the actual tensile stress in the intact rock below the
                        tension crack
                    sigma_t = sigma_d-sigma_rb;
                    %calculate the stress intensity factor at the crack tip
                    k1_e(i)= KI_edgeCrack(B.h,cl_e(i),sigma_t);



                    %if the stress intensity is less than the critical
                    if k1_e(i) <= B.k1_critical
                        %calculate the rate of crack growth (da/dt) based on Paris
                            law
                        %to do this we have to calculate the number of daily cycles
                            in this time step
                        %and round down to ensure we have an integer
                        N = floor(dt(i)/(24*60*60));

                        if sum(size(T.Tvar)) == 2
                            B.Thermal_dz = 1000000;
                            DoYrec = ones(N,1);
                        else
```

```
            %get the temperature variation at this depth / time
            DoYrec = zeros(N,1);
            DoYrec(1,1) = DoY;
            for j = 2:N
                if DoY == 365
                    DoY = 1;
                else
                    DoY = DoY+1;
                end
                DoYrec(j) = DoY;
            end
        end

        %calculate the change in length
        %da_P =  parisCalc(a0,B,delAlpha,v,m,c, E,N, Tvar, DoYrec,
            Thermal_dz);
        %find the closest depth in Tvar
         T_Zind = ceil(P.a0/B.Thermal_dz);
         Tvar_ave = sum(T.Tvar(T_Zind, DoYrec))/N

        %note: here we're assuming the propagating crack is always
            one grain long
        %this is the effective length of the stress variation
        da_P =  paris_noIterCalc(P.dg,P.B,P.delAlpha,P.v,P.m,P.c, P.
            E,N, Tvar_ave);
        %calculate the mean rate of propagation for Paris law in
            this time step
        dadt_p = da_P / dt(i);

        %calculate the rate of crack growth (da/dt) based on Charles
             law
        [dadt_c] =  charlesCalc(C.A,k1_e(i),B.k1_critical,C.n);
        %Obtain the length based on the elapsed time
        da_C = dadt_c*dt(i);
        %Add the new crack lengths to the previous crack length
        cl_e(i+1) = cl_e(i)+ da_C + da_P;

        %calculate the crack opening
        delCrack(i+1) = getCrackOpening(B.h,cl_e(i+1),sigma_t,P.G);

        %record if Charles law is fastest
        charlesProp(i) = dadt_c > dadt_p;

        %plot the new result
        if ~isnan(S.plotInt)
            plotPropagation(i, dt, time, S.yr, cl_e, k1_e, B.h, B.
                k1_critical, charlesProp, S.plotInt, delCrack);
        end

        %calculate a new dt based on the rate of the previous
            propagation
        dt(i+1) = new_dt(dadt_c, dadt_p, dt(i), S.minDT, S.maxDT, S.
            propEst);

        %update the time
        time(i+1) = time(i)+dt(i+1);
        %update counter
        i = i+1;
    else
        %tidy up the last stress intensity value we over-ran
        k1_e(i) = B.k1_critical;
        charlesProp(i) = charlesProp(i-1);
        %here we could also calculate the critical crack length
        %%%%%% but how??

        %plot the new result
        if ~isnan(S.plotInt)
            plotPropagation(i, dt, time, S.yr, cl_e, k1_e, B.h, B.
                k1_critical, charlesProp, i, delCrack);
        end
        exitCode = 0;
        break
```

```
                end
            end

            factorOfSafety = (sigma_rb+sigma_rt)/sigma_d;   %Update the factor
                of safety
        else
            if ~isnan(S.plotInt)
                'the base of the block provides stability'
            end
            k1_e = nan;
            charlesProp = nan;
            dt = nan;
            cl_e = nan;
            delCrack = nan;
            time = nan;
            exitCode = 1;
        end
    else
        if ~isnan(S.plotInt)
            'the block is unstable'
        end
        k1_e = nan;
        charlesProp = nan;
        dt = nan;
        cl_e = nan;
        delCrack = nan;
        time = nan;
        exitCode = 2;
    end
else
    if ~isnan(S.plotInt)
        'the block toppled'
    end
    k1_e = nan;
    charlesProp = nan;
    dt = nan;
    cl_e = nan;
    delCrack = nan;
    time = nan;
    exitCode = 3;
end
end


%% Check if the block Topple
function [isTopple, angleToCoM] = checkTopple(d,H,l)
    angleToCoM = d + atand((H/2) / (l/2));
    if angleToCoM < 90 %(Toopling)
            isTopple = 0;
        else   % If the value of angleToCoM  is >90, nothing is calculated
            because toppling happens.
            isTopple = 1;
    end

end

%% Block stability
function [sigma_d, sigma_rb, sigma_rt] = blockStability (phi, l, d, C, H, density,
    gravity, tens_strength, k1_critical, cl_e, cl_c)
%function [sigma_d, sigma_rb, sigma_rt] = blockStability (p, l, d, C, H, density,
    gravity, tens_strength, k1_critical, cl_e, cl_c)
a=l*1;  %(Square meter) base area of the block

w=a*H*density*gravity; % weight of the block

[sigma_rb, sigma_d]= calcDrivingResistingStress(C,d,a,phi,w);  %Calculate if the
    block is stable or not.
%sigma_rb= resisting stress
%simga_d= driving stress
% if the driving stress is higher than the ressisting stress the block wil  fail.
```

```
sigma_dt = sigma_d-sigma_rb;   % remaining stress in the remaining intact rock rock
    from the base to the fisure
% driving stress - resisting stress from base
% if the driving force is greater than the basal resistance

if sigma_dt > 0  %then check the stress intensity on the tension crack tip(s)
    k1_e=KI_edgeCrack(H,cl_e,sigma_dt); %Stress intensity factor for the edge crack

    %and check if they're stable. We assume the kritical stress intensity
    %of granite is 1 500 000 MN/m^2, if this critical stres is overcomed,
    %then a failure happens.
    stable_crack_e = k1_e<k1_critical;
else
    %otherwise the cracks will be stable
    stable_crack_e = 1;

end
    tens_height = H - cl_e ; %Length of the block from the base to the bottom of the
        fisure.
    sigma_rt = tens_height*tens_strength*stable_crack_e; % If one of the componets
        is 0 then the equation turns in 0
end

%% Calculate the driving and resisting stresses
function [sigma_rb, sigma_d] =  calcDrivingResistingStress(C,d,a,phi,w)
    sigma_rb = C*a+(w*cosd(d)*tand(phi)); % Resisting stress of the block base
    sigma_d =w*sind(d); % Driving force
end


%% Stress Intensity factor KI (mode 1) for edge crack. Tada Hiroshi. The stress
    analysis of crack handbook. pg 52
%see equation for Edge crack in a plate under uniaxial stress

%this function calls the lower two
%came from Validate_stress_intensity_kl.m
function [KI]= KI_edgeCrack(H,cl_e,sig_dt)
    %method can be: 'Gross_Brown', 'TadaV1', 'TadaV2')
    Fa_b = getKI_F(cl_e, H, 'TadaV2');
    KI = getK1(sig_dt, cl_e, Fa_b);
end
%this one calculates the second factor of the equation
function F =  getKI_F(a, b, method)

    vecLen = max(length(a), length(b));
    if length(a) < vecLen
        a = repmat(a,1,vecLen);
    end
    if length(b) < vecLen
        b = repmat(b,1,vecLen);
    end

    a_b = a./b;

    switch method
        case 'Gross_Brown'
            max_a_b = 0.6;
            a_b = a_b(a_b <= max_a_b);
            a = a(a_b <= max_a_b);
            b = b(a_b <= max_a_b);
            if ~isempty(a_b)
                F = 1.22-0.231*(a_b)+(10.55*(a_b).^2)-(21.71*(a_b).^3)+(30.382*(a_b)
                    .^4);
            else
                F = nan;
            end
        case 'TadaV1'
            max_a_b = 0.99;
            a_b = a_b(a_b <= max_a_b);
            a = a(a_b <= max_a_b);
            b = b(a_b <= max_a_b);
            if ~isempty(a_b)
```

```
            F = 0.265.*(1-a_b).^4+((0.857+0.265.*a_b)./(1-a_b).^(3/2));
        else
            F=nan;
        end
    case 'TadaV2'
        max_a_b = 0.99;
        a_b = a_b(a_b <= max_a_b);
        a = a(a_b <= max_a_b);
        b = b(a_b <= max_a_b);
        if ~isempty(a_b)
            var = (pi.*a)./(2.*b);
            F = sqrt(1./var.*tan(var))...
                .*((0.752+2.02.*a_b+0.37.*(1-sin(var)).^3)...
                ./(cos(var)));
        else
            F=nan;
        end
end

end
%and this one calculates the stress dependance
function KI = getK1(sig_t, a, Fa_b)
    KI = sig_t.*sqrt(pi.*a).*Fa_b;
end


%% Charles law
%da/dt= A*(KI/KIc)^n; % Eq.(3) Charles law. From: Ko and Kemney 2011 (pg.
%2)

function [dadt] = charlesCalc(A,k1_e,k1_critical,n)
    logdadt=log10(A) + n*log10(k1_e/k1_critical);

    dadt = 10^logdadt;
end




%% Paris law (with daily iterations for temperature - slower!!)--- NOT PARIS LAW (
    Eppes) --- Is Crack Evolution per Stress cycle!!!!!----------



%%
function [dadN] = parisCalc(a0,B,delAlpha,v,m,c, E,N, Tvar, DoYrec, Thermal_dz)
    %check we have a full cycle
    if N > 1
        %record the initial length
        a_init = a0;
        %propagate the crack through a number of cycles
        for i = 1:N
            %find the closest depth in Tvar
            T_Zind = ceil(a0/Thermal_dz);
            delSigMax = delAlpha*(E/1000000)*Tvar(T_Zind,DoYrec(i))/(1-v);  %Eppes
                text for Eq. 3; Emod should be in MPa for this calculation
            C1 = c * delSigMax^m*pi^(m/2);        %Eppes under Eq. 5 m; m = Effective
                stress amplitude

            a_len(i) = (a0^B + B*C1*1)^(1/B);
            a0 = a_len(i);
        end
        %just get the final change in length in (m)
        dadN = (a_len(i) - a_init)/1000;
    else
        dadN = 0;
    end
end

%% Paris law (without iterations)
function [dadN] = paris_noIterCalc(a0,B,delAlpha,v,m,c, E,N, Tvar_ave)
```

```
    %check we have a full cycle
    if N > 1
        %propagate the crack for a given a number of cycles
        %we assume everything is otherwise constant

        delSigMax = delAlpha*(E/1000000)*Tvar_ave/(1-v);  %Eppes text for Eq. 3;
            Emod should be in MPa for this calculation
        C1 = c * delSigMax^m*pi^(m/2);        %Eppes under Eq. 5 m; m = Effective
            stress amplitude

        a_len = (a0^B + B*C1*N)^(1/B);
        %just get the final change in length in (m)

        dadN = a_len/1000;
    else
        dadN = 0;
    end
end

%% calculate the time steps for the model
function [dt] = new_dt(dadt_c, dadt_p, dt_i, minDT, maxDT, propEst)
    %the minimum functional DT (anything faster is almost dynamic)
    %first find the faster rate of Charles law or Paris law
    max_dadt = max(dadt_c, dadt_p);
    %get the change in propagation rate from the previous step
    log10_ddt_i = log10(propEst/max_dadt) - log10(dt_i);
    %then update the time step to get approx (propRateEst)m
    %propagation in the next step
    if log10_ddt_i > 1
        dt = 10^(log10(dt_i)+log10_ddt_i*0.1);
    elseif log10_ddt_i < 1
        dt = 10^(log10(dt_i)-log10_ddt_i*0.1);
    else
        dt = propEst/max_dadt;

        %else
        %    dt = 10^(log10(dt_i)-2);
        %end
    end
    dt = max(dt, minDT);
    dt = min(dt, maxDT);
end

%% plot the propagation of the crack
function plotPropagation(i, dt, time, yr, cl_e, k1_e, H, k1_critical, charlesProp,
    plotInt, delCrack)
    %plot every XXth result to speed up the calc
    if mod(i,plotInt)==0 || plotInt == i
        %if the figure doesn't exist
        if ~ishandle(1)
            figure(1)
            subplot(5,1,1)        % add first plot in 5 x 1 grid
            title('log10(dt (in years)) vs. iteration')
            hold on
            subplot(5,1,2)        % add second plot in 5 x 1 grid
            title('edge crack length (% block height) vs. yr')
            hold on
            subplot(5,1,3)        % add third plot in 5 x 1 grid
            title('edge crack stress intensity (% K1c) vs. yr')
            hold on
            subplot(5,1,4)        % add fourth plot in 5 x 1 grid
            title('Crack opening vs. yr')
            hold on
            subplot(5,1,5)        % add fifth plot in 5 x 1 grid
            title('Variation from mean crack extension vs. yr')
            hold on
        end
        %set the plot point size
        ptsize = 4;
        xes = 1:i;
        subplot(5,1,1)        % add first plot in 3 x 1 grid
```

```
        scatter(xes( charlesProp)       ,log10(dt( charlesProp)/yr)        ,ptsize, '
            r', 'filled')
        %plot(xes,log10(dt/yr),'r')
        scatter(xes(~charlesProp)       ,log10(dt(~charlesProp)/yr)        ,ptsize, '
            k', 'filled')

        subplot(5,1,2)       % add second plot in 3 x 1 grid
        scatter(time( charlesProp)/yr  ,cl_e( charlesProp)./H        *100 ,ptsize, '
            r', 'filled')       % plot using + markers
        scatter(time(~charlesProp)/yr  ,cl_e(~charlesProp)./H        *100 ,ptsize, '
            k', 'filled')

        subplot(5,1,3)       % add second plot in 3 x 1 grid
        scatter(time( charlesProp)/yr  ,k1_e( charlesProp)/k1_critical*100,ptsize, '
            r','filled')
        scatter(time(~charlesProp)/yr  ,k1_e(~charlesProp)/k1_critical*100,ptsize, '
            k', 'filled')

        subplot(5,1,4)       % add second plot in 3 x 1 grid
        scatter(time( charlesProp)/yr  ,delCrack( charlesProp),ptsize, 'r','filled')
        scatter(time(~charlesProp)/yr  ,delCrack(~charlesProp),ptsize, 'k', 'filled'
            )

        drawnow
    end
    if plotInt > 1000 && plotInt == i
        subplot(5,1,5)
        xes = 1:i;
%         del_time = time(find(~charlesProp, 1,'last')) - time(1000);
%        del_cl_e = cl_e(find(~charlesProp, 1,'last')) - cl_e(1000);
        del_time = time(10000) - time(1000);
        del_cl_e = cl_e(10000) - cl_e(1000);
        ave_cl_e_per_time = del_cl_e/del_time;
        cl_e_tiepoint = cl_e(1000)-time(1000)*ave_cl_e_per_time;
        cl_e_var = cl_e-cl_e_tiepoint-time*ave_cl_e_per_time;
        plot(xes(~charlesProp), cl_e_var(~charlesProp), 'k');
        hold on
        plot(xes(charlesProp), cl_e_var(charlesProp), 'r');
    end
end

%% plot the summary of crack propagation for different geometries

function singleBlockPlots(S, critRec, crackSummary, d_Var, l_Var, h_Var)
    % Extract the crack geometry details
    %set times to failure to investigate
    S.TTFs = 4;
    TTF = nan(size(critRec, 1));
    LTF = nan(size(critRec, 1),S.TTFs+1);
    OTF = nan(size(critRec, 1),S.TTFs+1);
    for i = 1:size(critRec, 1)
        time_tmp = crackSummary(critRec(i,1),critRec(i,2),critRec(i,3)).time;
        length_tmp = crackSummary(critRec(i,1),critRec(i,2),critRec(i,3)).cl_e;
        opening_tmp = crackSummary(critRec(i,1),critRec(i,2),critRec(i,3)).delCrack;
        %get the time to failure
        TTF(i) = time_tmp(end);
        %and crack lengths for various times prior to failure
        for j = 1:S.TTFs+1
            if ~isempty(find(TTF(i) - time_tmp(:) > S.yr*10^(j-1), 1,'last'))
                LTF(i,j) = length_tmp(find(TTF(i) - time_tmp(:) > S.yr*10^(j-1), 1,'
                    last'));
                OTF(i,j) = opening_tmp(find(TTF(i) - time_tmp(:) > S.yr*10^(j-1), 1,
                    'last'));
            end
        end
        clear time_tmp length_tmp
    end
    %
        %-----------------------------------------------------------------------

    % plot images for all geometries at a given angle for a given time to failure
```

```
%
    %-------------------------------------------------------------------------


%make a grid to plot on
[xq,yq] = meshgrid(l_Var,h_Var);
figure(2)
cnt = 0;
%for one angle
ds_tmp = 1:ceil(length(d_Var)/5):length(d_Var);
TTFs_tmp = 0:S.TTFs;
for i = ds_tmp
    for k = 1:length(TTFs_tmp)
        j = length(TTFs_tmp)+1-k;
        cnt = cnt+1;
        %extract the data for this plot
        l_tmp = l_Var(critRec(critRec(:,1) == i, 2))';
        h_tmp = h_Var(critRec(critRec(:,1) == i, 3))';
        LTF_tmp = LTF(critRec(:,1) == i,j);
        LTFpercent_tmp = LTF_tmp./h_tmp *100;
        %grid the data
        vq = griddata(l_tmp, h_tmp', LTFpercent_tmp,xq,yq);

        subplot(length(ds_tmp),length(TTFs_tmp),cnt)       % add first plot in 3
            x 1 grid
        title(sprintf('%s%1.0f%s%1.0f%s', '% Len of ', 10^TTFs_tmp(j), 'yr to
            fail on ', d_Var(i),' deg'))
        hold on
        xlabel('Block length (m)');
        ylabel('Block height (m)');
        xticks = 5:5:length(l_Var);  %adjust as appropriate, positive integers
            only
        xlabels = l_Var(5:5:length(l_Var));  %time labels
        set(gca, 'XTick', xticks, 'XTickLabel', xlabels);
        yticks = 2:2:length(h_Var);  %adjust as appropriate, positive integers
            only
        ylabels = l_Var(2:2:length(h_Var));  %time labels
        set(gca, 'YTick', yticks, 'YTickLabel', ylabels);
        imagesc(vq, [0 100])
        axis square
        colorbar
    end
end
%
    %-------------------------------------------------------------------------

% plot increase in crack length for all geometries at a given angle for a given
    time to failure
%
    %-------------------------------------------------------------------------


%make a grid to plot on
[xq,yq] = meshgrid(l_Var,h_Var);
figure(3)
cnt = 0;
%for one angle
ds_tmp = 1:ceil(length(d_Var)/5):length(d_Var);
for i = ds_tmp
    j = S.TTFs+1;
    %extract the data for this plot
    l_tmp = l_Var(critRec(critRec(:,1) == i, 2))';
    h_tmp = h_Var(critRec(critRec(:,1) == i, 3))';
    LTF_tmp = LTF(critRec(:,1) == i,j);
    LTFpercent_ref = LTF_tmp;%./h_tmp *100;

    %for each time to failure
    for k = 1:S.TTFs
        j = S.TTFs+1 - k;
        cnt = cnt+1;
        %extract the data for this plot
        l_tmp = l_Var(critRec(critRec(:,1) == i, 2))';
```

```
            h_tmp = h_Var(critRec(critRec(:,1) == i, 3))';
            LTF_tmp = LTF(critRec(:,1) == i,j);
            LTFpercent_tmp = LTF_tmp;%./h_tmp *100;
            LTFpercentgrowth_tmp = LTFpercent_tmp - LTFpercent_ref;
            %grid the data
            vq = griddata(l_tmp, h_tmp', LTFpercentgrowth_tmp,xq,yq);
            LTFpercent_ref = LTFpercent_tmp;

            subplot(length(ds_tmp),S.TTFs,cnt)       % add first plot in 3 x 1 grid
            title(sprintf('%s%1.0f%s%1.0f%s%1.0f%s', 'Crack growth (m) from ', 10^j,
                'yr to ', 10^(j-1),'yr for fail on ', d_Var(i),' deg'))
            hold on
            xlabel('Block length (m)');
            ylabel('Block height (m)');
            xticks = 5:5:length(l_Var); %adjust as appropriate, positive integers
                only
            xlabels = l_Var(5:5:length(l_Var)); %time labels
            set(gca, 'XTick', xticks, 'XTickLabel', xlabels);
            yticks = 2:2:length(h_Var); %adjust as appropriate, positive integers
                only
            ylabels = l_Var(2:2:length(h_Var)); %time labels
            set(gca, 'YTick', yticks, 'YTickLabel', ylabels);
            imagesc(vq, [0 1.2])
            axis square
            colorbar
        end
    end

    %
        %-----------------------------------------------------------------------

    % plot images for all geometries at a given angle for a given time to failure
    %
        %-----------------------------------------------------------------------


    %make a grid to plot on
    [xq,yq] = meshgrid(l_Var,h_Var);
    figure(4)
    cnt = 0;
    %for one angle
    ds_tmp = 1:ceil(length(d_Var)/5):length(d_Var);
    TTFs_tmp = 0:S.TTFs;
    for i = ds_tmp
        for k = 1:length(TTFs_tmp)
            j = length(TTFs_tmp)+1-k;
            cnt = cnt+1;
            %extract the data for this plot
            l_tmp = l_Var(critRec(critRec(:,1) == i, 2))';
            h_tmp = h_Var(critRec(critRec(:,1) == i, 3))';
            OTF_tmp = OTF(critRec(:,1) == i,j);
            OTFpercent_tmp = OTF_tmp;
            %grid the data
            vq = griddata(l_tmp, h_tmp', OTFpercent_tmp,xq,yq);

            subplot(length(ds_tmp),length(TTFs_tmp),cnt)       % add first plot in 3
                x 1 grid
            title(sprintf('%s%1.0f%s%1.0f%s', 'Opening (mm) of ', 10^TTFs_tmp(j), '
                yr to fail on ', d_Var(i),' deg'))
            hold on
            xlabel('Block length (m)');
            ylabel('Block height (m)');
            xticks = 5:5:length(l_Var); %adjust as appropriate, positive integers
                only
            xlabels = l_Var(5:5:length(l_Var)); %time labels
            set(gca, 'XTick', xticks, 'XTickLabel', xlabels);
            yticks = 2:2:length(h_Var); %adjust as appropriate, positive integers
                only
            ylabels = l_Var(2:2:length(h_Var)); %time labels
            set(gca, 'YTick', yticks, 'YTickLabel', ylabels);
            imagesc(vq*1000, [0 1.5*10^-1])
            axis square
```

```
        colorbar
    end
end

%
    %-------------------------------------------------------------------------

% plot increase in crack opening for all geometries at a given angle for a given
     time to failure
%
    %-------------------------------------------------------------------------


%make a grid to plot on
[xq,yq] = meshgrid(l_Var,h_Var);
figure(5)
cnt = 0;
%for one angle
ds_tmp = 1:ceil(length(d_Var)/5):length(d_Var);
for i = ds_tmp
    j = length(TTFs_tmp);
    %extract the data for this plot
    l_tmp = l_Var(critRec(critRec(:,1) == i, 2))';
    h_tmp = h_Var(critRec(critRec(:,1) == i, 3))';
    OTF_tmp = OTF(critRec(:,1) == i,j);
    OTFpercent_ref = OTF_tmp;%./h_tmp *100;

    %for each time to failure
    for k = 1:S.TTFs
        j = S.TTFs+1 - k;
        cnt = cnt+1;
        %extract the data for this plot
        l_tmp = l_Var(critRec(critRec(:,1) == i, 2))';
        h_tmp = h_Var(critRec(critRec(:,1) == i, 3))';
        OTF_tmp = OTF(critRec(:,1) == i,j);
        OTFpercent_tmp = OTF_tmp;%./h_tmp *100;
        OTFpercentgrowth_tmp = OTFpercent_tmp - OTFpercent_ref;
        %grid the data
        vq = griddata(l_tmp, h_tmp', OTFpercentgrowth_tmp,xq,yq);
        OTFpercent_ref = OTFpercent_tmp;

        subplot(length(ds_tmp),S.TTFs,cnt)       % add first plot in 3 x 1 grid
        title(sprintf('%s%1.0f%s%1.0f%s%1.0f%s', 'Crack opening (mm) from ', 10^
            j, 'yr to ', 10^(j-1),'yr for fail on ', d_Var(i),' deg'))
        hold on
        xlabel('Block length (m)');
        ylabel('Block height (m)');
        xticks = 5:5:length(l_Var);  %adjust as appropriate, positive integers
            only
        xlabels = l_Var(5:5:length(l_Var));  %time labels
        set(gca, 'XTick', xticks, 'XTickLabel', xlabels);
        yticks = 2:2:length(h_Var);  %adjust as appropriate, positive integers
            only
        ylabels = l_Var(2:2:length(h_Var));  %time labels
        set(gca, 'YTick', yticks, 'YTickLabel', ylabels);
        imagesc(vq*1000, [0 1*10^-1])
        axis square
        colorbar
    end
end

%
    %-------------------------------------------------------------------------

% plot images for all exit codes at a given angle for a given time to failure
%
    %-------------------------------------------------------------------------


%make a grid to plot on
figure(6)
colormap(jet(5))
```

```
    cnt = 0;
    for i = ds_tmp
        cnt = cnt+1;
        %extract the data for this plot
        exitCode_tmp = [crackSummary(i,:,:).exitCode];
        %reshape the data to produce a grid again
        exitCode_tmp = reshape(exitCode_tmp, size(crackSummary, 2), size(
            crackSummary, 3))';
        %change 100 to -1
        exitCode_tmp = exitCode_tmp+1;
        exitCode_tmp(exitCode_tmp == 101) = 6;

        subplot(length(ds_tmp),1,cnt)       % add first plot in 3 x 1 grid
        title(sprintf('%s%1.0f%s', 'Stability modes for ', d_Var(i),' deg'))
        hold on
        xlabel('Block length (m)');
        ylabel('Block height (m)');
        xticks = 5:5:length(l_Var); %adjust as appropriate, positive integers only
        xlabels = l_Var(5:5:length(l_Var)); %time labels
        set(gca, 'XTick', xticks, 'XTickLabel', xlabels);
        yticks = 2:2:length(h_Var); %adjust as appropriate, positive integers only
        ylabels = l_Var(2:2:length(h_Var)); %time labels
        set(gca, 'YTick', yticks, 'YTickLabel', ylabels);
        image(exitCode_tmp)
        axis square
    end

        labels = {'Crack propagation to failure','Base is stable','block is unstable
            ','Toppling','dunno'};
        lcolorbar(labels,'fontweight','bold');

    %plot the FIELD DATA blocks.
         hold on
         cnt=0;
         for i = ds_tmp
             cnt=cnt+1;
             subplot(length(ds_tmp),1,cnt)       % add first plot in 3 x 1 grid

            %Scatter multiplied by 4 to get the same scale as image.
               % less than <40
               if cnt==1
                % Existing block
                scatter(Compileblocks.Length(1:19)*4,Compileblocks.Height(1:19)
                    *4,19)
                % Non existing block
                scatter(CompileNoneblocks1.Length(1:2)*4,CompileNoneblocks1.Height
                    (1:2)*4,19,'r')

                % Between < 40- 50
                 elseif cnt==2
                 % Existing block
                 scatter(Compileblocks.Length(20:56)*4,Compileblocks.Height(20:56)
                     *4,19)
                % Non existing block
                 scatter(CompileNoneblocks1.Length(3:10)*4,CompileNoneblocks1.
                     Height(3:10)*4,19,'r')

                 %Between < 50- 60
                elseif cnt==3
                % Existing block
                scatter(Compileblocks.Length(57:88)*4,Compileblocks.Height(57:88)
                    *4,19)
               % Non existing block
                scatter(CompileNoneblocks1.Length(11:end)*4,CompileNoneblocks1.
                    Height(11:end)*4,19,'r')
               end
         hold off
         end

end
```

```
%% Calculate the crack aperture
function [delCrack]= getCrackOpening(H,cl_e,sig_dt,E)
    %method can be: 'Gross_Brown', 'TadaV1', 'TadaV2')
    Va_b=getFormula_V(cl_e,H,'V_2');
    delCrack=getDelta(sig_dt,cl_e,Va_b,E);
end

function V=getFormula_V(a,b,method)
vecLen=max(length(a), length (b));
    if length(a)<vecLen
        a= repmat (a,1,vecLen);
    end

    if length (b)<vecLen
        b= repmat (b,1,vecLen);
    end

    a_b=a./b;

    switch method

      case 'V_1'
        % From: The stress analysis of cracks Handbook, Tada 2000.Crack opening at
            the edge (pag.53)
        %Gross 0.5% accuracy for 0.2< a/b <0.7
        max_a_b = 0.99;
        a_b=a_b(a_b <= max_a_b);
        a = a(a_b <= max_a_b);
        b = b(a_b <= max_a_b);

        if ~isempty(a_b)
            V=(1.46+3.42.*(1-cos(pi.*a_b/2))).*(cos(pi.*a_b/2).^2);
        else
            V=nan;
        end

      case 'V_2'
          %1%accuracy for any a/b
          max_a_b=1;
          a_b=a_b(a_b <= max_a_b);
          a = a(a_b <= max_a_b);
          b = b(a_b <= max_a_b);
         if ~isempty(a_b)
            V=(a_b./(1-a_b).^2).*(0.99-a_b.*(1-a_b).*(1.3-1.2*a_b+0.7*(a_b).^2));
         else
            V=nan;
         end
    end
end

function delta=getDelta(sig_t,a,Va_b,E1)
delta=4.*sig_t.*a.*Va_b./E1;
end
```

Bibliography

Abrecht, Jürgen (1994). "Geologic units of the Aar massif and their pre- Alpine rock associations : a critical review". In: *Schweizerische Mineralogische Und Petrographische Mitteilungen = Bulletin Suisse De Minéralogie Et Pétrographie = Bollettino Svizzero Di Mineralogia E Petrografia*. URL: http://dx.doi.org/10.5169/seals-56328{\%}0ANutzungsbedingungen.

Adhikary, D P et al. (1997). *A Study of the Mechanism of Flexural Toppling Failure of Rock Slopes*. Tech. rep. 2, pp. 75–93. URL: https://www2.cose.isu.edu/{~}crosby/teach/udec/reading/Adhikary{_}etal{_}mechs{_}of{_}flexural{_}toppling{_}RockMech{_}1997.pdf.

Agisoft (2018). *Agisoft PhotoScan User Manual*. URL: www.agisoft.ruhttp://pubs.acs.org/doi/10.1021/jp303597m.

Alzo'ubi, A K (2016). "Rock Slopes Processes and Recomendet Methods for Analysis". In: *International Journal of GEOMATE* 11.25, pp. 2520–2527. URL: http://geomatejournal.com/sites/default/files/articles/2520-2527-34052-Abdel-Sept-2016.pdf.

An-balagan, R. (1992). "Rock Mass Sta-bility Evaluation Using Modified SMR Approach". In: *6th Natural Symposium on Rock Mechanics*. Bangalore, India, pp. 258–268.

Anderson, T. et al. (2005). *Fracture Mechanics:Fundamentals and Applications*. Third Edit. New York, NY: CRC Press. ISBN: 13: 978-1-4200-5821-5.

Andres, Norina and Alexandre Badoux (2018). "Unwetterschäden in der Schweiz im Jahre 2017". In: pp. 67–74. URL: https://www.wsl.ch/fileadmin/user{_}upload/WSL/News{_}global/2018/03/Unwetterdaten{_}2017/WEL{_}1{_}2018{_}Unwetterschaeden{_}2017.pdf.

Aydan, O. and T. Kawamoto (1992). "The stability of slopes and underground openings against flexural toppling and their stabilisation". In: *Rock Mechanics and Rock Engineering* 25.3, pp. 143–165. ISSN: 0723-2632. DOI: 10.1007/BF01019709. URL: http://link.springer.com/10.1007/BF01019709.

Bailey, WA and JT Christian (1969). "ICES LEASE-I: A Problem-oriented Language for Slope Stability Analysis: Users Manual". In: URL: https://scholar.google.ch/scholar?hl=de{\&}as{_}sdt=0{\%}2C5{\&}q={\%}3A+A+problem-oriented+language+for+slope+stability+analysis.+1969+bailey{\&}btnG=.

Bishop, Alas W (1954). *First Technical Session : General Theory oj Stability of Slopes the Use of the Slip Circle in the Stability Analysis of Slopes*. Tech. rep. URL: https://www.icevirtuallibrary.com/doi/pdf/10.1680/geot.1955.5.1.7.

Bobet, A. (1999). "Analytical solutions for toppling failure". In: *International Journal of Rock Mechanics and Mining Sciences* 36.7, pp. 971–980. ISSN: 13651609. DOI: 10.1016/S0148-9062(99)00059-5. URL: http://linkinghub.elsevier.com/retrieve/pii/S0148906299000595.

Bolay, Stephan (2013). "Quantitative Measurements of Exfoliation Joint Spacing in the Central Aar Granites of the Grimsel Area (Central Swiss Alps)". PhD thesis. ETH.

Brown, W F and J E Srawley (1966). "Plane Strain Crack Toughness Testing of high Strength Metallic Materials". In:

Charles, R. J. (1958). "Static Fatigue of Glass. II". In: *Journal of Applied Physics* 29.11, pp. 1554–1560. ISSN: 0021-8979. DOI: 10.1063/1.1722992. URL: http://aip.scitation.org/doi/10.1063/1.1722992.

Chowdhury, Robin, Phil Flentje, and Gautam Bhattacharya (2010). *Geotechnical Slope Analysis*. February 2015. CRC Press. ISBN: 978-0-415-46974-6. URL: https://www.taylorfrancis.com/books/9780203864203.

Day, R. W. (1997). "Case Studies of Rockfall in Soft Versus Hard Rock". In: *Environmental & Engineering Geoscience* III.1, pp. 133–140. ISSN: 1078-7275. DOI: 10.2113/gseegeosci.III.1.133. URL: https://pubs.geoscienceworld.org/eeg/article/III/1/133-140/136983.

Delbo, Marco et al. (2014). "Thermal fatigue as the origin of regolith on small asteroids". In: *Nature* 508.7495, pp. 233–236. ISSN: 0028-0836. DOI: 10.1038/nature13153. URL: http://www.nature.com/nature/journal/v508/n7495/pdf/nature13153.pdfhttp://www.nature.com/doifinder/10.1038/nature13153.

Digvijay P., Salunkhe et al. (2017). "An Overview on Methods for Slope Stability Analysis". In: *International Journal of Engineering Research and* V6.03, pp. 528–536. ISSN: 2278-0181. DOI: 10.17577/IJERTV6IS030496. URL: http://www.ijert.org/view-pdf/16473/an-overview-on-methods-for-slope-stability-analysis.

Duncan, Michael (1996). "State of the Art: Limit Equilibrium and Finite-Element Analysis of Slopes". In: *Journal of Geotechnical Engineering* 122.July, pp. 577–596. URL: https://ascelibrary.org/doi/pdf/10.1061/{\%}28ASCE{\%}290733-9410{\%}281996{\%}29122{\%}3A7{\%}28577{\%}29.

Eberhardt, Erik (2002). "Numerical Analysis of progressive failure in natural rock slopes". In: *Geological Engineering/Earth and Ocean Sciences*, pp. 1–9.

Eppes, Martha Cary and Russell Keanini (2017). "Mechanical weathering and rock erosion by climate-dependent subcritical cracking". In: *Reviews of Geophysics* 55.2, pp. 470–508. ISSN: 19449208. DOI: 10.1002/2017RG000557.

Erismann, Theodor H. and Gerhard Abele (2001). *Dynamics of Rockslides and Rockfalls*. Berlin, Heidelberg: Springer Berlin Heidelberg. ISBN: 978-3-642-08653-3. DOI: 10.1007/978-3-662-04639-5. URL: http://link.springer.com/10.1007/978-3-662-04639-5.

Ernst, Kristina (2017). "Investigation of the Impact of Exfoliation Fractures on Post-Glacial Rock -Fall Hazards in the Upper-Aar Valley". PhD thesis. ETH Zurich.

Fredlund, D. (1984). "Analytical Methods for Slope Stability Analysis". In: *Fourth International Symposium on Landslides, State-of-the-Art*. Toronto, pp. 229–250. URL: https://soilvision.com/subdomains/unsaturatedsoil.com/Docs/\ResearchPapers/1984/ConferencePapers/Analyticalmethodsforslopestabilityanalysis.pdf.

Goodman, R. E. (1989). *Introduction to Rock Mechanics*. 2nd Editio. John Wiley & Dond. ISBN: 0-471-81200-5. URL: https://vdocuments.site/goodman-r-e-introduction-to-rock-mechanics-2nd-editionpdf.html.

Goodman, R.E. and J.W Bray (1976). "Toppling of Rock Slopes". In: *Specialty Conference on Rock Engineering for Foundations and Slopes*. Vol. 2. ASCE, pp. 201–234.

Goodman, Richard E and D Scott Kieffer (2000). "Behaviour Of Rock In Slopes". In: *Journal of Geotechnical and Geonviromental Engineering* 126. URL: https://ascelibrary.org/doi/pdf/10.1061/{\%}28ASCE{\%}291090-0241{\%}282000{\%}29126{\%}3A8{\%}28675{\%}29.

Gross, B, JE Srawley, and WF Brown Jr (1964). "Stress-intensity factors for a single-edge-notch tension specimen by boundary collocation of a stress function". In: URL: http://www.dtic.mil/get-tr-doc/pdf?AD=ADA398055.

Gross, Dietmar and Thomas Seelig (2011). *Fracture Mechanics*, p. 544. ISBN: 978-3-642-19239-5. DOI: 10.1007/978-3-642-19240-1. arXiv: arXiv:1011.1669v3.

Hack, Robert. (1998). *Slope stability probability classification, SSPC*. International Institute for Aerospace Survey and Earth Sciences (ITC). ISBN: 9061641543. URL: http://www.academia.edu/13317158/Slope{_}Stability{_}Probability{_}Classification{_}SSPC.

Hocking, G. (1976). "A method for distinguishing between single and double plane sliding of tetrahedral wedges". In: *International Journal of Rock Mechanics and Mining Sciences & Geomechanics Abstracts* 13.7, pp. 225–226. ISSN: 01489062. DOI: 10.1016/0148-9062(76)91697-1. URL: http://linkinghub.elsevier.com/retrieve/pii/0148906276916971.

Hoek, Evert (2007). *Practical Rock Engineering*. URL: https://www.rocscience.com/learning/hoeks-corner/course-notes-books.

Hoek, Evert and John Bray (1981). *Rock slope engineering*. Institution of Mining and Metallurgy, p. 358. ISBN: 0419160108. URL: https://books.google.ch/books/about/Rock{_}Slope{_}Engineering.html?id=VSccRRWxHf4C{\&}redir{_}esc=y.

Hossain, M M (2011). "Stability analysis of anchored rock slopes against plane failure subjected to surcharge and seismic loads". PhD thesis. Edith Cowan University. URL: https://ro.ecu.edu.au/theses/139.

Huang, Y H (2014). *Slope Stability Analysis by the Limit Equilibrium Method: Fundamentals and Methods*, p. 378. ISBN: 9780784412886. DOI: 10.1061/9780784412886.

Jaboyedoff, M. and M.-H Derron (2005). "Integrated risk assessment process for landslides". In: *Landslide risk management*. Ed. by R. O., Fell, R. R. Couture, and Eberhardt.

Jimenez-Rodriguez, R., N. Sitar, and J. Chacón (2006). "System reliability approach to rock slope stability". In: *International Journal of Rock Mechanics and Mining Sciences* 43.6, pp. 847–859. ISSN: 13651609. DOI: 10.1016/j.ijrmms.2005.11.011. URL: https://www.sciencedirect.com/science/article/pii/S136516090600\0128http://linkinghub.elsevier.com/retrieve/pii/S1365160906000128.

Kemeny, J (2003). "The Time-Dependent Reduction of Sliding Cohesion due to Rock Bridges Along Discontinuities: A Fracture Mechanics Approach". In: *Rock Mechanics and Rock Engineering* 36.1, pp. 27–38. ISSN: 0723-2632. DOI: 10.1007/s00603-002-0032-2. URL: https://link.springer.com/content/pdf/10.1007{\%}2Fs00603-002-0032-2.pdfhttp://link.springer.com/10.1007/s00603-002-0032-2.

Kim, Kyu-Sang et al. (2004). "Geographic Information System (GIS) based stability analysis of rock cut slopes". In: *Geosciences Journal* 8.4, pp. 391–400. ISSN: 1226-4806. DOI: 10.1007/BF02910475. URL: http://link.springer.com/10.1007/BF02910475.

Kirane, Kedar and Zdeněk P. Bažant (2016). "Size effect in Paris law and fatigue lifetimes for quasibrittle materials: Modified theory, experiments and micro-modeling". In: *International Journal of Fatigue* 83, pp. 209–220. ISSN: 01421123. DOI: 10.1016/j.ijfatigue.2015.10.015.

Kliche, C. A (2003). *Rock Slope Stability*, p. 205. ISBN: 9780471910213. DOI: 10.1016/0148-9062(75)90139-4. arXiv: EM1110-2-1902.

Ko, Tae Young and John Kemeny (2011). "Subcritical crack growth in rocks under shear loading". In: *Journal of Geophysical Research: Solid Earth* 116.1. ISSN: 21699356. DOI: 10.1029/2010JB000846.

Labhart, Toni P. (Toni Peter) (1977). *Aarmassiv und Gotthardmassiv*. Borntraeger, p. 173. ISBN: 3443150195. URL: https://books.google.ch/books?id=wnI1AAAAMAAJ{\&}hl=de{\&}source=gbs{_}ViewAPI{\&}redir{_}esc=y.

Le, Jia-Liang, Jonathan Manning, and Joseph F. Labuz (2014). "Scaling of fatigue crack growth in rock". In: *International Journal of Rock Mechanics and Mining Sciences* 72, pp. 71–79. ISSN: 13651609. DOI: 10.1016/j.ijrmms.2014.08.015. URL: http://dx.doi.org/10.1016/j.ijrmms.2014.08.015https://linkinghub.elsevier.com/retrieve/pii/S1365160914002299.

Leith, Kerry et al. (2017). "Development of a new thermally-induced fracture in a 12,000 year old bedrock surface". In: *Extended Abstracts of 2017 Progressive Rock Failure Conference*. Locarno: ETH Zurich, pp. 17–19. URL: https://www.research-collection.ethz.ch/handle/20.500.11850/223713.

Ling, Hoe I. and Alexander H.-D. Cheng (1997). "Rock sliding induced by seismic force". In: *International Journal of Rock Mechanics and Mining Sciences* 34.6, pp. 1021–1029. ISSN: 1365-1609. DOI: 10.1016/S1365-1609(97)80011-1. URL: https://www.sciencedirect.com/science/article/pii/S1365160997800111.

Liu, Ya-Ching and Chao-Shi Chen (2007). "A new approach for application of rock mass classification on rock slope stability assessment". In: *Engineering Geology* 89.1-2, pp. 129–143. ISSN: 00137952. DOI: 10.1016/j.enggeo.2006.09.017. URL: http://linkinghub.elsevier.com/retrieve/pii/S0013795206002614.

Mauldon, Matthew, Scott Arwood, and Christopher D. Pionke (1998). "Energy Approach to Rock Slope Stability Analysis". In: *Journal of Engineering Mechanics* 124.4, pp. 395–404. ISSN: 0733-9399. DOI: 10.1061/(ASCE)0733-9399(1998)124:4(395). URL: http://ascelibrary.org/doi/10.1061/{\%}28ASCE{\%}290733-9399{\%}281998{\%}29124{\%}3A4{\%}28395{\%}29.

Miller, Irwin and John E. Freund (1985). *Probability and statistics for engineers*. 3. ed. Englewood Cliffs N.J.: Prentice-Hall, p. 530. ISBN: 9780137119387. URL: https://www.worldcat.org/title/probability-and-statistics-for-engineers/oclc/797413419.

Paris, Paul C., Mario Gomes, and William Anderson (1961). "A rational analytic theory of fatigue". In: *Physical Review Letters* 13.4, p. 045501. URL: http://imechanica.org/files/1961ParisGomezAndersonArationalanalytictheoryoffatigue.pdf.

Price, David (2009). *Engineering Geology Principles and Practice*. Ed. by Michael H. de Freitas. Berlin, Heidelberg: Springer Berlin Heidelberg. ISBN: 978-3-540-29249-4. DOI: 10.1007/978-3-540-68626-2. URL: http://link.springer.com/10.1007/978-3-540-68626-2.

Pugno, N et al. "A generalized Paris' law for fatigue crack growth". In: *Journal of the Mechanics and Physics of Solids* 7, pp. 1333–1349. ISSN: 00225096. DOI: 10.1016/j.jmps.2006.01.007. URL: http://linkinghub.elsevier.com/retrieve/pii/S0022509606000196http://www.ncbi.nlm.nih.gov/pubmed/24335434http://www.pubmedcentral.nih.gov/articlerender.fcgi?artid=PMC3916382volume={54},year={2006}.

Raghuvanshi, Tarun Kumar (2017). "Plane failure in rock slopes – A review on stability analysis techniques". In: *Journal of King Saud University - Science*. ISSN: 10183647. DOI: 10.1016/j.jksus.2017.06.004. URL: http://dx.doi.org/10.1016/j.jksus.2017.06.004https://linkinghub.elsevier.com/retrieve/pii/S1018364717304470.

Raumer, J.F. (1993). *Pre-Mesozoic Geology in the Alps*. Ed. by J. F. von Raumer and Franz Neubauer. Vol. 134. 4. Berlin, Heidelberg: Springer Berlin Heidelberg, pp. 635–646. ISBN: 978-3-642-84642-7. DOI: 10.1007/978-3-642-84640-3. URL: http://link.springer.com/10.1007/978-3-642-84640-3.

Romana, M (1985). "New adjustement ratings for application of Bieniawski classification to slopes". In: *Proceedings of the International Symposium on the Role of Rock Mechanics in Excavations for Mining and Civil Works*. Zacatecas.

Schneeberger, Raphael Benedict (2017). "Interplay in 3D between faults and water flow paths in crystalline bedrock (Grimsel , Switzerland)". PhD thesis. Universität Bern. URL: https://boris.unibe.ch/108553/1/PhD{_}thesis{_}Schneeberger{_}reviewed.pdf.

Schumm, S. A. and R. J. Chorley (1964). "The fall of Threatening Rock". In: *American Journal of Science* 262.9, pp. 1041–1054. ISSN: 0002-9599. DOI: 10.2475/ajs.262.9.1041. URL: http://www.ajsonline.org/cgi/doi/10.2475/ajs.262.9.1041.

Segall, Paul (1984). "Formation and growth of extensional fracture sets". In: *Geological Society of America Bulletin* 95.4, p. 454. ISSN: 0016-7606. DOI: 10.1130/0016-7606(1984)95<454:FAGOEF>2.0.CO;2. URL: https://pubs.geoscienceworld.org/gsabulletin/article/95/4/454-462/202922.

Selby, M. J. (1982). *Hillslope Materials and Process*. Oxford University Press, p. 451. ISBN: 9780198741831. URL: https://global.oup.com/academic/product/hillslope-materials-and-processes-9780198741831?cc=us{\&}lang=en{\&}.

Sellmeier, Bettina (2015). *Quantitative Parameterization and 3D-run-out Modelling of Rockfalls at Steep Limestone Cliffs in the Bavarian Alps*. Springer Theses. Springer International Publishing, p. 159. ISBN: 978-3-319-24509-6. DOI: 10.1007/978-3-319-24510-2. arXiv: arXiv:1106.3562. URL: http://link.springer.com/10.1007/978-3-319-24510-2.

Shukla, S. K. et al. (2009). "Effect of Surcharge on the Stability of Anchored Rock Slope with Water Filled Tension Crack under Seismic Loading Condition". In: *Geotechnical and Geological Engineering* 27.4, pp. 529–538. ISSN: 0960-3182. DOI: 10.1007/s10706-009-9254-3. URL: http://link.springer.com/10.1007/s10706-009-9254-3.

Stead, D, E Eberhardt, and J.S. Coggan (2006). "Developments in the characterization of complex rock slope deformation and failure using numerical modelling techniques". In: *Engineering Geology* 83.1-3, pp. 217–235. ISSN: 00137952. DOI: 10.1016/j.enggeo.2005.06.033. URL: www.elsevier.com/locate/enggeohttp://linkinghub.elsevier.com/retrieve/pii/S0013795205002310.

Steward, T. et al. (2011). "Taylor's Slope Stability Charts Revisited". In: *International Journal of Geomechanics* 11.4, pp. 348–352. ISSN: 1532-3641. DOI: 10.1061/(ASCE)GM.1943-5622.0000093. URL: http://ascelibrary.org/doi/10.1061/{\%}28ASCE{\%}29GM.1943-5622.0000093.

Sutter, B. (2008). "Kluftmuster und Kluftgenese am Grimselpass: Geologisch- geotechnische Eigen- schaften und Tiefenwirkung der Trennflächensysteme". PhD thesis. ETH.

Tada, Hiroshi, Paul C. Paris, and George R. Irwin. *The Stress Analysis of Cracks Handbook, Third Edition*. Three Park Avenue New York, NY 10016-5990: ASME. ISBN: 0791801535. DOI: 10.1115/1.801535.

Tang, Huiming, Rui Yong, and M. A. M. Ez Eldin (2017). "Stability analysis of stratified rock slopes with spatially variable strength parameters: the case of Qianjiangping landslide". In: *Bulletin of Engineering Geology and the Environment* 76.3, pp. 839–853. ISSN: 1435-9529. DOI: 10.1007/s10064-016-0876-4. URL: https://link.springer.com/content/pdf/10.1007{\%}2Fs10064-016-0876-4.pdfhttp://link.springer.com/10.1007/s10064-016-0876-4.

Vallejo, Luis Gonzales de and Mercedes Ferrer (2012). *Geological engineering*. First Edit. CRC Press, p. 671. ISBN: 9780415413527.

Varnes, David J (1978). "Slope movements types and processes." In: *TRB Special Report* 176.Landslides: Analysis and Control, pp. 11–33. ISSN: 0360-859X. URL: http://worldcat.org/issn/0360859X.

Wang, Min and Ping Cao (2017). "Experimental Study of Crack Growth in Rock-Like Materials Containing Multiple Parallel Pre-existing Flaws Under Biaxial Compression". In: *Geotechnical and Geological Engineering* 35.3, pp. 1023–1034. ISSN: 0960-3182. DOI: 10.1007/s10706-017-0158-3. URL: https://link.springer.com/content/pdf/10.1007{\%}2Fs10706-017-0158-3.pdfhttp://link.springer.com/10.1007/s10706-017-0158-3.

Wijk, Gunnar (1978). *Some New Theoretical Aspects of Indirect Measurements of the Tensile Strength of Rocks*. Tech. rep., pp. 149–160.

Winter, Mike G. et al. (2014). "Economic Impact Assessment of Landslide Events". In: *Landslide Science for a Safer Geoenvironment*. Cham: Springer International Publishing, pp. 217–222. DOI: 10.1007/978-3-319-04999-1_28. URL: http://link.springer.com/10.1007/978-3-319-04999-1{_}28.

Wyllie, Duncan (2014). *Rock Fall Engineering*. CRC Press, p. 243. ISBN: 978-1-4822-1997-5. DOI: 10.1201/b17470. URL: https://www.taylorfrancis.com/books/9781482219982.

Wyllie, Duncan and Crhistopher Mah (2005). *Rock Slope Engineering: Civil and Mining*. 4th Editio. 4. CRC Press, p. 456. ISBN: 9781482265125.

Yang, Xiao-Li (2007). "Seismic displacement of rock slopes with nonlinear Hoek–Brown failure criterion". In: *International Journal of Rock Mechanics and Mining Sciences* 44.6, pp. 948–953. ISSN: 13651609. DOI: 10.1016/j.ijrmms.2007.01.002. URL: http://linkinghub.elsevier.com/retrieve/pii/S1365160907000159.

Ziegler, Martin (2013). "Age and formation mechanisms of exfoliation joints in the Aar Granites of the Central Alps (Grimsel region , Switzerland)". In: 21619, p. 169.

Declaration of Authorship

I hereby declare that the submitted thesis is the result of my own, independent work. All external sources are explicitly acknowledged in the thesis.

Signed: 

Date: 29.01.2019